LOCAL AND REGIONAL DRIVERS OF OXYGEN VARIABILITY IN COASTAL EMBAYMENTS ON THE SOUTHWEST SCOTIAN SHELF: IMPLICATIONS FOR NOVA SCOTIA ATLANTIC SALMON (SALMO SALAR) FARMING

by

Meredith Anne Burke

Submitted in partial fulfilment of the requirements
for the degree of Doctor of Philosophy

at

Dalhousie University
Halifax, Nova Scotia
August 2022

Dedicated to my parents
Brian and Brooke
For your unconditional support

TABLE OF CONTENTS

LIST OF TABLES vii
LIST OF FIGURES viii
ABSTRACT xiv
LIST OF ABBREVIATIONS AND SYMBOLS USED xv
ACKNOWLEDGEMENTS xviii
CHAPTER 1 INTRODUCTION 1
1.1 Drivers of Oxygen Distribution in the Ocean 1
1.2 Climate Change and the Future of Oxygen in the Ocean 2
1.3 Oxygen in Aquaculture Farms 4
1.4 Technological Innovations to Study DO 5
1.4.1 Optode-Based Sensors 5
1.4.2 Gliders 6
1.4.3 Numerical Models 6
1.4.4 Unit Conversion 7
1.5 Objectives and Thesis Outline 8
1.6 Statement of Co-Authorship 9
CHAPTER 2 OCEANOGRAPHIC PROCESSES CONTROL DISSOLVED OXYGEN VARIABILITY AT A COMMERCIAL ATLANTIC SALMON FARM: APPLICATION OF A REAL-TIME SENSOR NETWORK 10
2.1 Abstract 10
2.2 Introduction 11
2.3 Materials and Methods 14
2.3.1 Study Site 14
2.3.2 Data Collection 15
2.3.3 Statistical Analysis 16
2.4 Results 17
2.4.1 Temporal Variability 17
2.4.2 Spatial Variability 19
2.4.3 Drivers of Dissolved Oxygen 19
2.5 Discussion 23

2.5.1 Temporal Variability 24
2.5.2 Spatial Variability 25
2.5.3 Drivers of Dissolved Oxygen 26
2.6 Conclusion 29
CHAPTER 3 OXYGENATION EFFECTS ON TEMPERATURE AND DISSOLVED OXYGEN AT A COMMERCIAL ATLANTIC SALMON FARM 30
3.1 Abstract 30
3.2 Introduction 30
3.3 Materials and Methods 33
3.3.1 Study Site 33
3.3.2 Data Collection 34
3.3.3 Statistical Analysis 35
3.4 Results 36
3.4.1 Temperature 36
3.4.2 Dissolved Oxygen 42
3.5 Discussion 46
3.5.1 Temperature 47
3.5.2 Dissolved Oxygen 48
3.6 Conclusion 51
CHAPTER 4 TEMPORAL AND SPATIAL VARIABILITY IN HYDROGRAPHY AND DISSOLVED OXYGEN ALONG SOUTHWEST NOVA SCOTIA USING GLIDER OBSERVATIONS 52
4.1 Abstract 52
4.2 Introduction 52
4.3 Materials and Methods 56
4.3.1 Study Site 56
4.3.2 Field Measurements 59
4.3.3 Wind-Related Parameters and Water Mass Properties 60
4.4 Results 61
4.4.1 Water Mass Distribution 61
4.4.2 Along-Shore Variability 62

4.4.3 Cross-Shore Variability 65
4.4.4 The Role of Local Wind Forcing 67
4.4.5 Offshore-Inshore Interaction 69
4.5 Discussion 70
4.5.1 Water Mass Distribution 71
4.5.2 Along-Shore Dynamics 72
4.5.3 Cross-Shore Dynamics 73
4.5.4 The Role of Local Wind Forcing 74
4.5.5 Offshore-Inshore Interaction 75
4.6 Conclusion 77
CHAPTER 5 PROJECTIONS OF DISSOLVED OXYGEN VARIABILITY UNDER CLIMATE CHANGE SCENARIOS ON THE SOUTHWESTERN SCOTIAN SHELF 78
5.1 Abstract 78
5.2 Introduction 78
5.3 Methods 81
5.3.1 Study Domain 81
5.3.2 Model Setup 84
5.3.3 Numerical Experiments 86
5.4 Results and Discussion 88
5.4.1 Baseline Conditions 88
5.4.2 Temperature Increased 90
5.4.3 GSLC Weakened 93
5.4.4 Wind Increased 95
5.4.5 Wind Weakened 97
5.4.6 Combined Simulation 99
5.5 Conclusion 101
CHAPTER 6 CONCLUSION 103
6.1 Summary of Thesis 103
6.2 Research Contributions 105
6.3 Limitations and Research Opportunities 107
APPENDIX A 109

A.1 109
A.2 109
APPENDIX B 111
APPENDIX C 112
APPENDIX D 113
D.1 113
D.2 115
REFERENCES 122

LIST OF TABLES

Table 3.1 Mann-Whitney U test results for temperature difference between 2 m and 7 m in each cage during each time period; n = sample size 37

Table 3.2 Mann-Whitney U test results for temperature difference between satellite Sea Surface Temperature (SST) and 2 m in each cage during each time period; n = sample size 39

Table 3.3 Cross-correlation between wind or tide and temperature at 2 m; n = sample size 41

Table 3.4 Mann-Whitney U test results for DO difference between 2 m and 7 m in each cage during each time period; n = sample size 42

Table 3.5 Mann-Whitney U test results for DO difference between pre-oxygenation and oxygenation and between oxygenation and de-stratification for each depth; n = sample size 44

Table 3.6 Cross-correlation between wind or tide and DO at 2 m; n = sample size 45

Table 5.1 Summary of numerical experiments. NARR: North American Regional Reanalysis; GSLC: Gulf Stream/Labrador Current 87

LIST OF FIGURES

Figure 2.1 Site schematic showing (A) the location of the farm within Shelburne Bay including bathymetry (m) and an inset map of Nova Scotia, and (B) the layout of the farm with cages numbered.....15

Figure 2.2 Hourly (lighter lines) and daily (darker lines) average dissolved oxygen (DO) concentrations (mg L^{-1}), along with corresponding hourly temperatures (black), within (A) cage 1 (inner bay), (B) cage 5 (middle of the farm), (C) cage 10 (outer bay), and (D) a reference site. Red dots indicate oxygen below the maximum potential feed intake threshold (Remen et al. 2016) 18

Figure 2.3 Power spectral density (PSD) of dissolved oxygen (DO, mg L^{-1}) in cages 1 (blue; A,B), 5 (green; C,D) and 10 (red; E,F) for both the summer (A,C,E) and autumn periods (B,D,F). Black dashed line indicating the 12.42 h period, and purple dashed indicating the 6.21 h period.....20

Figure 2.4 Dissolved oxygen and tidal height over two weeks within cage 1 (blue; A,B), cage 5 (green; C,D) and cage 10 (orange; E,F) for summer (A,C,E) and autumn (B,D,F) 21

Figure 2.5 The correlation between tide and dissolved oxygen within each cage and 3 reference sites on either side of the farm (A) far from island, (B) close to island, for the summer period (white) and autumn period (black). Strength of correlation indicated as strong (shaded white), moderate (shaded yellow) and weak (shaded green).....23

Figure 3.1 Site schematic showing the layout of the cages within the Atlantic salmon farm in Aspotogan Bay including bathymetry (m) and an inset map of Nova Scotia.....34

Figure 3.2 Hourly (lighter lines) and daily (darker lines) average temperature within cages 1 (A), 2 (C) and 5 (E) at 2 m and 7 m in 2019, along with the sea surface temperature (SST) derived from satellite data (dashed line). Difference in temperature between observations at 2 m and satellite SST and between 2 m and 7 m in cages 1 (B), 2 (D), and 5 (F). The vertical dotted line indicates the onset of de-stratification, and the grey bars indicate approximate times when the oxygenation system was off.....38

Figure 3.3 Hourly (lighter lines) and daily (darker lines) average dissolved oxygen (DO, mg L^{-1}) within cages 1 (A), 2 (C) and 5 (E) at 2 m and 7 m in 2019, along with the reference (black). Difference in DO between 2 m and 7 m in cages 1 (B), 2 (D), and 5 (F). The vertical dotted line indicates the onset of de-stratification, and the grey bars indicate approximate times when the oxygenation system was off.....43

Figure 3.4 Relationship between oxygen consumption by the fish (mg O_2 hr^{-1}) and dissolved oxygen (DO, mg L^{-1}) over the average of both depths in cages 1 (circles), 2 (triangles) and 5 (diamonds) during pre-oxygenation (orange), oxygenation (blue), and de-stratification (red) 46

Figure 4.1 Major features of topography over the western Scotian Shelf and the Slocum glider transect (black line) depicting the route from Shelburne Bay (I), past Liverpool (II) and the weather station at Lunenburg (III) to St. Margarets Bay (IV), and an inset map of Nova Scotia 56

Figure 4.2 Two-month averaged model results of temperature, salinity and currents at three depths (0, 20 m, and 40 m) in September and October 2018 produced by a nested-grid shelf circulation model based on the ROMS (personal communication, Sheng 2022) 58

Figure 4.3 Temperature-salinity diagram based on Slocum glider observations along The full transect, including the isopycnals (-1000, kg m^{-3}). The colour Scheme corresponds to the DO (mg L^{-1}) distribution, with light blue indicating highest values and green indicating lowest. The relevant water masses are indicated as the surface mixed layer, Cabot Strait – Cold Intermediate Layer (CBS-CIL) and Warm Slope Water (WSW), with the major mixing line between the latter two 62

Figure 4.4 The distance to shore along the glider transect (a), the vertical distribution of temperature (°C; b), salinity (c), and dissolved oxygen (DO, mg L^{-1}; d), along the Slocum glider transect (September 25 – October 12 2020). The glider was programmed to turn 2 m above the seafloor, indicated by the white area in each plot. The shoreline waypoints are indicated by roman numerals (Shelburne Bay, I; Liverpool Bay, II; Lunenburg, III; St. Margarets Bay, IV). Dark red colours indicate highest temperature, salinity, oxygen while dark blue colours indicate lowest 63

Figure 4.5 Three cross-shore transects selected on the full along-shore glider track (a) and the subsequent temperature (°C; blue), salinity (red) and DO (mg L^{-1}; green) profiles for the transect near Shelburne (b), near to Liverpool (c) and near St. Margarets Bay (d). The lightest colours indicate the profiles closest to shore, while the darker colours indicate those furthest from shore 66

Figure 4.6 The distance to shore along the glider transect (a), temperature observations (°C) from the Slocum glider at 7 depths (5-50 m; b), the associated wind vectors (m s^{-2}; c), and the along-shore (U, m s^{-1}; purple) and cross-shore (V, m s^{-1}; teal) wind components (d) for the duration of the transect. In (f), the Ekman transport (I_w, m^2 s^{-1}) depicting upwelling (black) and downwelling (grey), as well as the wind impulse (orange). Each plot is between September 26 and October 12 2020. The grey bar indicates the strong upwelling event, while the purple bar indicates the wind components 25 h prior to this period. The black dotted lines indicate the transition between winds each of the three stations: Shelburne, Liverpool and Lunenburg; while the roman numerals indicate the coastline waypoints: Shelburne Bay, I; Liverpool Bay, II; Lunenburg, III; St. Margarets Bay, IV 68

Figure 4.7 Temperature (°C; a) and DO (mg L^{-1}; b) based on the Slocum glider observations at 5 m depth (red) and inshore observations from a sensor placed at 5 m within St. Margarets Bay (green) 70

Figure 5.1 Major features of topography over the western Scotian Shelf, including the basins (LaHave, Emerald) and banks (Roseway, Baccaro, LaHave, Sambro) and the isobaths at 30 m, 90 m, and 150 m relevant for the results, and an inset map of Nova Scotia 82

Figure 5.2 Model results of the control scenario (representing the conditions in 2018) with an overlay of the currents at 5 m (a, c) and 40 m (b, d) in August (a, b) and November (c, d). The black arrows indicate the path of the Nova Scotia Current (NSC) 83

Figure 5.3 Temperature profile along a vertical transect over the full study domain at 63.8ºW longitude (a), and an inset figure with a focus on the top 40 m depth (b) 89

Figure 5.4 Oxygen profiles along 3 vertical transects over the full study domain; (a) at 65ºW longitude; (b) at 64.5ºW longitude; and (c) 63.8ºW longitude. The inset figure depicts the top 60 m of the profile along the 63.8ºW transect (d) 90

Figure 5.5 The relative difference (%) in DO between the monthly-means of the control and the increased temperature numerical experiment along southwest Nova Scotia (Canada). The results are presented for August at 5 m (a) and 40 m (b) depth, and November at 5 m (c) and 40 m (d) depth. The banks/basins relevant for the results are indicated as LBn (LaHave Basin), RB (Roseway Bank), BB (Baccaro Bank), and LBk (LaHave Bank) 91

Figure 5.6 The relative difference (%) in DO between the monthly-means of the control and the weakened Gulf Stream/Labrador Current numerical experiment along southwest Nova Scotia (Canada). The results are presented for August at 5 m (a) and 40 m (b) depth, and November at 5 m (c) and 40 m (d) depth. The banks/basins relevant for the results are indicated as LBn (LaHave Basin), EB (Emerald Basin), RB (Roseway Bank), BB (Baccaro Bank), and LBk (LaHave Bank) 94

Figure 5.7 The relative difference (%) in DO between the monthly-means of the control and the increased wind forcing numerical experiment along southwest Nova Scotia (Canada). The results are presented for August at 5 m (a) and 40 m (b) depth, and November at 5 m (c) and 40 m (d) depth. The banks/basins relevant for the results are indicated as LBn (LaHave Basin), EB (Emerald Basin), SB (Sambro Bank), RB (Roseway Bank), BB (Baccaro Bank), and LBk (LaHave Bank) 96

Figure 5.8 The relative difference (%) in DO between the monthly-means of the control and the decreased wind forcing numerical experiment along southwest Nova Scotia (Canada). The results are presented for August at 5 m (a) and 40 m (b) depth, and November at 5 m (c) and 40 m (d) depth. The banks/basins relevant for the results are indicated as LBn (LaHave Basin), RB (Roseway Bank), BB (Baccaro Bank), and LBk (LaHave Bank) 98

Figure 5.9 The relative difference (%) in DO between the monthly-means of the control and the combined numerical experiment of increased winds, weakened GSLC, and weakened wind forcing along southwest Nova Scotia (Canada). The results are presented for August at 5 m (a) and 40 m (b) depth, and November at 5 m (c) and 40 m (d) depth. The banks/basins relevant for the results are indicated as LBn (LaHave Basin), EB (Emerald Basin), RB (Roseway Bank), BB (Baccaro Bank), and LBk (LaHave Bank) 100

Figure A.1 The relationship between temperature (blue), dissolved oxygen (red) and photoperiod (yellow bars indicating daylight) 109

Figure B.1 The relationship between satellite derived sea surface temperature (SST) and temperature in cages 1 (circles), 2 (triangles) and 5 (diamonds) during pre-oxygenation (orange), oxygenation (blue), and de-stratification (red) 111

Figure D.1.1 The relative difference (%) in ocean temperature between the monthly-means of the control and the increased temperature numerical experiment along southwest Nova Scotia (Canada). The results are presented for August at 5 m (a) and 40 m (b) depth, and November at 5 m (c) and 40 m (d) depth. The banks/basins relevant for the results are indicated as LBn (LaHave Basin), Roseway Bank (RB), BB (Baccaro Bank), and LBk (LaHave Bank) 113

Figure D.1.2 Model results of the control scenario (representing the conditions in 2018) with an overlay of the difference in currents between the control and the increased wind forcing simulation at 5 m (a, c) and 40 m (b, d) in August (a, b) and November (c, d) 114

Figure D.1.3 Model results of the control scenario (representing the conditions in 2018) with an overlay of the difference in currents between the control and the weakened wind forcing simulation at 5 m (a, c) and 40 m (b, d) in August (a, b) and November (c, d) 115

Figure D.2.1 Major topographic features and domains of three submodels for a nested-grid coupled circulation-ice modelling system for the southeastern Canadian shelf and adjacent deep ocean waters of the northwestern Atlantic Ocean. The horizontal resolutions of submodels (a) L1, (b) L2, and (c) L3 are respectively 1/12°, 1/36° and 1/108°. The color image in each subplot represents water depths (from Pei MSc thesis, Dalhousie University, 2022)..... 116

Figure D.2.2 Time series of observed (red) and simulated (blue) (a) total, (b) tidal and (c) non-tidal surface elevations at Yarmouth tidal gauge station from 5 February to 27 March 2018. The simulated results are produced by submodel L1 (from Pei MSc thesis, Dalhousie University, 2022) 117

Figure D.2.3 Co-phases (black contour lines) and co-amplitudes (red contour lines) of the M_2 tidal elevations calculated from results produced by submodel L1 using t_tide (left panels) and taken from OTIS dataset (right panels; (from Pei MSc thesis, Dalhousie University, 2022). The ground truth data are from m_map Matlab program (Pawlowicz, 2020) 118

Figure D.2.4 Monthly-mean SST (a,b) and SSS (c,d) over the domain of submodel L1 in March 2018 calculated respectively from (a,c) results produced by submodel L1 and (b) satellite remote sensing SST data, and (d) extracted from the Sea Surface Salinity Essential Climate Variable (ECV) dataset (version 1.8) produced by the European Space Agency's (ESA) Climate Change Initiative (CCI; adapted from Pei MSc thesis, Dalhousie University, 2022) 119

Figure D.2.5 Monthly-mean temperature (a,d), currents (arrows in a,d), and DO (b,e) produced by L3COM at (a,b) the surface and (d,e) 70 m over the L3 domain in March 2018. For clarity, velocity vectors are plotted at every 6th model grid point. Figure 4.3c,f presents the March-mean DO in 2018 at the sea surface and 70 m over the L3 domain calculated from the daily-mean product of the GRB29 dataset (from Pei MSc thesis, Dalhousie University, 2022) 120

Figure D.2.6 Vertical profiles of observed (red dots) and simulated (blue lines) DO at Points B, C, and D over the southwestern Scotian Shelf in July 2018. The blue line in each subplot represents the daily-mean DO by averaging model results at four grid points around each observation point (from Pei MSc thesis, Dalhousie University, 2022) 121

ABSTRACT

Globally, the coastal ocean is increasingly threatened by climate change-related stressors, such as ocean warming and deoxygenation. As a result, anthropogenic activities such as sea cage aquaculture, which often occurs in these ecosystems, are left vulnerable. Additionally, coastal oxygen deficits are intensified due to eutrophication as there is increased nutrient input from coastal development, which then affect cultured fish directly through stress, vulnerability to diseases and ultimately, increased mortality. Therefore, it is important to effectively monitor aquaculture farms and the adjacent coastal zone to ensure optimal fish welfare and marine management. This thesis explores the local and regional drivers of dissolved oxygen and temperature dynamics in coastal embayments within southwest Nova Scotia. Novel real-time oxygen and temperature sensors were used to understand local dynamics. First, a dense array of 63 sensors was deployed through an aquaculture farm to explore the drivers of oxygen variability. Tidal driven currents were determined to have the most significant impact on oxygen, with the influence varying depending on the position of the cage within the farm (Chapter 2). Second, the sensors were used to determine how an oxygen supplementation system affects oxygen distribution within 3 sea cages. Overall, oxygenation likely resulted in the upwelling of cool waters to the surface, increasing oxygen solubility and lowering fish metabolism, subsequently increasing oxygen concentrations (Chapter 3). To explore regional along-shore and cross-shore oxygen distribution and variability, a Slocum glider was deployed in a zigzagging pattern along the inner southwest Scotian Shelf. Wind direction had a significant affect, with strong cross-shore winds advecting water masses of differing properties to the coast, and persistent southwesterly winds causing upwelling of high DO from the subsurface. This data was then compared to a sensor within a bay to examine the offshore-inshore interaction, which has the potential to impact aquaculture farms located in these coastal embayments. A strong upwelling event 10 km from the coast was captured 30 h later within the bay, depicting possible interaction between the shelf and the bay (Chapter 4). Lastly, numerical experiments using an oxygen model were conducted for the Southwest Scotian Shelf. The effect of four potential climate change-related stressors on oxygen dynamics were examined: increased temperatures, weakened Gulf Stream-Labrador Current, increased winds, and weakened winds. To simulate the interactive effect of these stressors, a final scenario combined increased temperature, weakened currents, and weakened winds (Chapter 5). Individually, weakened Gulf Stream-Labrador Current resulted in the most significant decrease in oxygen on the inner Scotian Shelf, while increased winds (due to stronger storm events) resulted in the highest decreases in oxygen on the mid-outer Scotian Shelf. When stressors were combined, there was an overall decline in DO across the domain, whereby weakened currents caused the most significant decrease on the inner shelf. The exception to this was in the LaHave and Emerald Basins, as weakened winds caused an increase in oxygen. Improved knowledge of the drivers of oxygen dynamics within aquaculture farms and the adjacent shelf waters is important for the management of the region as well as for the future of aquaculture production and other coastal economies.

LIST OF ABBREVIATIONS USED

ABBREVIATION	DESCRIPTION
ADCP	Acoustic Doppler Current Profiler
AMOC	Atlantic Meridional Overturning Circulation
ANCOVA	Analysis of Covariance
AVHRR	Advanced Very-High Resolution Radiometer
BB	Baccaro Bank
CBS	Cabot Strait
CBS-CIL	Cabot Strait-Cold Intermediate Waters
CICE	Los Alamos Sea Ice Model
CMIP5	Coupled Model Intercomparison Project Phase 5
CTD	Conductivity, Temperature, Depth
DO	Dissolved Oxygen
EB	Emerald Basin
GSL	Gulf of St. Lawrence
GSLC	Gulf Stream-Labrador Current
K-S	Kolmogorov-Smirnov Test
LB	LaHave Bank
LBn	LaHave Basin
M_2	Principal Lunar Semidiurnal Tidal Constituent (12.42 h)
M_4	Shallow Water Overtides of Principal Lunar Constituent (6.21 h)
NARR	North American Regional Reanalysis
NOAA	National Oceanic and Atmospheric Administration
NSC	Nova Scotia Current
NWR	Net Water Respiration
PSD	Power Spectral Density
RAS	Recirculating Aquaculture System
RCP	Representative Concentration Pathway
RB	Roseway Bank

ROMS	Regional Ocean Modelling System
SB	Sambro Bank
ScS	Scotian Shelf
SOC	Sediment Oxygen Consumption
SST	Sea Surface Temperature
UNIANOVA	Regression Analysis/Analysis of Variance
WSW	Warm Slope Water

SYMBOLS	**DESCRIPTION**
a,b	Coefficients of the respiration rate
$\boldsymbol{C}$	Concentration of a tracer
$\overline{\boldsymbol{C'w'}}$	Tracer flux
$\mathbf{C_D}$	Dimensionless drag coefficient
Chl	Chlorophyll
$\mathbf{D}(\boldsymbol{u}, \boldsymbol{v}, \boldsymbol{C})$	Horizontal diffusive terms
F	Forcing (u, v); source/sink for the tracer (C)
$\boldsymbol{f(x,y)}$	Coriolis parameters
$\boldsymbol{h(x,y)}$	Local water depths
$\boldsymbol{I}$	Wind impulse
I	Intensity of luminescence in the presence of oxygen
$\mathbf{I_O}$	Intensity of the dye luminescence in the absence of oxygen
$\boldsymbol{I_w}$	Ekman transport
$\boldsymbol{K_h}$, $\boldsymbol{K_v}$	Horizontal, vertical molecular diffusion coefficients
$\mathbf{K_q}$	Quencher rate or Stern-Volmer coefficient
$\boldsymbol{O_2}$	DO concentrations
$\boldsymbol{O_{2sat}}$	Saturated DO
$\boldsymbol{\rho_{air}}$, $\boldsymbol{\rho_a}$	Air density
$\boldsymbol{\rho_w}$	Density of seawater
PP	Primary production rate
$\mathbf{p_{O2}}$	Partial pressure of oxygen
R	Respiration rate

$\boldsymbol{Sc_{ox}}$	Schmidt number for oxygen
$\boldsymbol{\tau_a}$	Along-shore wind stress
$\boldsymbol{t}$	Time
T	Ocean temperature (°C)
u, $\boldsymbol{v}$, $\boldsymbol{w}$	Eastward (x), northward (y), upward (z) components of ocean currents
$\overline{\boldsymbol{u'w'}}, \overline{\boldsymbol{v'w'}}$	Reynolds stresses
$\boldsymbol{V}$	Ttotal wind velocity
$\boldsymbol{Vk_{O2}}$	Gas transfer velocity
$\boldsymbol{v}$,$\boldsymbol{v_\theta}$	Molecular viscosity and diffusivity
W	Salmon weight (g)
$\boldsymbol{z}$	Vertical Cartesian coordinate
$\emptyset(\boldsymbol{x}, \boldsymbol{y}, \boldsymbol{z}, \boldsymbol{t})$	Dynamic pressure
$\boldsymbol{\eta}(\boldsymbol{x}, \boldsymbol{y})$	Sea surface elevations

ACKNOWLEDGMENTS

First and foremost, I would like to thank my supervisors, Drs. Jon Grant and Ramon Filgueira, for their thoughtful ideas, immense knowledge, support and motivation throughout my PhD. Allowing me to conduct such relevant and applicable research has been so rewarding, and I am extremely grateful. I would also like to thank my committee members, Vincent Sieben and Jinyu Sheng. Vince's encouragement and knowledge of sensors has been invaluable for my research, while Jinyu's input on anything physical oceanography-related has allowed me to grow as a scientist. To my external examiner, Karen Wild-Allen, thank you for taking the time to read my thesis and provide feedback. Lastly, I'd like to acknowledge that funding for my research was provided by Dalhousie, the Ocean Frontier Institute, and the Natural Sciences and Engineering Research Council (NSERC).

I would also like to acknowledge the hard work of the farmers from Cooke Aquaculture and to Kyle Gosley, for deploying the sensors, tending to them and transporting me endlessly around the farms. Also, thank you to Tim Stone and InnovaSea, for teaching me about their real-time sensors and working with me to improve them. To the Glider Team, and Clark Richards, for the guidance around the glider mission. To Qiantong (Albert) Pei, for the incredible work on the oxygen model, and the invaluable insights into the data. None of this work could have been done without all of you.

My sincere thanks go to the Grant and Filgueira Lab members past and present including Anne McKee, Jenny Weitzman, Laura Steeves, Megan Rector, Hart Koepke, and Jennie Korus for their continued encouragement and motivation. A special thanks to both my office mates, Stephen Finnis and Sarah de Mendonça for creating an amazing atmosphere for both work and occasionally play.

I am so grateful to my friends, near and far. I have the best support network, from those in Montreal (CATSMANEK) to Boston (Three Seas) and here in Halifax, and I am thankful to be surrounded by amazing people. I want to thank in particular Natalie Davis, Emily Horonowitsch, Jessica Sadko, Jessica Bennett, Meghan Troup, and Graeme Guy for the laughter, the distraction and, of course, their incredible, unwavering support; I would not have gotten here without you.

Finally, thank you to my family. My parents, Brian and Brooke, who have wholeheartedly supported every crazy decision I have made along this academic path; this dissertation is dedicated to you. From moving me to Halifax (then Boston and back to Halifax again), to instilling within me a love for the ocean and travel, and for loving me and helping me through the more challenging times, I cannot thank you enough. To my siblings, Austin and Olivia, you have grounded and encouraged me, and knowing that you'll always be there has given me a lot of strength. I love you all, thank you.

CHAPTER 1 INTRODUCTION

1.1 Drivers of Oxygen Distribution in the Ocean

The oceanic oxygen inventory is a balance that relies primarily on the exchange of oxygen through air-sea flux, through photosynthesis by marine plants, and consumption through respiratory, chemical and enzymatic oxidation throughout the water column (Thistle, 2003, Richards, 1957). The distribution of oxygen can vary seasonally and geographically (Joint and Pomroy, 1986). Primary production occurs in the euphotic zone, above the thermocline, which varies depending on the season as it relates to irradiance/heat flux (thermal stratification) and wind forcing (mixing). There is often shoaling of the thermocline in the summer when irradiance (stratification) is high and wind forcing (mixing) is low. While production occurs in the photic zone, oxygen can ventilate the deep ocean through physical transport.

Geographically, circulation and local currents control water mass movement and the horizontal distribution of oxygen. In areas of downwelling, notably the north Atlantic, oxygenated surface waters are moved to the deep where currents then circulate this highly oxygenated water, in a process called the Atlantic Meridional Overturning Circulation (AMOC). AMOC is driven by thermohaline circulation, or temperature and salinity density gradients, and has been termed the “ocean conveyor belt”, as it transports water between the ocean basins through surface and deep currents (Broecker, 1991).

Along the coast, tidal currents and freshwater discharge strongly influence oxygen concentrations. Many coastal zones are eutrophic, or have an excess amount of nutrients, due to runoff from land, especially in populated areas. As almost half of the world’s population live on the coast, this is a major concern as eutrophication greatly increases phytoplankton growth, and thus oxygen consumption (D’Avanzo & Kremer, 1994). While phytoplankton growth is limited to the photic zone due to light constraints, consumption occurs throughout the water column, therefore oxygen production is usually outpaced by respiration, and the depletion of oxygen in bottom waters occurs.

1.2 Climate Change and the Future of Oxygen in the Ocean

Ocean deoxygenation is one of the major threats of climate change. Globally, dissolved oxygen (DO) has decreased around 2% since the 1950s and projections for the representative concentration pathway (RCP) 8.5 from the Coupled Model Intercomparison Project phase 5 (CMIP5) describe a decline of 3-4% by 2100 (Breitburg et al., 2018; IUCN, 2019). This projected decline is due to the effects of (i) increased sea temperatures, which increase biological metabolism and oxygen consumption rates, while decreasing oxygen solubility, (ii) warming on biological production, respiration and remineralization, and (iii) increased stratification on ventilation of the deep ocean, which is due to reduced upwelling, deep-water formation, and turbulent mixing (Helm et al., 2011; Shepherd et al., 2017). The latter also reduces oxygen in newly formed water masses which circulate slowly through the oceans (Schmidtko et al., 2017). While climate models predict the continuing decline of oxygen in the ocean due to the aforementioned effects, they do not reproduce or correctly estimate oxygen changes that have been observed, and generally only simulate about half of the oxygen loss inferred from observations. For instance, climate models do not show oxygen changes in the ocean's thermocline and often underestimate observed temporal variability of oxygen concentrations (Oschlies et al., 2018).

Deoxygenation is exacerbated on the coast where there is the added challenge of eutrophication from land runoff (Gilbert et al., 2010). Eutrophication is the enrichment of a body of water with minerals and nutrients, which leads to increased phytoplankton productivity and ultimately decomposition of the phytoplankton by bacteria, a process which consumes oxygen. Eutrophication is predominantly caused by sewage discharge and the runoff of agricultural fertilizer. This has been a dominant issue for the last 100 years, however it has increased in more recent years due to the growing global population (Breitburg et al., 2018).

Decreases in oxygen can alter the biogeochemisty of the ocean, specifically for the nitrogen, phosphorus, and carbon cycles. Low oxygen controls denitrification, which converts nitrate to nitrogen gas in anaerobic conditions, removing bioavailable nitrogen. The loss of fixed nitrogen in the ocean limits nitrate for ocean productivity while producing N_2O, a potent greenhouse gas. Low DO also affects the marine phosphorus

cycle as there are greater levels of recycled phosphorus from sediments when DO is low in the overlying waters. Higher levels of phosphorus lead to higher ocean productivity and subsequent oxygen demand (Wallmann, 2003; Keeling et al., 2009; Watson et al., 2017). DO is also directly connected to the carbon cycle through the production and remineralization of organic matter. The effects of low DO on these biogeochemical cycles can result in changes to ecosystem health through shifts in biodiversity, suitable habitats, and overall ecosystem functioning (Vaquer-Sunyer and Duarte, 2008). There are three lower limits of DO that are important for biogeochemistry: hypoxia, suboxia and anoxia (Ridder and England, 2014). First, hypoxia refers to those conditions where certain species have insufficient oxygen to respire, rendering the region uninhabitable for that species. The general guidelines often use 2 mg L^{-1} as the threshold for hypoxia, as this is the limit for fisheries production. Next, suboxic conditions are those where nitrogen, specifically denitrification, is used in remineralization rather than oxygen. This becomes an issue in areas where nitrate is already in low quantities and thus processes that utilize nitrate become constrained. Dead zones and oxygen minimum zones are characterized by suboxic conditions, the threshold of which has been generalized as between 0.03-0.66 mg L^{-1} (Spietz et al., 2015). Lastly, anoxic waters are those below 0.03 mg L^{-1}, usually completely devoid of oxygen, which results in sulphate reduction replacing nitrate respiration (Paulmier and Ruiz-Pino, 2009). When respiration occurs in the absence of oxygen, the electron acceptors that are subsequently used (nitrate, then sulphate), yields less and less energy. This results in reduced biodiversity, biomass, and energy expensive ecological interactions, like predation. Energy is transferred to microbes instead of larger animals, which results in the loss of diverse ecosystems and reduced ecosystem services (Breitburg et al., 2018). The composition and distribution of organisms in the water column are also likely to change, such as with zooplankton, as shoaling of oxygen minimum layers compresses their habitat (Seibel et al., 2016). Species specifically adapted to low oxygen environments through physiological, structural, enzymatic, metabolic, molecular or behavioural adaptions will thrive (Levin, 2003). For example, those organisms with the ability to reduce metabolic rate quickly to lower their energy requirements, use anaerobic metabolism, or those with high hydrogen sulphide tolerances, which is produced in anoxic sediments and is toxic to most aerobic

organisms. Additionally, some species that are vagile, or able to move, can leave deoxygenated areas, and studies have shown that larvae of species with a sessile adult phase, can avoid hypoxic waters and delay settlement until more suitable habitat is located (Lagos et al., 2015).

1.3 Oxygen in Aquaculture Farms

There are conditions in which an organism is not able to escape or adapt from low oxygen conditions, such as a settled adult sessile organism, or fish in aquaculture farms. As fish farms are located predominantly in coastal regions, they may be vulnerable to the acceleration of deoxygenation. Atlantic salmon (*Salmo salar*) are the dominant species farmed in Canada (Doelle and Saunders, 2015). These fish are vulnerable to changes in temperature and oxygen as they are contained and cannot escape when waters become unsuitable. Fish species can differ in their response to decreased oxygen conditions. Salmonids are considered oxygen conformers, as their metabolic rate decreases with decreasing oxygen, due to their highly active lifestyle (Barnes et al., 2011). In other words, they require high oxygen concentrations to sustain their metabolic demands. Their oxygen threshold, below which fish become stressed and more susceptible to disease, depends on temperature, size of the fish, and species (Remen et al., 2013, 2016; Hvas et al., 2017; Oldham et al., 2019). It can range from 4.5 mg L^{-1} for Atlantic salmon to 8.85 mg L^{-1} for sockeye salmon (Barnes et al., 2011).

Physical transport is essential to meet oxygen requirements in sea cages within aquaculture farms. Cage size, location, configuration, mesh size of the net walls, and net biofouling can affect DO concentrations as these factors can reduce water exchange. Moreover, aquaculture farms located in more stagnant regions can exacerbate these effects. Fish biomass within the cages also influence DO within cage environments due to the oxygen demands of the fish (Cronin et al., 1999). Aquaculture farm managers that do not account for the effect of cage size, location, and fish biomass on oxygen concentrations, especially during the summer and early autumn when oxygen is lowest, are vulnerable to low production and higher fish mortality. Adequate monitoring of oxygen conditions within farms is important to keep cultured fish healthy and production high (Taranger et al., 2015).

1.4 Technological Innovations to Study DO

1.4.1 Optode-Based Sensors

The measurement of DO in the ocean has been documented since the mid-1800s. It began with ship-based measurements, including a study by Dittmar (1884) on the H.M.S. Challenger, which was the first to document the general distribution of oxygen in the global ocean (Richards, 1957). Winkler (1888) developed a precise analytical chemical method for measuring oxygen in water samples, and this has been the most common method used (with few improvements) to this day (Bittig et al., 2018). Although Winkler Titration is useful and accurate, it takes time to perform, requires a laboratory and a knowledge of chemistry. Thus, electrode- and optode-based oxygen sensors were developed for in situ measurements of oxygen. Electrode sensors, however, ultimately did not satisfy the long-term accuracy goal defined by Gruber et al. (2010) of 1 μmol kg^{-1} (Kanwisher, 1959; Bittig et al., 2018).

Optodes were developed based off the fluorescence quenching principle and remains the most common form of optical sensing today, though it has only recently become commercially available. In essence, the sensor consists of a sensing element containing a luminescent dye, an LED, and a photodetector. The light excites the electrons in the dye, which releases energy in the form of luminescence and is then measured by the photodetector (Bittig et al., 2018). The concentration of DO is inversely proportional to the luminescence lifetime through the Stern-Volmer equation:

$$\frac{I_O}{I} = 1 + K_q \cdot p_{o_2} \quad (1)$$

where I_O is the intensity/lifetime of the dye luminescence in the absence of oxygen, I is the intensity/lifetime of luminescence in the presence of oxygen, K_q is the quencher rate or Stern-Volmer coefficient, and p_{O2} is the partial pressure of oxygen (Bittig et al., 2018). Optical sensors have a fast reaction time, do not consume oxygen (whereas Winkler titration and electrodes do), are highly sensitive, and are not affected by water quality or electromagnetic interference. Additionally, they are subject to less drift and do not require as frequent calibration or maintenance compared to electrodes, and thus are a good tool for long-term deployment. Additionally, Tengberg et al. (2006) found that optodes can be stable without cleaning for 20 days, though many companies now include

wipers on the sensor to clear it of biofouling or specialized dark tubing to block light and reduce algal growth, allowing them to remain deployed for longer periods.

The development of fiber-optics has resulted in smaller and less costly optical sensors, which are easily portable and deployable, and have high sensitivity at low oxygen concentrations. It also allows for the transmission of signals at longer distances compared to the electrodes, which lends itself to remote deployment and incorporation into a network of sensors (Wolfbeis, 2015).

1.4.2 Gliders

Underwater gliders have transformed the way that researchers can study the ocean interior. Gliders are a type of autonomous underwater vehicles that are small and relatively inexpensive, compared to shipboard measurements, and are able to sample at high frequencies (Bishop et al., 2009). Various sensors can be placed on gliders, including CTDs (conductivity, temperature, depth), fluorometers, and ADCPs. The addition of optodes on gliders can generate comprehensive oxygen profiles over long distances. This allows for exploration of the spatial and temporal variability in both physical and biogeochemical parameters governing the dynamics in the ocean. The data can be received in near-real-time, as the data is offloaded at each surfacing (Bishop et al., 2009). The advances in autonomous underwater vehicles have allowed researchers to acquire a much larger, more detailed dataset, compared to using ship-based measurements, and reveal variability that may have otherwise been missed (Santana et al., 2018).

1.4.3 Numerical models

Oceanographic processes often occur at scales that are too large or small for controlled experiments. In recent years, the projected effects of climate change and how ocean dynamics will change in the future have come to the forefront of oceanography research. Thus, computer models are required to represent processes or concepts that scientists are otherwise unable to study in situ. Numerical models use a series of mathematical equations that represent biogeophysical processes to find solutions to intricate problems. Since the 1990s, increasingly complex numerical models have been used to study the climate, ocean circulation, and other biophysical mechanisms in the

ocean (Edwards, 2011). Using numerical models to simulate and characterize the state of the oceans and the response to climate change provides a hypothesis for understanding the future of the planet. As computational costs are decreasing with improved computing power, the accuracy of the models is increasing, allowing scientists to have a more comprehensive analysis of oceanic processes (Griffies, 2005).

1.4.4 Unit Conversion:

The amount of dissolved oxygen in seawater can be expressed in various units including mg L^{-1}, mL^{-1}, µmol L^{-1}, µmol kg^{-1}, and percent saturation. While mg L^{-1} is primarily used in aquaculture literature, it is important to understand how it relates to oxygen units commonly used in other aquatic sectors. The following conversions were acquired through the St. Lawrence Global Observatory (www.ogsl.ca).

For some applications, such as the output of some oxygen sensors, mL L^{-1} is common. mg L^{-1} can be converted to mL L^{-1} through:

$$mL\ L^{-1} = \frac{mg}{L} \times \left(\frac{1\ mL}{1.429\ mg}\right) = \frac{mg}{L} \times 0.70 \quad (2)$$

A mole is the SI unit for an amount of any substance. It is useful to use moles in situations where the molecule of oxygen is important, as a mole is the same number of atoms or molecules (6.02 x 10^{23}) regardless of the substance being measured. This allows for comparisons between substances. In oceanic oxygen studies, a commonly used unit is µmol L^{-1}. This can be converted to mg, as:

$$1\ \mu mol\ of\ oxygen = 0.022391\ mg\ of\ oxygen$$

Thus, 100 µmol L^{-1} oxygen is equal to 2.2 mg L^{-1} oxygen. Similarly, mmol m^{-3} (or µM) is commonly used where:

$$mmol\ m^{-3} = mL\ L^{-1} \times 44.66 \quad (3)$$

or

$$mmol\ m^{-3} = mg\ L^{-1} \times 31.262 \quad (4)$$

Many optical sensors output oxygen values as percent saturation. 100% air saturation indicates that a body of water is holding as many dissolved oxygen molecules as it can in equilibrium. Water will absorb oxygen from the air until it reaches equilibrium, which depends on temperature, salinity, pressure. Thus, the same concentration of oxygen at different temperatures, salinities, and depths will result in

different percent saturations (i.e., as temperature and salinity increases, and pressure decreases, the solubility of oxygen decreases). Percent saturation corresponds to:

$$\%sat = \frac{O_{2_{obs}}}{O_{2_{100\%sat}}} \times 100\% \quad (5)$$

Where the O_2 at 100% saturation is determined using the observed water temperature, salinity and pressure (atmospheric and hydrostatic).

1.5 Objectives and Thesis Outline

This thesis explores the drivers of oxygen variability both within aquaculture farms in coastal embayments and on the Southwest Scotian Shelf. This is not only necessary to improve the management of this region, but also for aquaculture production and farm management. The thesis is divided into 6 chapters. Chapter 1 is the general introduction presented here, followed by 4 data chapters. In chapter 2, 63 optode-based oxygen sensors were deployed in a dense array within and around an aquaculture farm in Shelburne, Nova Scotia (Canada). Local drivers of oxygen, such as tide, winds and photoperiod, were analyzed for their effect on oxygen and temperature dynamics within the cage and how this ultimately affects fish welfare and production. In chapter 3, the same sensors were used to examine the effectiveness of an oxygen supplementation system, and how the drivers identified in chapter 2 influenced the system. While chapter 2 provides a baseline of oxygen distribution through an aquaculture farm, chapter 3 explores how an oxygen supplementation system affects this baseline. Chapter 4 focuses on the distribution and variability in oxygen (and temperature, salinity) both in the cross-shore and along-shore directions of the inner southwestern Scotian Shelf using observations collected by a Slocum glider. In chapter 5, numerical experiments were conducted using an oxygen model. The numerical experiments were designed to explore the effects of four climate change-related stressors on DO dynamics in the southwestern Scotian Shelf. The four stressors that were examined were: increased temperatures, weakened Gulf Stream-Labrador Current, increased winds (storms), and weakened winds. However, these stressors are expected to occur together, therefore a last numerical experiment combined them together to explore the interactions. Lastly, chapter 6 is the conclusion and provides a general summary of the results for each chapter and their significance. This chapter delves deeper into the thesis' contributions to the scientific

literature, and the importance of understanding the oxygen dynamics in and around aquaculture farms. Overall, this work aims to contribute to the knowledge of the current and future trajectories of oxygen on the Scotian Shelf.

1.7 Statement of Co-Authorship

This thesis contains four data chapters written in manuscript structure for publication in a peer-reviewed scientific journal. Though I was the main contributor to the research design, data analyses and written manuscripts, there were co-authors for each chapter that were essential in creating the finished product. My specific contributions were to the conceptualization, methodology, formal investigation and analysis of data, writing of the original draft, and all visualizations. The co-authors contributed in comments, advice for the research design and methods, as well as interpretation of the results and edits of the drafts.

Chapter 2 (published): Burke, M., Grant, J., Filgueira, R., Stone, T., 2021. Oceanographic processes control dissolved oxygen variability at a commercial Atlantic salmon farm: Application of a real-time sensor network. Aquaculture 533, 736143.

Chapter 3 (accepted): Burke, M., Grant, J., Filgueira, R., Swanson, A., 2022. Oxygenation effects on temperature and dissolved oxygen at a commercial Atlantic salmon farm. Aquaculture Engineering.

Chapter 4 (under revision): Burke, M., Grant, J., Filgueira, R., Sheng, J., 2022. Temporal and spatial variability in hydrography and dissolved oxygen along southwest Nova Scotia using glider observations. Continental Shelf Research.

Chapter 5 (in preparation for submission): Burke, M., Pei Q., Filgueira, R., Grant, J., Sheng, J. Projections of dissolved oxygen variability under climate change scenarios on the southwestern Scotian Shelf.

CHAPTER 2 OCEANOGRAPHIC PROCESSES CONTROL DISSOLVED OXYGEN VARIABILITY AT A COMMERCIAL ATLANTIC SALMON FARM: APPLICATION OF A REAL-TIME SENSOR NETWORK[1]

2.1 Abstract

Open ocean fish farming involves containment of cultured animals under environmental conditions influenced by seasonal variation and water quality. Recently, an important area of research focus has been on water quality monitoring to improve aquaculture management. The development of novel sensors that report in real-time is critical to improve the monitoring capacity of farms, while increasing the understanding of the dynamics of environmental variables. In this study, commercially available, real-time dissolved oxygen and temperature sensors were distributed in the center of 19 cages at a commercial Atlantic salmon (*Salmo salar*) farm located within Shelburne Bay, Nova Scotia (Canada) and four reference sites. The site had an average depth of 15 m, while the cages consisted of nets 10 m deep. The dense deployment allowed for insight into the spatial and temporal variability of dissolved oxygen throughout the farm. Tide was determined to have the most significant impact on dissolved oxygen levels, with its influence varying depending on cage location within the farm. As waters flow from one end of the farm to the other, driven by tidal advection, fish behaviour and physiology, as well as flow restriction from cage infrastructure reduce oxygen levels in cages downstream. This results in oxygen concentrations out of phase on opposite ends of the farm, with higher oxygen levels at one end of the farm (i.e. 8.24 ± 0.29 mg L^{-1}) and lower oxygen levels at the other (i.e. 5.38 ± 0.34 mg L^{-1}) at any given phase of the tidal cycle. As Atlantic salmon become stressed and exhibit a reduced appetite at oxygen levels below 4-6 mg L^{-1}, depending on temperature, it is important to accurately monitor the entirety of the farm. This study examined the patterns and drivers, specifically tide, of

[1] Burke, M., Grant, J., Filgueira, R., Stone, T., 2021. Oceanographic processes control dissolved oxygen variability at a commercial Atlantic salmon farm: Application of a real-time sensor network. Aquaculture 533, 736143.

dissolved oxygen throughout a commercial salmon farm to understand the oxygen dynamics and make informed decisions that impact fish growth and welfare.

2.2 Introduction

Fish farming can often involve challenging conditions for cultured animals including poor water quality, weather, and disease. Through the recent development of "Precise Fish Farming", the benefits of increasing technological tools in aquaculture farms to monitor the cultured fish are recognized as ways to increase the knowledge base and optimize production (Fore et al. 2018). Recent implementation of sensor networks at ocean-based farms enhances management capabilities regarding environmental monitoring, fish welfare, feeding, stocking, and harvesting (O'Donncha and Grant 2019). Among water quality parameters to be monitored, dissolved oxygen and temperature can have considerable impacts on the welfare of farmed fish as it relates to the metabolic demands of respiration and thermoregulation (Nobel et al. 2018). All organisms have an optimal range of oxygen and temperature, and if water quality is not suitable, vagile organisms can leave the area. However, fish in an aquaculture sea cage cannot avoid poor water quality, making monitoring even more important.

Dissolved oxygen (DO) is an essential parameter to examine since oxygen concentrations can fluctuate rapidly. DO is one of the main factors affecting fish metabolism, and ultimately, welfare and growth (Claireaux and Lagardère 1999). The consequences of oxygen concentrations outside organism optimal ranges are twofold; impacting fish growth and mortality directly through hypoxia (Wilding 1939), as well as indirectly through stress and vulnerability to diseases (Mayer 1970; Snieszko 1974). Remen et al. (2014) reported that salmon kept in normoxic conditions with intermittent rounds of hypoxia (1 h at 50% DO) every 6 h reduced growth rates by 13%. Additionally, Burt et al. (2014) determined the impact of intermittent hypoxia (for 30, 60, 90, 120 or 150 minutes) on growth rates and found that salmon growth rates were reduced by 24% in the group that were fed during these periods. To optimize growth rates and fish welfare, maximum feed intake has been studied in Atlantic salmon, indicating that intake declines linearly below 4-6 mg L^{-1} , depending on temperature and size of the fish (Remen et al. 2013, 2016; Hvas et al. 2017; Oldham et al. 2019). At higher temperatures,

the threshold for maximum intake occurs at a lower oxygen concentration, compared to at lower temperatures. However, it is important to note that farmers often use a fixed threshold of 6 mg L^{-1} when deciding to feed, and this can be harmful to fish exposed to lower levels of oxygen at lower temperatures, where feed intake is still maximal (Burt et al. 2012).

Temperature remains one of the most important factors governing oxygen availability, as it directly affects the solubility of oxygen, as well as fish metabolism (Bopp et al. 2002; Neubauer and Andersen 2019). As temperature increases, the metabolism of ectothermic organisms also increases, which raises the oxygen requirement for fish to survive and grow (Hvas et al. 2017). This is becoming more relevant as climate change increases ocean temperatures and deoxygenation threatens coastlines. In addition to temperature, there are biological factors which affect dissolved oxygen in the ocean including photosynthesis, organismal respiration, and physical factors such as wind, tide, or currents (Burt et al. 2012). Wildish et al. (1993) determined that within an Atlantic salmon (*Salmo salar*) cage, photosynthesis alone is likely insufficient to meet the oxygen requirements of the fish. The study estimated oxygen requirements for Atlantic salmon, the reaeration due to air-sea exchange, phytoplankton production, and physical transport, and it was determined that the physical transport of oxygen from outside the farm due to tidal currents and wind driven circulation were likely the main controlling processes for oxygen renewal. Additionally, at the farm-scale, fish are often exposed to a decline in oxygen due to reduced water exchange from net structure, fouling, sea lice barriers, and high stocking densities (as discussed by Remen et al. 2016; Klebert et al. 2020).

A consequence of reduced oxygen in salmon farms is diminished appetite, and if feeding is not reduced in response, food waste will accumulate below the cages (Wu 2002; Remen et al. 2016). According to Axler et al. (1993), 36% of the total oxygen demand in a farm is due to microbial decomposition of waste, which ultimately leads to anoxic conditions in bottom waters, and negative impacts on biota (e.g. Silvert and Sowles 1996; Bianchi et al. 2000). Additionally, if the fish do continue to feed, there is an increase in metabolic demands and thus even greater oxygen stress. It has become common practice to measure oxygen levels at the farm, and to withdraw feeding when

oxygen levels become suboptimal. However, monitoring has often been minimal, limited to once or twice daily measurements, as it is generally conducted manually by the farmers and is time-consuming. The recent development of real-time sensors, allows for cost-effective continuous monitoring of these parameters, improving farm management and reducing economic and ecological waste (Xu et al. 2019).

Real-time sensors have revolutionized both the agriculture and aquaculture industries, allowing for continuous and efficient monitoring (Raju and Varma 2017). Advancement in sensor technology applied to oxygen has made a substantial contribution to capable sensor networks. Oxygen optodes measure DO by emitting light and measuring the luminescence emanating from the oxygen molecules in the water sample (Bittig et al. 2018). Optodes require less maintenance than their membrane electrode counterpart, often used in CTD/oxygen casts. Furthermore, through the development of fibre-optics, oxygen optodes are small in size and cost-effective. Sensors requiring wires are problematic at fish farms where there is already crowded infrastructure underwater. Through wireless networks and an Internet of Things approach, an array of these sensors can be established around farms with remote access to real-time water quality data. An understanding of factors driving oxygen variation within and beyond fish farms, coupled with real-time monitoring, allows adjustment of feeding, stocking, harvesting, and site and cage locations. This level of control leads to improved farm management, fish welfare, and sustainable husbandry.

Real-time capabilities allow deployment of sensors at multiple locations within a farm and increase visibility of oxygen dynamics. In recent years, the relatively dense deployment of sensors has also allowed researchers to determine the existence of temporal and spatial oxygen variations within sea cages (e.g. Stehfest et al. 2017; Oldham et al. 2018; Solstorm et al. 2018). Generally, these studies agree that physical transport through currents and wind, as well as fish behaviour, have the greatest impact on dissolved oxygen within sea cages. However, there has generally been low temporal and spatial resolution of fish farm oxygen levels, and limited knowledge of the variation in oxygen between sea cages. To improve the knowledge of DO dynamics throughout a farm, this study explored the patterns and physical drivers of oxygen in an Atlantic salmon farm in southwest Nova Scotia (Canada). The use of commercially available real-

time sensors allowed for extensive deployment of sensors, with high frequency sampling, providing higher spatial and temporal resolution than most previous research in this field.

2.3 Materials and Methods

2.3.1 Study Site

Shelburne Harbour (43.76°N, 65.32°W) is a large bay (7.3 km at the mouth) on the southwest shore of Nova Scotia (Figure 2.1a). The bay has a depth of ~8 m, deepening toward the open ocean to depths of 11-20 m. Dissolved oxygen and temperature measurements were collected between September and December 2018 at a Cooke Aquaculture salmon farm located in the center of the opening to Shelburne Harbour, adjacent to McNutts Island. The farm consisted of 19 circular cages, in two parallel rows (Figure 2.1b). Each cage was 32 m in diameter and had a cylindrical net (mesh size: 57 mm) to a depth of 8 m (~6 365 m^3 volume). The adult post-smolt Atlantic salmon had average weight of 4.3 kg, and the average stocking density was 16.4 kg m^{-3}. A remotely operated vehicle cleaned the nets of biofouling throughout the study, as per the farm's maintenance program.

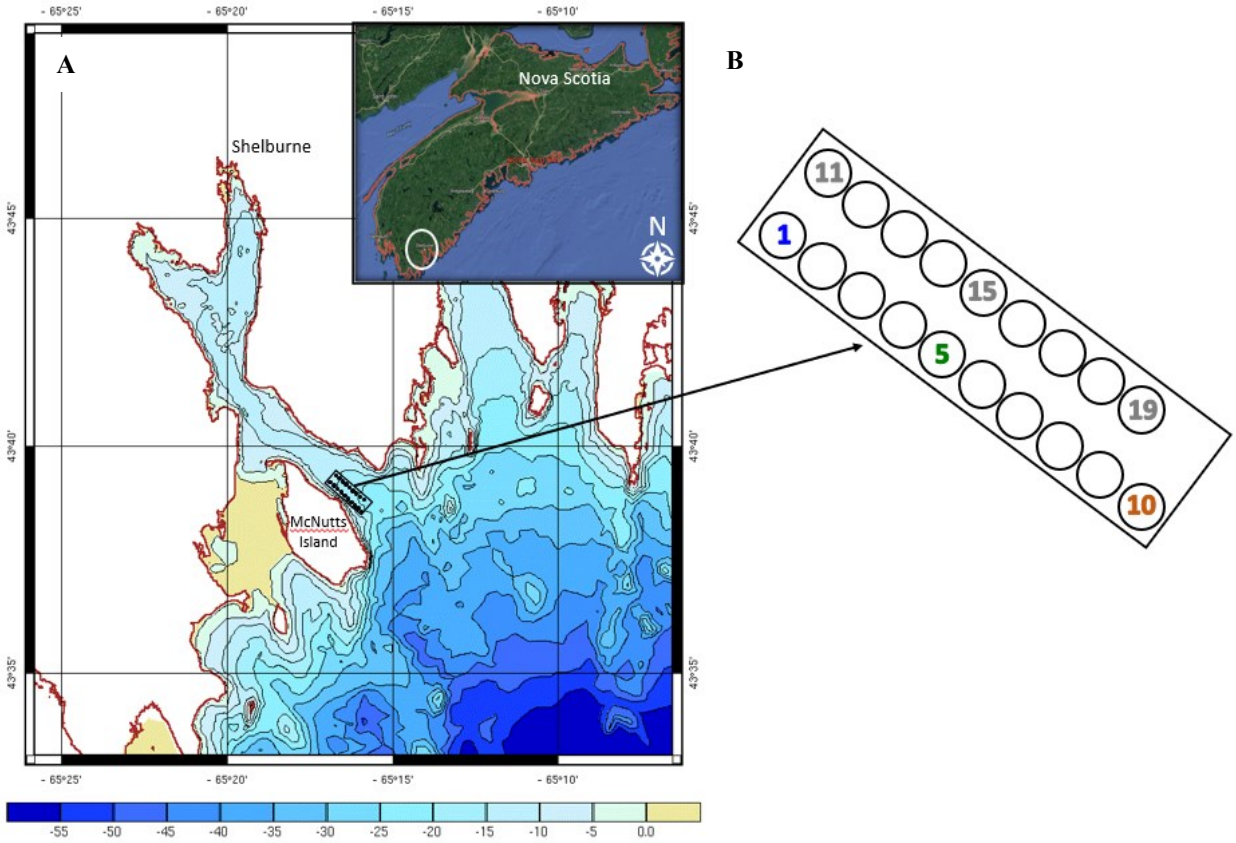

Figure 2.1 Site schematic showing (A) the location of the farm within Shelburne Bay including bathymetry (m) and an inset map of Nova Scotia, and (B) the layout of the farm with cages numbered.

Nova Scotia has a temperate continental climate, where temperatures fluctuate more on a daily and seasonal basis compared to a maritime climate. This results in a more moderate winter compared to inland Canada, with a mean air temperature of 0.4°C in Shelburne. The Gulf Stream, which is located offshore in the winter, moves further inshore between July and September resulting in a prolonged summer well into October, with a mean air temperature of 13.7°C in Shelburne. Water temperatures in Shelburne are warmest in August with an average of 16°C, and coolest in March, with an average of 4°C. Water circulates through the bay with a semi-diurnal tide that ranges from 0.2 m low to 2.6 m high throughout the year.

2.3.2 Data Collection

Temperature and DO were recorded every 5 minutes using wireless, real-time, optode based sensors (AquaMeasure, InnovaSea Systems, Inc., Bedford, Nova Scotia). The data were transmitted to cloud storage in real-time, within a hub located on site, and logged

internally. A sensor was deployed at 2 m depth in the center of each of the 19 cages, while single reference sensors were placed at each of the four corners of the site, 14 m from the adjacent cages, also at 2 m depth (cleaning and quality control of the sensors are discussed more in Appendix A.2). The center of the cage was chosen to reduce bias caused by randomly selecting a side of the cage, while this depth was selected to capture the dissolved oxygen above the thermocline. The thermocline was observed during the first two weeks of August 2018, with 0 – 2 m at 13°C, followed by a steep decrease to 9°C between 3 and 10 m.

Wind data was acquired by an Environment Canada weather station located at nearby Sandy Point, NS, however a storm in mid-October disrupted the station and resulted in a 1.5-week gap in the data. Tidal height was acquired through a station located in Shelburne Harbour, from the Department of Fisheries and Oceans. Cubic interpolation of tidal maxima and minima was used to acquire hourly tidal heights.

2.3.3 Statistical Analysis

Within the cages, an examination of the time series in full indicated a decline in temperature that coincided with an increase in oxygen in mid-October (Figure 2.2). A two-sample Kolmogorov-Smirnov (K-S) test was used to determine significance between these time periods ($p<0.001$, $D=0.92$, $n=527$). All statistics were conducted via Python programming language (Python Software Foundation, https://www.python.org/). Because there was a statistically significant decrease in temperature in mid-October, the time series was divided into two 3.5-week periods to satisfy stationarity. The 'summer' months were those that fell before the sharp decrease in temperature (September 19th to October 15th), while the 'autumn' months were those that fell after the decrease (October 17th to November 14th; Figure 2.2). Subsequent to the division in the data, two sample K-S tests were used to examine the differences in oxygen between the mean of the cages and the outside reference levels. Coefficient of variation was also used as a parameter to determine the amount of fluctuation in dissolved oxygen.

A low-pass filter with a cutoff at 6.3 h was used on the oxygen time series to remove high frequency oscillations ostensibly due to fish behaviour and physiology, and better examine low frequency variability (Santana et al. 2018). Subsequently, to determine factors affecting these low frequency oscillations, the time domain data was transformed

into the frequency domain to perform spectral analysis. In essence, spectral analysis uses periodograms to visualize the frequencies of various sine/cosine waves that have the highest correlation with the time series in question (Priestly 1981).

Once the tidal frequency had emerged as the physical parameter with the highest power in the periodograms, a cross-correlation was conducted between oxygen and tide in 6 cages, two on each end of the farm (cages 1, 11 and 10, 19) and two in the middle of the farm (cages 5, 15; see Figure 2.1 for sea cage positioning). Cross-correlation analyses were also conducted between dissolved oxygen and wind direction, speed, and stress. Wind stress is defined as the shear stress that wind exerts on the surface of the ocean which results in the motion of surface waters and plays a large role in ocean circulation; it can be calculated from wind speed (Talley et al. 2011). Wind speed was the only factor determined to be significant, thus wind speed was rotated 360° and a series of correlations was used to determine threshold and direction of speed significantly affecting dissolved oxygen.

2.4 Results

2.4.1 Temporal Variability

The complete DO and temperature time series between September and December 2018 were examined in three cages: cage 1, 5 and 10, located in the inner, middle, and outer bay, respectively (Figure 2.1). Between September and early October (summer months), the three cages showed an average oxygen concentration of 7.0 ± 0.07 mg L^{-1} (S.D.) with an average temperature of 16.9 °C. In mid-October, there was a transition to autumn conditions and a significant decrease in temperature to 8.7 ± 0.1°C ($p<0.001$, $D=0.95$, $n=527$), which was associated with a significant increase in DO to a mean of 8.7 ± 0.3 mg L^{-1} ($p<0.001$, $D=0.92$, $n=527$; Figure 2.2). As the Nova Scotia climate is heavily influenced by the prevailing westerly winds, the shift in winds from southwest and west in the summer to northwest and west in the winter, results in distinct summer and autumn periods. However, the temperature change was not monotonic. On October 15, the initial temperature decrease was to 7.5°C, and subsequently rose on November 1 to 10°C, before falling to 6.5°C on November 12. Similar patterns were observed between the two

rows of cages, thus the figures that follow will only depict an example row (cages 1,5,10).

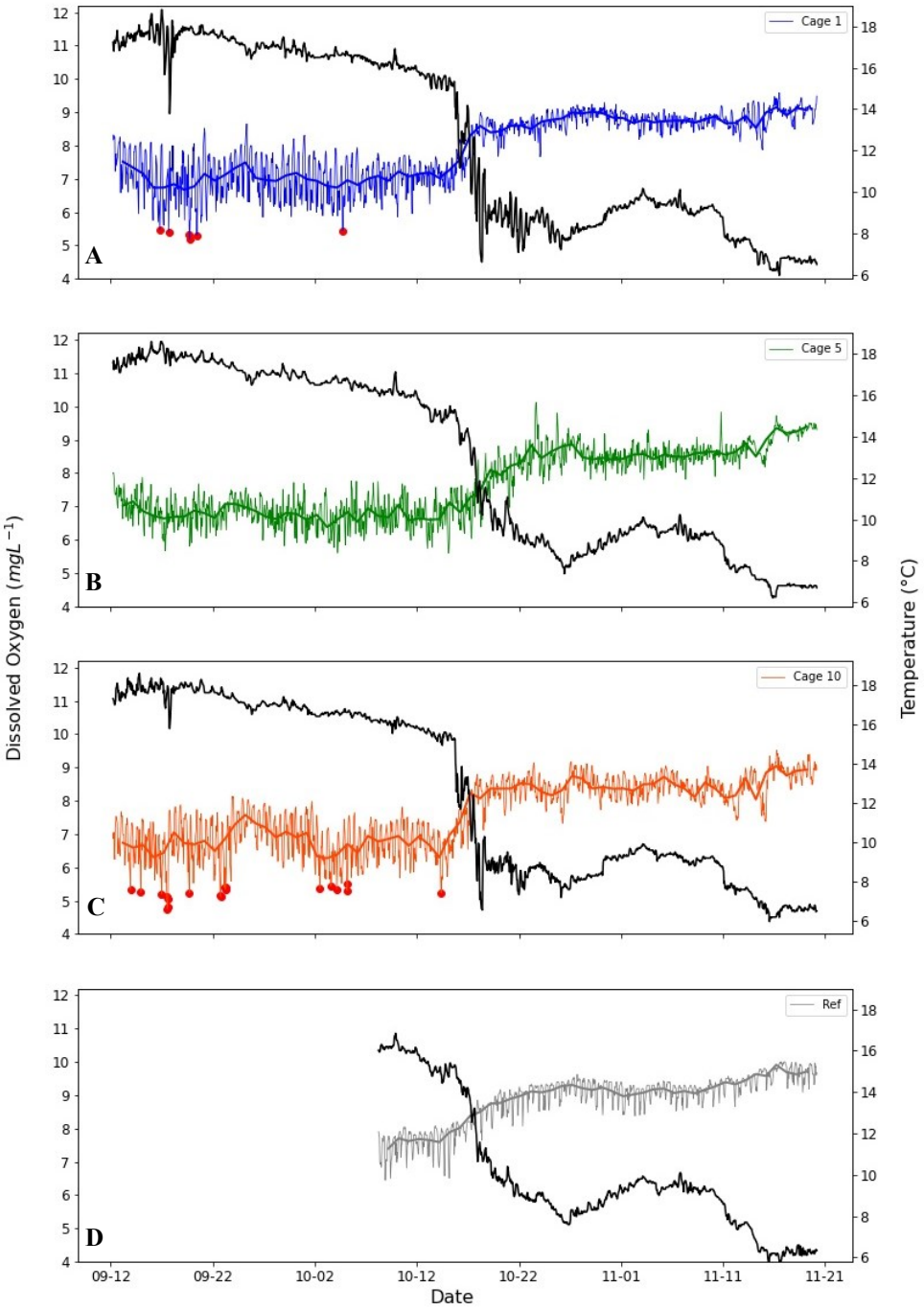

Figure 2.2 Hourly (lighter lines) and daily (darker lines) average dissolved oxygen (DO) concentrations (mg L^{-1}), along with corresponding hourly temperatures (black), within (A) cage 1 (inner bay), (B) cage 5 (middle of the farm), (C) cage 10 (outer bay), and (D) a reference site. Red dots indicate oxygen below the maximum potential feed intake threshold (Remen et al. 2016).

2.4.2 Spatial Variability

Across the full time series, the temperature between cages and reference sites, located at the corners of the farm, were not significantly different from each other ($p=0.98$). Although, a comparison between 3 of the cages and the average of 3 of the reference sensors indicated that DO within the cages was significantly lower than the reference levels, during both seasons ($p<0.001$, $D=0.83$, $n=429$; Figure 2.2). The average coefficient of variation for the cages across the full time series was 2.6 %, higher than the reference sites, which was 2.0 %.

In the summer months, there were higher fluctuations in DO within the cages on the outskirts of the farm, with coefficients of variation of 8.76 % and 9.35 % for cages 1 and 10, respectively, while inner cage 5 had a coefficient of variation of 5.81 %. In autumn, these oscillations decreased, with coefficients of variation of 2.68 %, 3.32 %, and 4.11% for cages 1, 5 and 10, respectively (Figure 2.2). A similar pattern was observed in the cages in the row opposite, with coefficients of variation of 8.18%, 5.92%, 9.32% for cages 11, 15, 19, respectively in the summer, and 2.56%, 3.84%, 5.49% respectively in the autumn.

Low oxygen conditions were determined following Remen et al. (2016), which indicated feed intake due to stress occurs below 4.8 mg L^{-1} at 11°C, and below 5.5 mg L^{-1} at 15°C. This occurred in each of the three cages during the summer, and if the oxygen fell below this threshold for more than 1 h, it was termed a "low oxygen event". During the summer, there were no low oxygen events in cage 5, cage 1 had 6 events, and cage 10 had 19 events (Figure 2.2). A similar pattern was observed in the cages in the row opposite where cage 19 had the highest number of low oxygen events (25 events; not shown), while cages 11 and 15 had no low oxygen events. No events occurred in any of the cages during the autumn period.

2.4.3 Drivers of Dissolved Oxygen

Wind and tide were examined as parameters that would likely impact the variability in DO concentrations within the farm. Wind had a positive impact on DO at speeds higher than ~33 km h^{-1} (maximum speed = 37 km h^{-1}) , which only occurred over five 30-minute periods throughout the summer and autumn; winds throughout the period were relatively low, with minimum, mean and median speeds of 0 km h^{-1}, 9 km h^{-1} and 8

km h^{-1}, respectively (not shown). To explore the effects of tide, a periodogram was used to determine the most important frequencies governing the DO time series for cages 1, 5 and 10, for both summer and autumn. In the summer, for cages 1 and 10, there was a dominant period of 12.42 h, and a lower peak at 6.21 h; cage 5 (15), however, had a dominant but minor peak related to the 6.21 h period (Figure 2.3 A, C, E). In autumn, there were small peaks also related to the 12.42 h period in each of the cages, as well as small peaks for the period of 6.21 h in cages 1 and 5, though the latter frequency was not apparent in cage 10 (Figure 2.3 B, D, F). These dominant frequencies correspond to the principal tidal constituents: the principal lunar semidiurnal constituent (M_2) with a period of 12.42 h, and the shallow water overtides of the principal lunar constituent (M_4) of 6.21 h.

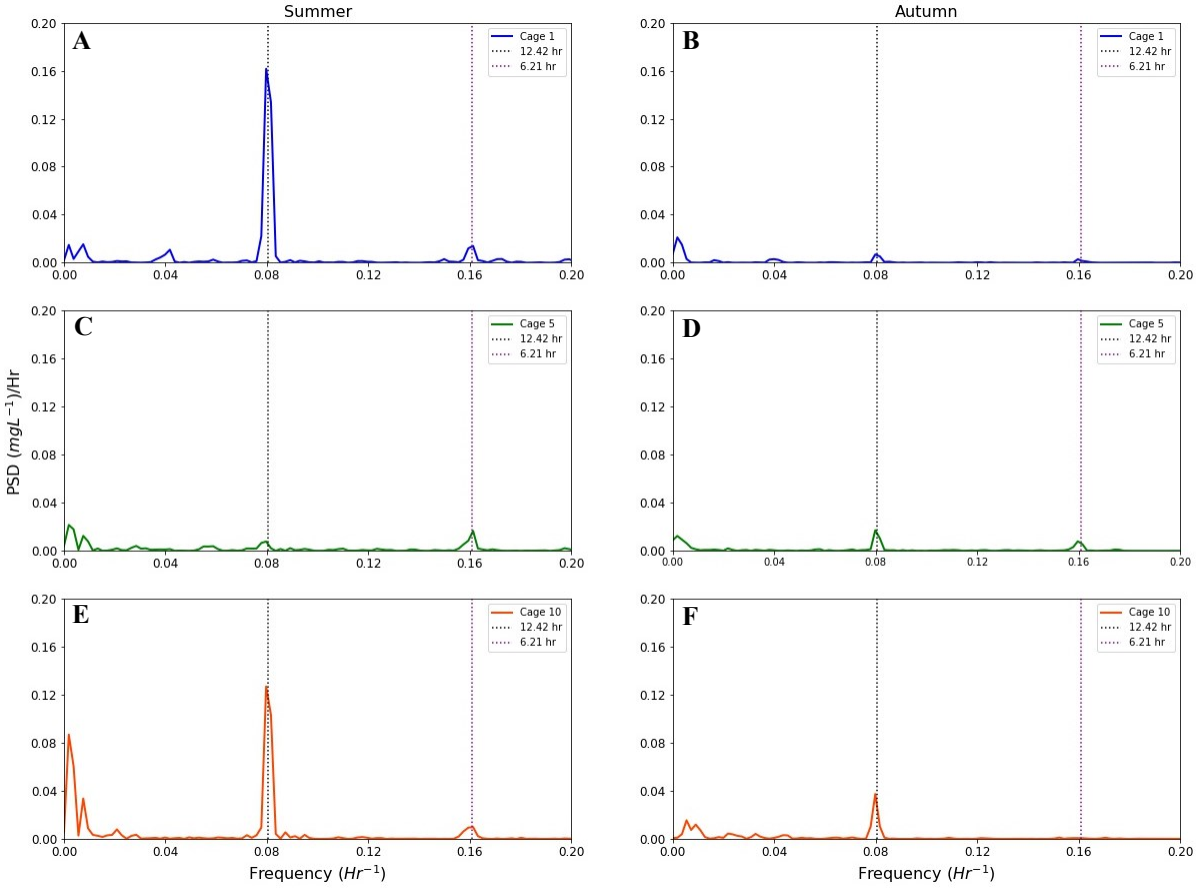

Figure 2.3 Power spectral density (PSD) of dissolved oxygen (DO, mg L^{-1}) in cages 1 (blue; A,B), 5 (green; C,D) and 10 (red; E,F) for both the summer (A,C,E) and autumn periods (B,D,F). Black dashed line indicating the 12.42 h period, and purple dashed indicating the 6.21 h period.

The low-pass filter of 6.3 h was employed to remove the high frequency oscillations and focus on the longer-term trends relating to the principal lunar constituent. This revealed a correlation between DO and tide for cages 1 and 10 (Figure 2.4 A, E). The DO in cage 1 was oscillating at a phase shift of 180 degrees, opposite to tidal height, while cage 10 had a phase shift of 0 degrees, indicating that it was oscillating in tandem with tidal height. In other words, cage 1 (inner bay) had a negative correlation with tide ($R= -0.73$, $p<0.05$; Figure 2.4A), while cage 10 (outer bay) had a positive correlation ($R=0.63$, $p<0.05$; Figure 2.4E). Cage 5 (middle of the farm), however, did not appear to have as clearly defined a relationship, as it had a differing periodicity to cages 1 and 10, and a maximum correlation coefficient of 0.24 ($p<0.05$; Figure 2.4C).

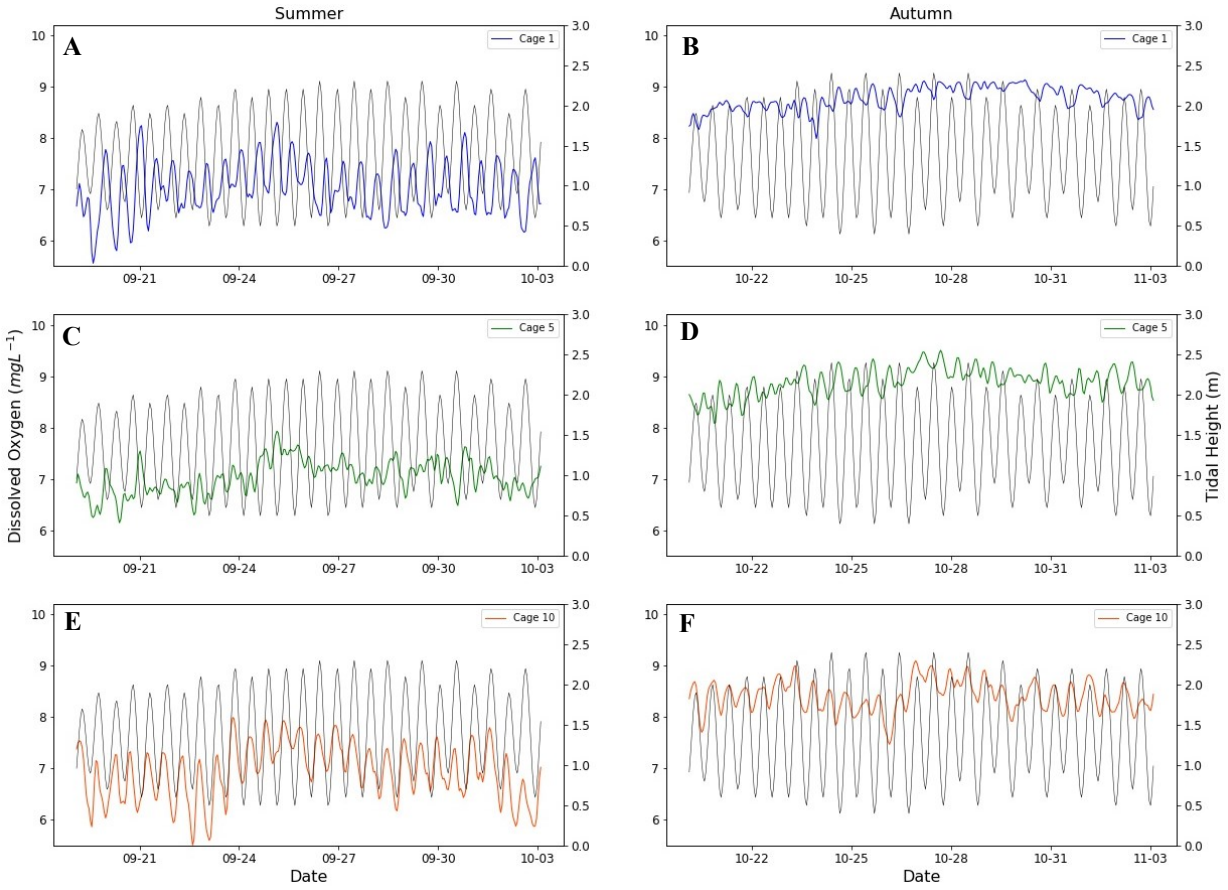

Figure 2.4 Dissolved oxygen and tidal height over two weeks within cage 1 (blue; A,B), cage 5 (green; C,D) and cage 10 (orange; E,F) for summer (A,C,E) and autumn (B,D,F)

During the autumn months, the amplitude and cyclical nature of the DO time series were less pronounced compared to the summer period. The DO oscillations in cage

1 again had a predominant phase shift of 180 degrees relative to tidal height, however the correlation coefficient was lower at -0.42 ($p<0.05$ Figure 2.4B). Similarly, Cage 10 had the same phase shift as in the summer months, 0 degrees, and a lower correlation coefficient of 0.45 ($p<0.05$, Figure 2.4F). Cage 5 had an increase in correlation with tide during the autumn, in the negative direction ($R= -0.55$, $p<0.05$), indicating a phase shift of 180 degrees with respect to tide (Figure 2.4D). The reference sites showed no significant differences between correlation in the summer compared to the autumn period, with an overall low correlation coefficient ($R = 0.2$, $p = 0.7$). Each of the above results and patterns were also observed in the cages in the row opposite (11, 15, 19), however for simplicity, they have not been shown.

While examining the cross-correlation between tide and DO for the entirety of the site, a pattern emerged where correlation decreased towards the middle of the farm (Figure 2.5). During summer, the highest correlation between tide and DO occured in the four corner cages of the site. Three of the cages at the corners of the farm, cages 1,10 and 11, had strong correlations above 0.6, while the cage at the fourth corner, cage 19, had moderately high correlation, 0.48. There were moderate correlations (between 0.3 and 0.6) in those cages towards the outskirts of the farm (average of 0.42 ± 0.08) and finally, the weakest correlation (between 0.1 and 0.3) were in the cages in the middle of the farm (average of 0.16). In autumn, the overall correlation between DO and tide decreased but the pattern remained the same (Figure 2.5). There were no cages with strong correlations, the cages predominantly on the outskirts had moderate correlations (average of 0.40 ± 0.07), and cages in the middle of the farm had weak correlations (average of 0.19 ± 0.08). Additionally, the correlation between DO and tide for the reference sites were weak during both periods (~0.2). Essentially, as the tides shift, the oxygen concentrations in the perimeter cages on the end that is refreshed has a moderate-high correlation with tide, and this relationship decomposes as the tidal current is transported through the farm.

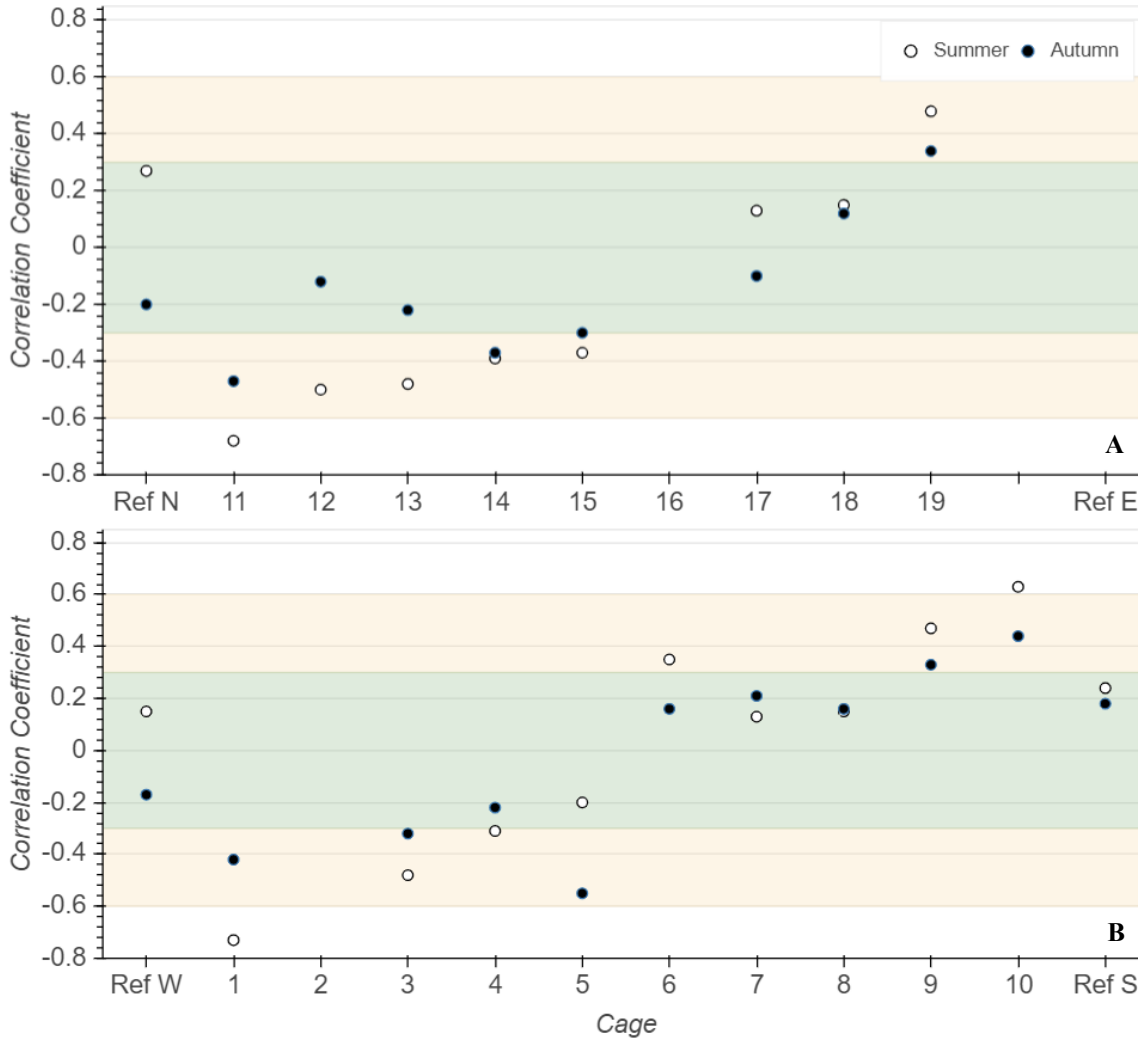

Figure 2.5 The correlation between tide and dissolved oxygen within each cage and 3 reference sites on either side of the farm (A) far from island, (B) close to island, for the summer period (white) and autumn period (black). Strength of correlation indicated as strong (shaded white), moderate (shaded yellow) and weak (shaded green).

2.5 Discussion

Using a dense array of real-time DO and temperature sensors, this study examined the spatial and temporal variation in DO across a salmon aquaculture farm. Oxygen is a critical variable for health, welfare, and growth of farmed salmon, and accordingly there have been studies measuring DO in commercial cages. However, while studies have examined DO using CTD casts within a single cage or in multiple cages for short-term experiments (e.g. Johansson et al. 2006, Oldham et al. 2017, Oldham et al. 2018,

Solstorm et al. 2018), to the best of our knowledge, the study presented here is the first to include high spatial and temporal resolution within a commercial farm to establish this larger scale variation in ambient DO. Overall, our results first indicated that oxygen significantly increased in mid-October concurrent with a decrease in water temperature. Secondly, DO within cages was significantly lower than those at the reference sites, located outside of the farm. Lastly, tide had a dominant effect on the variability of DO across the farm. The use of real-time optical sensors, which require less maintenance than their electrode counterparts, allows farmers to utilize this technology for improved management, rather than shorter deployments for experimental use.

2.5.1 Temporal Variability

In this study, temperature dropped sharply in mid-October, with a concomitant rise in oxygen throughout the farm. The decreased temperature likely triggered a rise in oxygen availability as cooler water has both a higher potential for DO solubility, resulting in an increase in the exchange of oxygen across the air-sea interface, and a decrease in metabolism and subsequent oxygen consumption by fish (Hvas et al. 2017; Brett, 1972; Davis, 1975). After examining the DO in percent saturation, there was no significant difference between the summer and the autumn, supporting the idea that temperature had a critical impact. The abrupt decrease in temperature in mid-October was likely due to high winds that were documented in the area at this time. These high winds would overturn the water column, disrupting the thermocline and raising cooler water from depth (Ikeda 1987). Petrie et al. (1987) intimated that upwelling favourable winds to the northeast are a source of cold-water advection during the fall in Nova Scotia. This autumn convection deepens the mixed layer, breaking up the summer stratification, and greatly affects the biology of the North Atlantic. It upwells nutrients from depths and results in an autumn phytoplankton bloom, ultimately fueling upper trophic levels (Wihsgott et al. 2019). Additionally, Johansson et al. (2006) and Oppedal et al. (2011) reported that salmon prefer warmer waters, occurring above the pycnocline, therefore through the disruption of the thermocline in the autumn period, the salmon likely took advantage of the increase in suitable habitat, and moved down through the water column, allowing for oxygen to replenish near the surface.

Few studies have had the opportunity to examine the seasonal pattern between oxygen and temperature, due to the length required of the studies. Burt et al. (2012) and Cheshuk et al. (2003) observed similar patterns to the present study, along with the same concentrations of oxygen (~6-10 mg L^{-1}). Johansson et al. (2006), however, described the opposite trend, with a slight decrease in oxygen as autumn progressed (8 mg L^{-1} to 7.2 mg L^{-1}). The latter concluded that decreased light, resulting in decreased primary production and increased respiration, as well as increased fish density had a negative effect on oxygen concentrations in autumn and winter. Variability due to light intensity was examined in this study and had no significant effect on oxygen concentrations (R=0.07, Appendix A). Stocking density was also disregarded, as cage 13 had double the number of fish as cages 12 and 14, yet did not contain significantly less oxygen (not shown). Therefore, among the biological physical drivers, temperature emerges as the main driver to explain the temporal variation in dissolved oxygen observed in this study.

2.5.2 Spatial Variability

Oxygen concentrations within salmon cages were significantly lower than those outside the farm. A study conducted by Solstorm et al. (2018) examined the variability in oxygen within a cage and demonstrated that the center of the cage had the absolute lowest oxygen and was likely caused by the swimming behaviour and oxygen consumption of fish coupled with slow current speeds due to the presence of cage infrastructure. This may explain the differences in oxygen found in between the cages and the reference sites, as each of the sensors used were placed in the center of their respective cages, and the reference sensors were not impeded by these factors. Additionally, the DO concentrations were more variable within cages compared to reference levels, also observed by Oldham et al. (2018).

Within the farm, the three cages that were focused on, had on average similar oxygen levels. Winthereig-Rasmussen et al. (2016) reported that the current velocity was the weakest downstream from and within the middle cage, therefore, it was hypothesized that the center of the farm would have the lowest DO, due to the restrictive nature of the cages on the flow of oxygenated waters to the middle of the farm. As the tide floods or ebbs, and the cages downstream are insufficiently aerated, the middle of the farm would presumably be chronically undersaturated in oxygen. However, cage 5 (middle) had an

average of only 0.25 mg L^{-1} less oxygen in the summer than cages 1 (inner) and 10 (outer). Furthermore, cage 5 had 0.42 mg L^{-1} more than the two perimeter cages during the autumn period. This indicates that the average oxygen concentrations are similar between cages; however, they do not reflect differences in oxygen that were observed at smaller temporal scales, which could affect the conditions that fish are experiencing across the farm.

Following Remen et al. (2016), low oxygen events were periods of time over 1 h in length where oxygen fell below the maximum potential feed intake threshold of 4.8 mg L^{-1} at 11°C and 5.5 mg L^{-1} at 15°C. Low oxygen events occurred in each of the three cages during the summer, most frequently in cage 10, followed by cage 1, and cage 5 having the fewest. Reference sensors indicated that the pool of oxygen in the inner bay is lower than that towards the open ocean. Water flowing through to the outer cages as the tide ebbs will thus contain lower oxygen levels compared to those waters coming from the outer bay. With 19 low oxygen events in cage 10, along with 25 events occurring in the row opposite (cage 19), the fish in cages towards the outer bay during low tide will suffer increased stress relative to those in the inner bay. However, it is important to note that the majority of the measurements were within range of suitable oxygen levels for optimal Atlantic salmon production. Monsour et al. (2008) and Burt et al. (2012) found that there were intermittent hypoxic periods in Newfoundland, at times of the year coinciding with the low oxygen events observed in this study, indicating that this may be common in a cage environment during this time of year.

2.5.3 Drivers of Dissolved Oxygen

Although the average oxygen concentrations were similar between cages, there were differences on an hourly basis. Temperature, winds and tides were explored as the main drivers to explain the high frequency, inter-cage variability in oxygen. Temperature was disregarded as a driver due to the little variation between cages, which did not match the changes in dissolved oxygen. Examination of the effects of wind speed indicated that only speeds above ~33 km/h influenced oxygen concentrations, which is related to storm events; storms are known to cause an increase in oxygen transport across the air-sea interface and briefly increase oxygen concentrations (Boyd and Tucker 2019). Tides were determined to govern the dissolved oxygen time series on the outer edges of the farm,

particularly during the summer period, with the dominant frequency relating to the M_2 tidal constituent. Other studies have also concluded that the M_2 constituent is the dominant driver of DO variability in locations where the prevalent tidal type is semidiurnal (e.g. Pastore et al. 2019, Santana et al. 2018, Roegner et al. 2011). Cages in the middle of the farm (5 and 15) did not exhibit such a relationship with the M_2 constituent. It is likely that biological or other physical factors, rather than tide, dominate the middle cages. Other processes that can influence water flow between cages, and consequently oxygen dynamics are the presence of fish consumption, their swimming behaviour, cage infrastructure (nets causing drag), and biofouling (Klebert et al. 2013; Bi et al. 2013). Therefore, cages in the middle of the farm receive oxygen influenced by these processes, and thus are more correlated with their neighbouring cage, rather than tide. Results from Burt et al. (2012) support this concept, as no relationship between tide and DO was observed during a relatively long-term study on cages located in the center of the farms.

In autumn, the relationship with the M_2 frequency decreased for the perimeter cages, with only a slight peak at 12.42 h for each cage. This change was likely due to cooler waters lowering the oxygen demands from the fish. Although fish metabolism and behaviour was not specifically studied, the metabolism and oxygen demand likely decreased 28.8 % between summer (102 mg O_2 kg^{-1} hr^{-1}) and autumn (76.9 mg O_2 kg^{-1} hr^{-1}), due to the observed drop in temperature (Brett 1964; Hvas et al. 2017). With the reduced metabolic rate during autumn, oxygen within the cages remained high, likely diminishing the role of the tide in reaerating the farm. This was further supported as there was no significant difference in correlation between tide and oxygen at the reference sites, where fish metabolism had little to no effect.

A low-pass filter was used to remove the high frequency oscillations in oxygen which were potentially due to fish behaviour and physiology, as the reference sensors contained significantly less variation in DO. These filtered time series provided better insight into how tide and oxygen were related after eliminating the noise caused by the animals. In summer, high tidal height was correlated with high oxygen levels in cage 10 (outer bay), while it was correlated with low oxygen levels on the opposite end of the farm in cage 1 (inner bay). The proposed explanation is that water exchange, through

tidal advection, is driving DO dynamics At flood tide, cages on the outer bay reaerate and as the water is transported through the farm, fish respiration decreases the oxygen concentrations until ultimately, the cages on the inner bay receive a decreased quantity of oxygen. The opposite is then true for ebb tide, creating a gradient of oxygen through the farm depending on the direction of the tidal current. This is further exacerbated by the reduced current speeds through the farm, largely due to the occlusion of cage netting, allowing for increased water residence time, and increased respiration time for salmon within the cages (Hayton and Barron 1990). This pattern of oxygen variation through the farm, directly relating to the tidal cycle is a novel discovery. Previously, most studies on oxygen in sea cages only obtain measurements over short time scales, which precludes researchers from determining relationships with variables that occur over longer timescales, such as the tidal cycle (e.g. Johansson et al. 2007, Monsour et al. 2008, Oldham et al. 2018). While Wildish et al. (1993) also examined the role that tide played on oxygen levels at a salmon farm in the nearby Bay of Fundy, the spatial and temporal resolution was low, and full support for their conclusions could not be documented. In the present study, despite a differing research design, tide as a driver of oxygen dynamics was clearly demonstrated.

However, it may also be location and cage specific, as the cages used in this study are smaller than those used in Newfoundland, Norway or Australia, with a circumference of 100m whereas the other sites have circumferences of ~160-240 m (e.g. Cheshuk et al. 2003, Stehfast et al. 2017, Oldham et al. 2018, Solstorm et al. 2018). Oldham et al. (2018) determined that larger cages have lower DO, through reduced surface area to volume ratio, ultimately leading to decreased water exchange. This finding may reveal why the effect of tidal height is not apparent in those studies.

The natural variation in DO, determined through the reference points is relatively low, therefore the farm itself is the driving force of the observed variability. Vigan (2008) determined that water velocity alone does not influence oxygen levels, it is the combine effect of water velocity and fish presence. This study supports this as oxygen at the reference sites had a low correlation with tide. Due to this inherent variability in DO within the cages due to tidal currents, fish respiration, and cage infrastructure, it is evident that a one sample a day regime, often employed at farms, is insufficient and can

lead to over- or underestimation in DO concentrations (Page et al. 2005). This exemplifies the requirement for increased monitoring to ensure the welfare of the fish across all cages, an aspect of husbandry that will be improved with wider implementation of sensor networks (O Donncha and Grant 2019).

2.6 Conclusion

Extensive monitoring of a stocked Atlantic salmon aquaculture farm revealed the role that seasonality, the cages themselves, and most importantly tide play in DO variability. Perimeter cages are reaerated with higher oxygen levels as the tide transports water from outside the bay (flood tide) or inside the bay (ebb tide). This results in differing environments for the fish living on either end of the farm at opposite phases of the tidal cycle. As farmers restrict feeding when DO levels fall below 6 mg L^{-1}, ample spatial coverage of monitoring is required, in addition to employing proper feed intake thresholds, to ensure that feeding regimes are accurate and that fish welfare in each cage is considered. The utility of the oxygen sensors used in this study is ultimately in potential feedback to automated systems for finer grained control to optimize feeding, while minimizing impacts on welfare.

CHAPTER 3 OXYGENATION EFFECTS ON TEMPERATURE AND DISSOLVED OXYGEN AT A COMMERCIAL ATLANTIC SALMON FARM[2]

3.1 Abstract

As climate change continues to warm oceans and exacerbate deoxygenation, coastal ecosystems and anthropogenic activities that occur there are left vulnerable. Fish cultured in ocean net pens are increasingly subjected to oxygen stress. Aeration and oxygenation have been utilized to improve oxygen conditions in pond aquaculture; however, their use in open ocean net pens is still in its infancy. In this study, liquid oxygen was distributed through the NetOx Net system within sea cages in a commercial Atlantic salmon (*Salmo salar*) farm located off Saddle Island, Nova Scotia (Canada). Real-time sensors were used to measure temperature and oxygen before oxygenation, between oxygenation and the onset of de-stratification due to mixing, and after mixing had resulted in full de-stratification. Oxygenation likely resulted in the upwelling of cold deep water, lowering the cage temperature by ~4°C which in turn increased oxygen solubility and decreased fish metabolism; these factors resulted in an overall increase in oxygen concentrations by ~1.5 mgL^{-1}. Following de-stratification, the effects of the oxygenation system were diluted, and mixing due to oceanographic processes dominated the system. As climate change increases hypoxia in coastal regions, where aquaculture practices continue to expand, oxygenation systems may become commonplace. Therefore, it is important to understand whether they will work in an environment that is open to other elements.

3.2 Introduction

Ocean warming threatens biological communities through temperature and oxygen related stressors. As temperature rises, the capacity of the ocean to hold dissolved oxygen decreases while biological consumption increases (Richards 1957). Surface ocean temperatures have risen an average of 0.7°C over the last 100 years, contributing to the

[2] Burke, M., Grant, J., Filgueira, R., Swanson, A., 2022. Oxygenation effects on temperature and dissolved oxygen at a commercial Atlantic salmon farm. Accepted in Aquaculture Engineering.

expansion of dead zones worldwide (Gruber 2011; Altieri and Gedan 2015). Coastal ecosystems have the additional challenge of increased nutrients through expanding development. Eutrophication can result in the proliferation of primary production, organic sedimentation, and an increase in benthic oxygen consumption via decomposition of organic matter (Diaz 2001). Both warmer waters and higher nutrient loads have resulted in intensification of coastal oxygen deficits (Breitburg et al. 2018).

Understanding oxygen dynamics within coastal ecosystems is important for marine aquaculture farms, as they are often located in coastal areas that are experiencing increased oxygen stress. Additionally, adequate dissolved oxygen (DO) concentrations through a farm are paramount in finfish aquaculture, as low oxygen can directly impact the health and growth of fish. Oxygen below certain thresholds, usually between 4-6 mg L^{-1} (dictated by temperature and size of the fish) impact feed intake and feed conversion rates, and if prolonged, can result in fish stress, vulnerability to diseases, and mortality (Hvas et al. 2017; Oldham et al. 2019). The oxygen regime in marine cages is primarily governed by physical processes, through tides, winds, and currents, and through oxygen consumption by the fish (Wildish et al. 1993; Oldham et al. 2018; Burke et al. 2021). The principal way in which aquaculture companies can prevent oxygen related issues is during site selection, where farms can be located in areas that are well ventilated and thoroughly mixed through adequate hydrodynamic conditions (Bergheim et al. 2006). However, at certain times of year, now exacerbated by climate change conditions, when DO is low companies must implement forced aeration.

Water aeration is any process by which oxygen is introduced to the water body, however it is most commonly achieved through the utilization of air-sea contact to transfer atmospheric air to the water column. The aim of using aeration systems is to increase DO and consequently the carrying capacity of the aquaculture system (Lawson 1995). Since the 1980s, studies have emerged on the effectiveness and economic viability of aerators, often in catfish ponds in the USA (Boyd 1982; Engle 1989; Boyd et al. 2018). Aeration in a common topic of study in fish ponds due to the static nature of these systems, where stagnant waters and low primary productivity can result in chronically low oxygen, especially at night when respiration exceeds production (e.g. Boyd et al. 2018). Electrically powered paddlewheels are the most common type of aeration in

catfish ponds, while sea cages utilize air-stones, air-lift pumps, and submerged pumps (Beveridge 2008; Kumar and Engle 2017). The primary uses of aeration systems in sea cages are to create inhospitable environments for sea lice and harmful algae, or increasing water movement to maintain ice-free conditions, dispel waste and increase wave action and oxygen transfer across the air-sea interface (Beveridge 2008). To a lesser degree, farms that contain high stocking densities or exhibit low oxygen during warmer months may use aeration devices to improve oxygen conditions (Berillis et al. 2016).

In the effort to increase oxygen above equilibrium or above concentrations that can be obtained through aeration, the injection of pure oxygen to the system has also been in development (Lekang 2007). For example, Vinci and Summerfelt (2015) suggested that the use of oxygenation in recirculating aquaculture systems (RAS) can increase the carrying capacity by a factor of 3 compared to aeration. However, the transport and distribution of oxygen can be costly in open ocean environments, thus oxygenation is more commonly used in RAS (Lekang 2007). There are multiple types of oxygenation techniques, ranging from systems that disperse micro- or nano-bubbles of pure oxygen as liquid or gas into the cages, to replacing nitrogen with oxygen, or even using hydrogen peroxide which dissociates to release oxygen (Endo et al. 2008; Bögner et al. 2021). Studies of oxygenation success and efficiency are few, particularly in sea cage environments. A study by Bergheim et al. (2006), examined the use of a novel oxygen injection system and found that the system increased oxygen by an average of 10-15% when the DO saturation fell below 85%. Additionally, a study by Endo et al. (2008) determined that micro-bubbles of oxygen injected into marine cages raised oxygen concentrations significantly compared to reference concentrations, nearly saturating the entire water column while slightly decreasing cage temperatures.

One of the main challenges for coastal aquaculture in Nova Scotia (Canada), is the onset of low oxygen conditions during the summer and autumn. The Atlantic Ocean off Nova Scotia is influenced by both the southward flow of the cold and fresh Labrador Current as well as the northward flow of the warm and saline Gulf Stream further offshore. As summer progresses into autumn, the Gulf Stream shifts closer inshore, transporting warmer waters with reduced oxygen solubility. Studies have suggested that in the future, the onset of this inshore transport is likely to occur earlier in the year and be

prolonged (Greenan et al. 2018). Therefore, the main concern for managers with farms located in coastal zones is to plan ways to increase oxygen concentrations to protect the production and welfare of cultured fish. The goal of this study was to examine the effectiveness of an oxygenation system deployed at a coastal, sheltered Atlantic salmon farm in southwestern Nova Scotia. Oxygen concentration as well as associated temperature was examined in detail over 5 months in 2019 including 2 months prior to the use of oxygenation and 3 months through its use. Environmental variables such as wind and tides, as well as biological processes such as fish metabolism were also considered to determine how oxygenation may interact with these processes.

3.3 Materials and Methods

3.3.1 Study Site

Saddle Islands (44.50°N, 64.05°W) are a small cluster of islands located off the Aspotogan Pensinsula on the outskirts of Aspotogan Harbour, Nova Scotia (Canada). A Cooke Aquaculture Atlantic salmon farm is located between shore and the main island, hereinafter referred to as Saddle Island (Figure 3.1). The average depth of the waters surrounding the farm is 15 m, with the deepest areas of the bay reaching 22 m. The farm consists of a row of 6 circular cages, each 48 m in diameter with cylindrical nets (mesh size: 57 mm) to a depth of 10 m (~18 100 m^3 volume). A remotely operated vehicle cleaned the nets of biofouling throughout the study in conjunction with the farm's maintenance program. The farm was stocked with adult post-smolt Atlantic salmon that averaged 3.2 kg during the study period, resulting in an average stocking density of 11 kg m^{-3}.

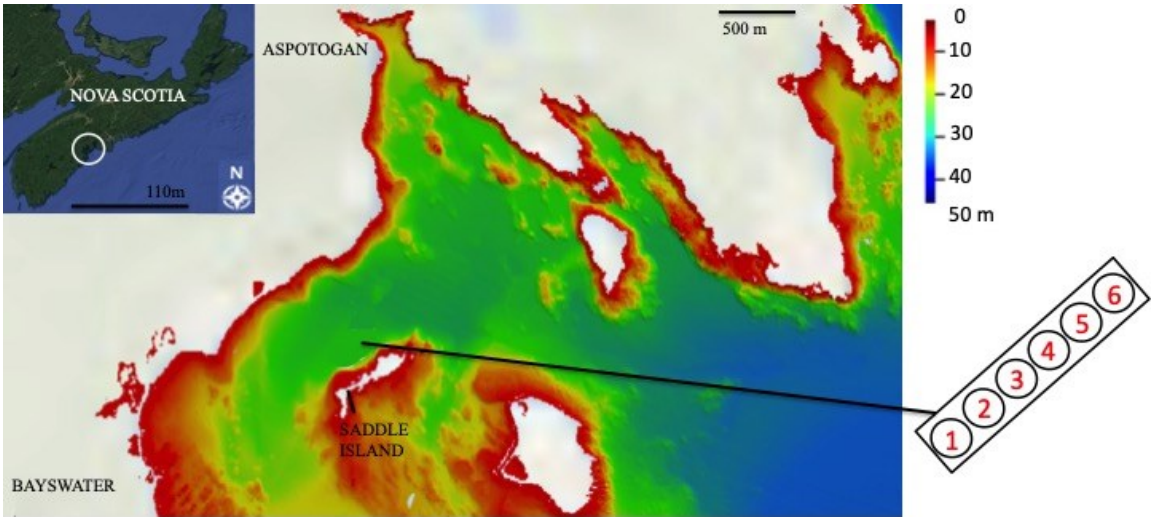

Figure 3.1 Site schematic showing the layout of the cages within the Atlantic salmon farm in Aspotogan Bay including bathymetry (m) and an inset map of Nova Scotia.

The study was conducted between June 1 and October 31 2019, while oxygenation systems were deployed within each cage at 8 m depth beginning on August 4 2019 and continuing until the end of the study period. In 3 of the cages, liquid oxygen was distributed using NetOx Net (OxyVision AS, Norway), which is a diffuser grid consisting of perforated tubing releasing 65-190 L micro-bubbles of oxygen per minute as a curtain along the bottom of the cages (www.biomarine.no/en/sea-cages/netox-net/). The remaining 3 cages contained a different system that was not evaluated in the current study. Additionally, no control cage was used as the oxygen is depleted at this site during the late summer and autumn, and the farm could not risk potential fish mortality. Due to technical aspects, the system did not operate continuously during the trial (indicated by grey bars in the figures). The managers recorded the system interruptions and thus there is a potential error on these bars of ~12 h, depending on the time of day.

3.3.2 Data Collection

Each of the cages contained 2 temperature and DO sensors (center of the cage at 2 m and 7 m depth), which recorded in 5 min intervals and transmitted the data to cloud storage in real-time (AquaMeasure, InnovaSea Systems, Inc., Bedford, Nova Scotia). A single reference sensor was deployed off a nearby barge (~75 m away) at 5 m depth, however this sensor was only deployed in mid-September. Cages 1,2 and 5 had the

oxygenation system under examination, thus the following analysis concerns these three cages.

Tidal height was collected through a tidal gauge operated by the Department of Fisheries and Oceans situated in Blandford, located on the opposite side of the Aspotogan Peninsula, 5 km south of the aquaculture site. Cubic interpolation of tidal maxima and minima was used to acquire hourly tidal heights. Wind speed was acquired through an Environment Canada weather station located in Lunenburg, NS, located 25 km south of the site. Wind stress (τ) was calculated using the wind speed data as:

$$\tau = C_D \cdot \rho_{air} \cdot {u_{10}}^2 \quad (6)$$

where C_D is the dimensionless drag coefficient (0.0013), ρ_{air} is air density (1.22 kg m^{-3}), and u_{10} is wind speed. Satellite daily sea surface temperature (SST) was used to compare to the temperature in the cage, as the reference sensor was deployed late in the trial period. Satellite SST was retrieved from 4km AVHRR Pathfinder Version 5.3, produced by NOAA National Centers for Environmental Information (Saha et al. 2018). Only data of a quality level greater than 4 were chosen, with gridded averages covering the area between 44.54-44.34°N and 64.16-63.86°W. Subsequently, linear interpolation was used to fill data gaps and create daily satellite SST values. Oxygen consumption due to fish respiration in the cages was calculated as standard metabolic rate according to equation A1 in Trudel and Welch (2005):

$$log_e R_s = -2.94(0.07) + 0.87(0.01) \cdot log_e W + 0.064(0.003) \cdot T \quad (7)$$

Where W is salmon weight (g) and T is temperature (°C). Standard errors are indicated in parentheses.

3.3.3 Statistical Analysis

All statistics were conducted via Python (Python Software Foundation, https://www.python.org/). Though the temperature and DO time series were examined between June and October 2019, for temporal consistency, analyses on the effect of oxygenation were conducted over three 3 week time periods: before the deployment of oxygenation ("pre-oxygenation"; July 13-August 3), between the deployment of oxygenation and the onset of mixing caused by de-stratification of the water column ("oxygenation"; August 4-August 25), and finally, after the de-stratification of the water column while oxygen continued to be supplied ("de-stratification"; August 26-September

16). To test for differences in temperature/DO between these periods, Mann-Whitney U tests were used. Model II linear regressions were conducted between fish calculated respiration and oxygen concentrations in the cage, as well as between satellite SST and 2 m temperature, among the three time periods in question, with ANCOVA and UNIANOVA to determine significance.

To explore the effects that other environmental and physical parameters could have on oxygen and temperature aside from the system itself, cross-correlations were conducted between wind stress, speed and direction, tidal height, and photoperiod. Wind stress was determined to be the most highly correlated with oxygen and temperature, and therefore spectral analysis and periodograms were used to explore the dominant frequencies during the study period. In order to maximize the power of these time series analyses the entirety of the time series was used.

3.4 Results

3.4.1 Temperature

Prior to oxygenation, between June and July, the average temperature between the cages at both depths showed an overall increase from 11.0±2.10℃ (mean ±SD) and 9.91±2.27℃ in June, to 16.27±2.03℃ and 13.98±1.77℃ by the end of July at 2 m and 7 m, respectively (Figure 3.2A, C, E). Thermal stratification was strong during these two months; the average temperatures at 2 m were 1.65±1.32℃ warmer than at 7 m, although not statistically significant in cage 2 (Figure 3.2B, D, F; Table 3.1).

Table 3.1 Mann-Whitney U test results for temperature difference between 2 m and 7 m in each cage during each time period; n = sample size.

Cage	Period (Daily)	*n*	*U*	*P*
1	Pre-Oxygenation	50	645	**<0.001**
2		38	660	0.26
5		50	695	**<0.001**
1	Oxygenation	13	36	**0.007**
2		22	118	**0.002**
5		22	123	**0.003**
1	De-stratification	67	2075	0.23
2		67	2075	0.23
5		67	2027	0.17

This is a typical summer warming progression for coastal Nova Scotia. Despite the long-term increase, temperatures at both depths displayed variation of 1-2℃ over short time scales (days). Temperatures at 2 m were more stable than at 7 m, which showed greater changes such as the July 9 decrease of ~4℃, persisting for 1-2 days before rebounding in each cage.

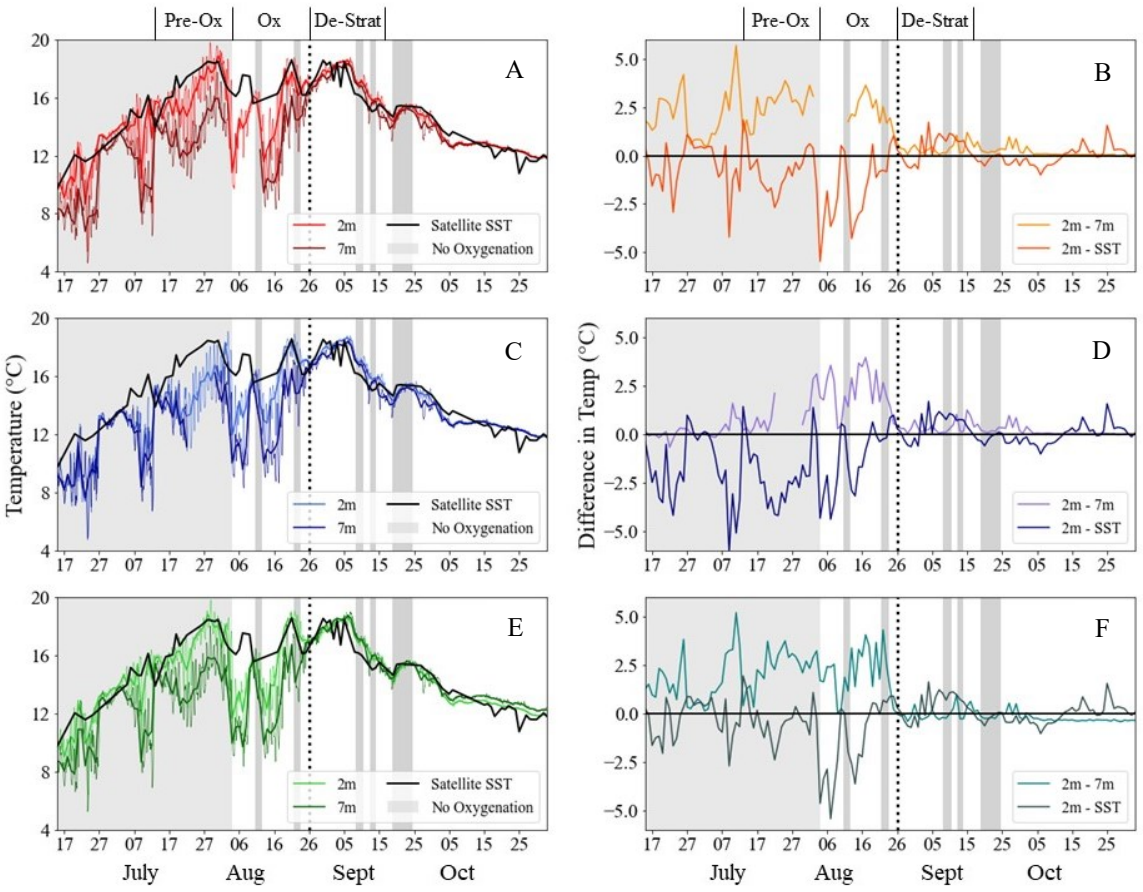

Figure 3.2 Hourly (lighter lines) and daily (darker lines) average temperature within cages 1 (A), 2 (C) and 5 (E) at 2 m and 7 m in 2019, along with the sea surface temperature (SST) derived from satellite data (dashed line). Difference in temperature between observations at 2 m and satellite SST and between 2 m and 7 m in cages 1 (B), 2 (D), and 5 (F). The vertical dotted line indicates the onset of de-stratification, and the grey bars indicate approximate times when the oxygenation system was off.

During the pre-oxygenation period, the satellite SST pattern agreed with sea cage temperature at 2 m depth, but the coarser temporal resolution of satellite SST did not display higher frequency variation observed at the cage level (Figure 3.2A, C, E). While temperatures at 2 m in cages 1 and 5 were not significantly different from satellite SST during this period, cage 2 was significantly lower than satellite SST (Table 3.2). Overall, standard major axis regression indicated that 80% of the variance in cage temperature could be explained by satellite SST (Appendix B). The consistency between these signals indicates that the satellite SST can provide far field temperature values independent of the local sea cage effects.

Table 3.2 Mann-Whitney U test results for temperature difference between satellite SS and 2 m in each cage during each time period; n = sample size.

Cage	Period (Daily)	*n*	*U*	*P*
1			1097	0.15
2	Pre-	50	806	**0.001**
5	Oxygenation		1189	0.34
1			119	**0.002**
2	Oxygenation	22	151	**0.02**
5			151	**0.02**
1			2202	0.43
2	De-stratification	67	2179	0.39
5			2200	0.42

The oxygen system was activated on August 4, which coincided with a sharp drop in temperature at both depths in each cage, and on average from 16.4±1.56 to 11.8±2.01℃ at 2 m and 13.2±1.30 to 10.0±1.08℃ at 7 m in one day (Figure 3.2A, C, E). Overall, the temperature decreased from 15.9±1.82℃ and 14.2±1.43℃ during pre-oxygenation to 15.3±2.32℃ and 13.1±2.65℃ during oxygenation at 2 m and 7 m, respectively. This decrease was not observed in satellite SST when comparing the same periods, resulting in a significant difference between 2 m and satellite SST for each cage during the oxygenation period (Table 3.2). Although significant, standard major axis regression indicated that only 23% of the variance in cage temperature could be explained by satellite SST during the oxygenation period (Appendix B).

Oxygenation also magnified the differences in temperature between the two depths, from 1.65±1.32 during pre-oxygenation to 2.24±1.05℃ during oxygenation (Figure 3.2B, D, F). The differences between depths were significant before and during oxygenation in cages 1 and 5, and they also became significant in cage 2 during oxygenation (Table 3.1). When the system was activated, temperatures remained low until August 9 when both depths increased in temperature and converged to 15.2±0.38℃. Following this, both depths rapidly decreased again on August 13 to 12.6±1.42℃ and

9.79±0.85°C at 2 m and 7 m respectively, before increasing on August 15, rising to similar temperatures observed during pre-oxygenation. Temperatures at both depths then converged once more to 16.5±0.45°C on August 25, coinciding with the onset of full water column mixing.

On August 26, stratification broke down and the average difference in temperature between depths became negligible in each cage due to wind mixing (Figure 3.2B, D, F; Table 3.1). Winds from the southwest were strong and persistent in late August (not shown), resulting in shallow water convection and water column overturn on August 26. The oxygenation system may have maintained mixing in the cages, prohibiting water re-stratification for the remainder of the trial until full autumn convection. Following August 26, temperatures at both depths continued to warm, reaching an average among the cages of 18.5±0.18°C by September 6, and then steadily declined for the remainder of the oxygenation trial until reaching 12.5±0.34°C by the end of October (Figure 3.2A, C, E). Once wind mixing increased and the water became de-stratified, temperature at 2 m became statistically similar to satellite SST in each cage (Table 3.2), and satellite SST again became strongly related to cage temperature, reaching an R^2 of 0.92 ($p<0.001$; Appendix B).

Wind stress had the highest correlation with temperature. Winds were relatively strong in this area, with maximum, mean and median speeds of 74 km h^{-1}, 16 km h^{-1} and 14 km h^{-1}, respectively. The correlations between wind and temperature at 2 m differed between each period, though there was always a dominant frequency of 24 h. During pre-oxygenation, there were negative correlations of R = -0.36, -0.26 and -0.43 for cages 1,2 and 5, respectively (each $p < 0.05$; Table 3.3), indicating that higher wind stress correlated with cooler temperatures. This correlation then decreased during the oxygenation period and became positively correlated with R = 0.31, 0.27 and 0.26 for cages 1,2 and 5, respectively (each $p < 0.05$; Table 3.3), indicating that higher wind stress correlated with increased temperatures at 2 m. During the de-stratification period, there was no longer a significant correlation between these two variables (Table 3.3).

Table 3.3 Cross-correlation between wind or tide and temperature at 2 m; n = sample size.

Cage	Period	Parameter	*n*	*R*	*P*
1		Wind		-0.36	**<0.05**
2		Wind		-0.26	**<0.05**
5	Pre-Oxygenation	Wind	816	-0.43	**<0.05**
1		Tide		-0.11	**<0.05**
2		Tide		-0.13	**<0.05**
5		Tide		-0.11	**<0.05**
1		Wind		0.31	**<0.05**
2		Wind		0.27	**<0.05**
5	Oxygenation	Wind	528	0.26	**<0.05**
1		Tide		0.24	**<0.05**
2		Tide		0.21	**<0.05**
5		Tide		0.20	**<0.05**
1		Wind		-0.05	>0.05
2		Wind		-0.05	>0.05
5	De-stratification	Wind	1608	-0.05	>0.05
1		Tide		0.02	>0.05
2		Tide		0.02	>0.05
5		Tide		0.01	>0.05

Tide had a low, though statistically significant correlation with cage temperature at 2 m. During pre-oxygenation, there was a negative correlation of R = -0.11, -0.13, and -0.11 for cages 1,2 and 5, respectively (each $p<0.05$; Table 3.3), indicating higher tidal height correlated with cooler temperatures. During the oxygenation period, as with wind, tidal height became positively correlated with temperature with R = 0.24, 0.21, and 0.20 for cages 1, 2 and 5, respectively (each $p<0.05$; Table 3.3), thus higher tidal height correlated with warmer waters. Finally, this correlation was non-significant during de-stratification (Table 3.3).

3.4.2 Dissolved Oxygen

During pre-oxygenation, the average DO among the cages at both depths was 7.46±0.90 mg L^{-1} and 8.53±0.82 mg L^{-1} at 2 m and 7 m, respectively (Figure 3.3A, C, E). Oxygen at 7 m was significantly higher than at 2 m in cages 1 and 5, but not in cage 2 (Figure 3.3B, D, F; Table 3.4). There were noticeable increases in oxygen during periods coinciding with the fluctuations in temperature mentioned above, such as the July 9 increase of ~ 2 mg L^{-1}.

Table 3.4 Mann-Whitney U test results for DO difference between 2 m and 7 m in each cage during each time period; n = sample size.

Cage	Period (Daily)	*n*	*U*	*P*
1		50	309	**<0.001**
2	Pre-	38	584	0.08
5	Oxygenation	50	8603	**<0.001**
1		13	33	**0.004**
2	Oxygenation	22	133	**0.005**
5		22	1930	**<0.001**
1		67	1552	**0.001**
2	De-stratification	67	2170	0.37
5		67	38641	**0.001**

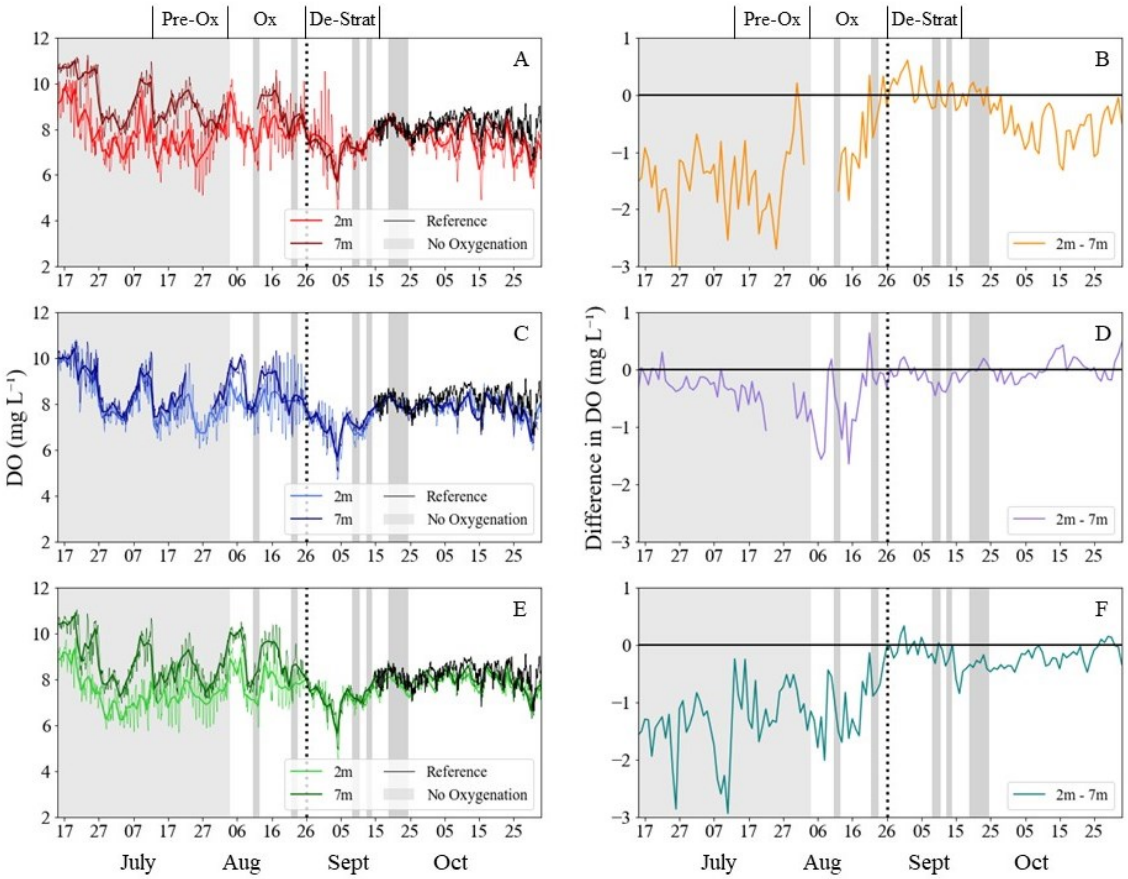

Figure 3.3 Hourly (lighter lines) and daily (darker lines) average dissolved oxygen (DO, mg L^{-1}) within cages 1 (A), 2 (C) and 5 (E) at 2 m and 7 m in 2019, along with the reference (black). Difference in DO between 2 m and 7 m in cages 1 (B), 2 (D), and 5 (F). The vertical dotted line indicates the onset of de-stratification, and the grey bars indicate approximate times when the oxygenation system was off.

While the temperatures declined at the onset of oxygenation, there was a concurrent increase in DO (Figure 3.3A, C, E). DO then continued to follow the same inverse pattern as temperature, with a decrease in each cage to an average of 7.30 ± 0.82 at 2 m and 8.53 ± 0.36 at 7 m on August 13, followed by an increase to 7.80 ± 0.85 at 2 m and 9.50 ± 0.32 at 7 m on August 15. By August 25, the DO in the cages became relatively stable at 8.23 ± 0.73 at 2 m and 8.26 ±0.24 at 7 m. As in the pre-oxygenation period, oxygen concentration at 7 m was significantly higher than at 2 m in all cages (Figure 3.3B, D, F; Table 3.4). During oxygenation, the average DO was 8.06 ± 0.91 mg

L^{-1} and 8.88 ± 0.86 mg L^{-1} at 2 m and 7 m, respectively, which is significantly higher than the values observed during pre-oxygenation at both depths (Table 3.5).

Table 3.5 Mann-Whitney U test results for DO difference between pre-oxygenation and oxygenation and between oxygenation and de-stratification for each depth; n = sample size.

Cage	Period	Depth	*n (pre/ox)*	*U*	*P*
1		2 m	505/505	72878	**<0.001**
		7 m	503/298	62598.5	**<0.001**
2	Pre-oxygenation – Oxygenation	2 m	505/505	71531.5	**0.001**
		7 m	306/502	35383.5	**<0.001**
5		2 m	505/505	80637	**<0.001**
		7 m	505/505	73086.5	**<0.001**
1		2 m	505/505	68315.5	**<0.001**
		7 m	298/505	6105	**<0.001**
2	Oxygenation – De-stratification	2 m	505/505	43463.5	**<0.001**
		7 m	502/505	12039	**<0.001**
5		2 m	505/505	65737	**<0.001**
		7 m	505/505	15699.5	**<0.001**

De-stratification due to mixing, on August 26 resulted in a significant difference in oxygen between the oxygenation and de-stratification periods (Table 3.5). This difference was due to the convergence of oxygen between depths within each cage to 7.44±0.30 mg L^{-1} for cage 1, 7.48±0.25 mg L^{-1} for cage 2, and 7.92±0.16 mg L^{-1} for cage 5. The average daily difference between 2 m and 7 m within the 3 cages was -0.17±0.31 mg L^{-1} during this period (Fig 3 B, D, F). The difference between depths was not significant in cage 2, and while it was significant in cages 1 and 5, it was less so than in the oxygenation period (Table 3.4). On September 4, during oxygenation and despite the mixing, there was an oxygen drop to 4.3 mg L^{-1}, which is a hypoxic level at 18.5 °C, and resulted in fish mortalities.

As with temperature, wind stress also had the highest correlation with DO at the farm with a periodicity of 24h, reflecting the effect of wind on temperature. During pre-

oxygenation, there were positive correlations of R = 0.18, 0.16 and 0.31 for cages 1, 2 and 5, respectively (each $p < 0.05$; Table 3.6). During the oxygenation period, these correlations increased and became negative with R=-0.33, -0.44, and -0.47 for cages 1, 2 and 5 respectively (each $p < 0.05$; Table 3.6). Finally, after de-stratification, the correlation was once again positive and lower at R=0.15, 0.18 and 0.15 for cages 1, 2 and 5, respectively (each $p < 0.05$; Table 3.6). The correlations for tide followed the same pattern observed for wind, with a positive correlation during pre-oxygenation of R=0.14, 0.12 and 0.20 for cages 1, 2 and 5, respectively (each $p<0.05$; Table 3.6). During oxygenation, the correlation again became negative at R=-0.15, -0.21 and -0.28 for cages 1, 2 and 5 respectively (each $p<0.05$; Table 3.6). During de-stratification, there was no longer a significant relationship between tide and DO.

Table 3.6 Cross-correlation between wind or tide and DO at 2 m; n = sample size.

Cage	Period	Parameter	*n*	*R*	*P*
1		Wind		0.18	**<0.05**
2		Wind		0.16	**<0.05**
5	Pre-Oxygenation	Wind	816	0.31	**<0.05**
1		Tide		0.14	**<0.05**
2		Tide		0.12	**<0.05**
5		Tide		0.20	**<0.05**
1		Wind		-0.33	**<0.05**
2		Wind		-0.44	**<0.05**
5	Oxygenation	Wind	528	-0.47	**<0.05**
1		Tide		-0.15	**<0.05**
2		Tide		-0.21	**<0.05**
5		Tide		-0.28	**<0.05**
1		Wind		0.15	**<0.05**
2		Wind		0.18	**<0.05**
5	De-stratification	Wind	1608	0.15	**<0.05**
1		Tide		0.05	>0.05
2		Tide		0.04	>0.05
5		Tide		0.04	>0.05

Given the potential effect of fish metabolism on oxygen dynamics within marine cages, a correlation analysis between the calculated oxygen consumption and observed DO was conducted for the three time periods (Figure 3.4). The reduced major axis regression models for each period were significant, however the R^2 was lowest during pre-oxygenation at 0.15, which increased to 0.53 during oxygenation and then decreased once more after de-stratification at 0.33. Pairwise comparisons between the 3 time periods using the estimated marginal mean for consumption revealed that during oxygenation the mean DO was significantly higher than during the pre-oxygenation and de-stratification periods ($p<0.001$). Thus, at similar levels of oxygen consumption, there were higher concentrations of oxygen within the cages during oxygenation.

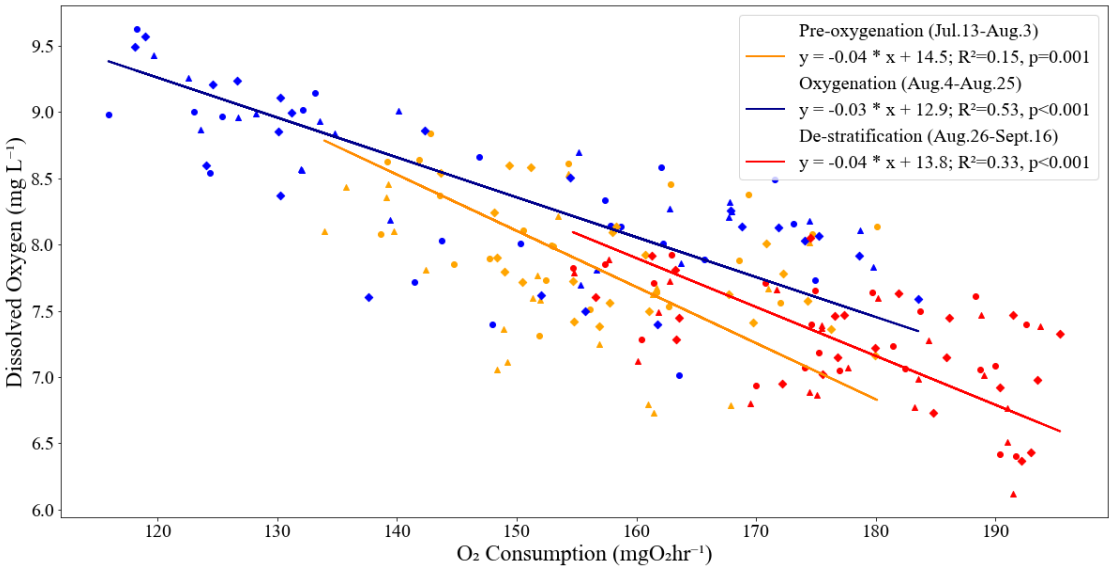

Figure 3.4 Relationship between oxygen consumption by the fish (mg O_2 hr^{-1}) and dissolved oxygen (DO, mg L^{-1}) over the average of both depths in cages 1 (circles), 2 (triangles) and 5 (diamonds) during pre-oxygenation (orange), oxygenation (blue), and de-stratification (red).

3.5 **Discussion**

Open ocean finfish aquaculture can be challenged by low oxygen events, especially in the summer and autumn. As climate change continues to warm the oceans, these events are likely to become more frequent. Oxygen supplementation within aquaculture farms is occasionally used to increase DO concentrations; however, studies on these systems are rare, especially in marine cages. It is important to monitor the use of

oxygenation as it must be regulated properly to avoid oversaturation, which can force increased fish respiration and become detrimental to fish health (Kepenyes and Váradi 1984). The majority of studies on oxygenation and aeration are primarily conducted in lake or pond environments, where the waters are relatively quiescent, or in small bays where freshwater input results in regular stratification (e.g. Boyd 1982; Hargreaves et al. 1991; Stehfast et al. 2017; Boyd et al. 2018; Oberle et al. 2019). Additionally, many of these studies use aeration to break up the stratification and promote mixing, or only require oxygenation in the early morning hours when oxygen concentrations are lowest. To the best of our knowledge, this is one of the only studies on a months-long time scale for the use of oxygenation to increase DO in open ocean aquaculture.

Overall, the results of this study suggest that oxygenation may have caused an upwelling of cooler waters which decreased temperatures throughout the cage. Combined with strong winds in the area, this ultimately resulted in a breakdown of stratification at the end of August allowing for oxygen replenishment in the upper layers. Furthermore, this decrease in temperature resulted in conditions that allowed for increased oxygen solubility and decreased fish metabolism, which resulted in an overall increase in oxygen concentrations. The effects of oxygenation became less apparent after de-stratification, leading to the conclusion that these systems are more effective while waters are stratified.

3.5.1 Temperature

Prior to oxygenation, there was a consistent thermal stratification between 2 and 7 m, specifically observed in cages 1 and 5. Thermal stratification is caused by surface warming, where absorption of solar radiation decreases with depth and results in a pycnocline as cooler waters sink (Losordo and Piedrahita 1991). In contrast, cage 2 did not show this stratification. It is hypothesized that either the sensor was not placed in the correct location, or the sensor may not have been measuring correctly as it is unlikely that stratification, a common phenomenon during the summer in Nova Scotia waters, did not occur in cage 2 but was statistically significant in two adjacent cages.

After the oxygenation system was activated, there was an abrupt decrease in temperature at 2 m in all cages, which was not observed in SST from satellite data, indicating that this was likely due to the oxygenation system. The same pattern was observed in a study by Endo et al. (2008) in which micro-bubble oxygenation was

implemented within sea bream cages. During that study, the authors noted a significant decrease in temperature within the oxygenated cages and determined that the micro-bubbles were forcing the upwelling of cooler waters from depth.

The temperature at this site was stratified between 2 m and 7 m until August 26. Satellite SST measurements began to converge again with those at 2 m in the cage on August 17, as 7 m cage temperature increased towards 2 m temperatures. On August 26, winds likely combined with aeration resulted in temperature convergence of both depths and water column overturn in the cages. Studies at shellfish farms indicate the effectiveness of forced upwelling via aeration to help overturn the water column and enhance primary production (e.g. McClimans et al. 2002; Aure et al. 2007; Handå et al. 2013), therefore the relatively constant flow of oxygen bubbles may have resulted in mixing of the water column.

Wind stress and temperature had a periodicity of 24h likely due to the proximity to land and the resulting sea breeze (Boyd and Tucker 2019). Wind and tide exhibited similar patterns in correlation as both were negatively correlated with temperature pre-oxygenation, but during oxygenation this correlation became positive. Both wind and tide promote mixing, which was evident prior to oxygenation as higher wind/tide correlated with lower temperatures (Rumyantseva et al. 2019). During oxygenation however, as the system interrupted the natural environment, wind and tide had a warming effect counter to the upwelling caused by oxygenation. Once mixing de-stratified the cages, tide and wind no longer had a significant effect on temperature indicating that mixing had dominant control on the temperature dynamics compared to oxygenation. Overall, the oxygenation system was successful at upwelling cooler waters from depth and promoting mixing which then supported oxygen solubility while lowering fish metabolism.

3.5.2 Dissolved Oxygen

As temperature increased through June and July, oxygen decreased at both 2 m and 7 m, reflecting the temperature effects on oxygen solubility and fish consumption. Thermal stratification highly influences oxygen distribution, as oxygen in upper layers can be replenished through the air-sea interface, but stratification prevents the reaeration of deeper waters, limiting oxygen saturation below the thermocline (Oberle et al. 2019). However, previous studies on salmon depth distribution have shown that farmed salmon

prefer to be in the upper layers of the cage, particularly at night and during feeding (Johansson et al. 2006; Oppedal et al. 2011; Wright et al. 2017). If the fish prefer 2 m depth, population respiration can result in depleted oxygen concentrations near the surface, as opposed to the conventional cage structure of deep-water deoxygenation due to thermal stratification. Usually within cages, temperature and oxygen follow a typical pattern with higher temperatures and oxygen in the surface layer due to the proximity to the air-sea interface, and both variables decreasing with depth (Oldham et al. 2017). However, during this study, the oxygen was significantly lower at 2 m than 7 m prior to de-stratification, suggesting that the fish were congregating in the upper water layers. Upwelling by the oxygenation system and de-stratification then allowed for oxygen replenishment of the surface waters.

Though the present study did not include reference oxygen values until mid-September, oxygen at the reference was higher than the cage throughout the remainder of the trial. Similar findings were documented in Bergheim et al. (2006), which used the same NetOx system as was employed in this study within similar salmon sea cages in Norway. The authors documented that oxygen concentration increased due to oxygenation; however, reference concentration remained consistently higher than within the cages. In contrast, the oxygenation study by Endo et al. (2008) utilized their own micro-bubble generating system within red sea bream cages in Japan and observed that oxygen concentrations were 0.52-0.87 mg L^{-1} above reference concentrations. The analogous methods between this research and that done in Bergheim et al. (2006) likely explains the similarities in results; however, it is important to consider the farm environments in which each of these studies were performed. Though the Endo et al. (2008) research was conducted in a similarly sheltered bay as this study, compared to the more exposed location of the Bergheim et al. (2006) study, the Japanese bay was almost 10°C warmer than Nova Scotian or Norwegian waters. It is also important to consider that the red seabream used in the Endo et al (2008) study have a different physiology than the Atlantic salmon used in this and the Bergheim et al. (2006) study.

Oxygen variability at aquaculture farms has been noted at both the cage- (e.g. Solstorm et al. 2018) and farm-scale (e.g. Burke et al. 2021). Parameters influencing oxygen dynamics are primarily physical (wind, tides, currents) and to a lesser degree

biological (primary production, respiration). There are also inherent variabilities due to the nature of a sea cage, from the effect of cage infrastructure on hydrodynamics and water mixing, fish through respiration and movement, or through biofouling (Bi et al. 2013; Klebert et al. 2013; Solstorm et al. 2018). To determine sources of variability in the oxygenation system, other parameters impacting oxygen were examined. Wind stress and to a lesser degree tide, were the two physical parameters that had a significant impact on DO. The effects of wind stress are primarily due to increased wave action which promotes the natural diffusion of oxygen across the air-sea interface while promoting water column mixing (Talley et al. 2011). The effects of tide are more direct, advecting aerated waters from outside of the bay at high tide replenishing oxygen within the cages (Burke et al. 2021). These effects were corroborated in the findings during the pre-oxygenation period, where there was a positive relationship between oxygen and wind stress/tide, however, at the onset of oxygenation, these correlations became negative. As stated above, the opposite occurred in temperature, with negative correlations pre-oxygenation, and positive correlations during the oxygenation period, reflecting the effect that temperature had on oxygen. This pattern change suggests that oxygenation had a dominant impact on oxygen and temperature dynamics compared to the effect that wind and tide had during the pre-oxygenation period. While oxygenation encouraged upwelling of cooler waters from depth, wind countered with mixing warmer waters from above, while tide transported relatively warmer waters from outside of the cage. Finally, after de-stratification, mixing became dominant and there was no longer an effect due to wind or tide, while also creating conditions under which oxygenation was less effective.

Fish respiration also has a direct impact on oxygen (Solstorm et al. 2018). Therefore, the relationship between calculated oxygen consumption by fish and the observed oxygen within the cage was examined to determine whether oxygenation may disrupt this correlation. The regression model revealed that while there were higher concentrations of DO during the oxygenation period, there was overall lower oxygen consumption. The calculated consumption was dependent on temperature, thus lower temperatures due to oxygenation resulted in lower consumption. This also resulted in higher oxygen concentrations at similar consumption compared to the other two periods. Subsequently, de-stratification resulted in similar concentrations and calculated

consumption as prior to the activation of oxygenation. Thus, oxygenation likely had less of an effect once there was an overturn of the water column, rendering the system ineffective after this point.

3.6 Conclusion

Oxygenation was effective at mixing and upwelling cooler waters from depth ultimately resulting in improved solubility conditions for increased oxygen, rather than directly increasing oxygen concentrations. This implies that the oxygenation system need not run for the entire duration of the warm season, it may only be useful until stratification breaks down, saving the farmer the associated economic costs. Moreover, stripping of oxygen from air and transporting liquid oxygen cylinders to remote aquaculture sites is expensive and energy intensive, whereas other, cheaper mixing methods such as bubbling air may achieve the desired conditions for improved oxygen solubility. Additionally, this site is located behind an island in a relatively sheltered bay, and this may explain some of the improvements the oxygenation system seemed to have caused. More exposed locations are less likely to have oxygen fall to critical concentrations often enough to require an oxygenation system. This is a novel study as research on oxygenation in open ocean aquaculture is minimal, though many farms already use these systems to improve fish welfare. Therefore, understanding the effectiveness of oxygenation is paramount to improving farm management.

CHAPTER 4 TEMPORAL AND SPATIAL VARIABILITY IN HYDROGRAPHY AND DISSOLVED OXYGEN ALONG SOUTHWEST NOVA SCOTIA USING GLIDER OBSERVATIONS

4.1 Abstract

By the end of the century, dissolved oxygen (DO) in the global ocean is projected to decline 3-4% with increased severity in coastal waters. The decline in DO could degrade coastal habitats, impacting conditions that are required for sustainable aquaculture. It is important to have 3-dimensional quantitative knowledge of coastal ocean circulation, especially in reference to DO dynamics, for improved farm management (e.g., site selection). Accordingly, the main objective of this study was to quantify along-shore and cross-shore variability in DO dynamics, as well as onshore advection of offshore waters to the bays that could contain aquaculture farms. For that purpose, a Slocum underwater glider was deployed between September 25 and October 12, 2020 to collect high-resolution data of temperature, salinity and DO along a transect between Shelburne Bay and St. Margarets Bay (Nova Scotia, Canada), with an average distance of about 15 km from shore. The observations demonstrate that wind direction had a significant effect on the variability of hydrography and DO over the inner shelf. The strong cross-shore winds advected offshore transient water masses to the coast, creating a mosaic of differing water properties, with warmer, fresher, and less oxygenated shoreward waters. Strong and persistent southwesterly winds created coastal upwelling of sub-surface waters, which cooled the upper water layers by 6°C and increased DO by 1.4 mg L^{-1}. This strong upwelling event detected at 10 km from the coast was also captured 30 h later within St. Margarets Bay, depicting a potential offshore-inshore interaction. Therefore, bay-wide ecosystems and aquaculture production could be affected by intrusions of offshore waters.

4.2 Introduction

Ocean deoxygenation has accelerated over the last 70 years (Breitburg et al., 2018). By 2100, as the global ocean warms and nutrient discharges increase, the

dissolved oxygen (DO) content is projected to decline 3-4%, with evidence that DO is declining more severely over coastal waters than in the open ocean (Gilbert et al., 2010). This loss in DO can impact ocean ecosystem functioning by degrading coastal habitats, potentially affecting regional fisheries stocks (Brennan et al., 2016). With this potential impact on food security, well-suited coastal habitats for aquaculture are necessary. It is important to have comprehensive knowledge on coastal ocean dynamics, especially in reference to DO, as climate-driven hypoxia can threaten seafood production. Additionally, DO plays a key role in many biogeochemical cycles, such as the nitrogen and carbon cycles, especially as deoxygenated deep waters can produce nitrous oxide, carbon dioxide and methane, which can then be upwelled to the surface and released to the atmosphere (Zehr and Ward, 2002; Laffoley and Baxter, 2019).

The Nova Scotia coastline is vast, stretching about 7,400 km, with many inlets and bays suitable to net pen aquaculture. As an underwater extension of Nova Scotia's Atlantic coast, the Scotian Shelf (ScS) is physically complex, and the hydrodynamics have been widely studied (Smith et al., 1978; Umoh and Thompson, 1994; Burt et al., 2013; Townsend et al., 2015; Brickman et al., 2018; Rutherford and Fennel, 2018). The ScS is characterized by deeper inner-shelf basins that cause cyclonic circulation features, and shallow outer-shelf banks then cause anticyclonic circulation features (Han and Loder, 2003). These basins and banks are linked through cross-shelf channels where advection transports slope waters onto the shelf, creating a dynamic environment with circulation patterns that have both biological and environmental importance (Brennan et al., 2016). Coastal upwelling is an important oceanographic feature on the ScS, as it can upwell nutrients to the surface which supports primary production and subsequently the upper trophic levels (Greenan et al., 2004). Upwelling has thus been subject of several studies in the past, to better understand the mechanisms behind it (Hachey, 1937; Petrie et al., 1987; Andrade, 1991; Shan and Sheng, 2022). According to the classic Ekman Theory (Ekman, 1905), prevailing winds blowing parallel to the coast with ocean waters on the right-hand side of the wind direction in the northern hemisphere result in the offshore transport of surface waters, which is then replaced by cool and nutrient-rich waters from below. On the ScS, strong southwesterly winds result in coastal upwelling

and is correlated to lower-than-normal sea surface temperatures in summer months (Hachey, 1937; Petrie et al., 1987).

Most previous studies on the hydrography on the ScS focused on the general circulation, while the DO distribution has not been as well characterized (Dever et al., 2016; Song et al., 2010; Shan and Sheng, 2022). The DO budget is governed by both biological processes (production and respiration) and physical processes (advection and diffusion from outside sources and via air-sea gas exchange). The latter relies on temperature and salinity for oxygen solubility. Additionally, density-induced vertical stratification reduces DO in bottom waters due to the isolation from the surface oxygen flux, and biological respiration of DO occurs throughout the water column and in the bottom sediments (Brennan et al., 2016). Furthermore, DO in bays is also affected by internal dynamics and other processes such as eutrophication, which can consume oxygen through the proliferation and subsequent respiration and decomposition of phytoplankton (Bonsdorff et al., 1997). DO in bays can also have spatial heterogeneity, with localized minima from aquaculture production through fish respiration, especially at night when photosynthetic oxygen replenishment is low, or by oxygen renewal through the tidal cycle (Srithongouthai et al., 2006; Burke et al., 2021).

Traditional oceanographic observations such as ship-board and moored measurements are essential for understanding the role of the ocean in earth's system and for validating and improving numerical ocean models (Gould et al., 2013). Autonomous underwater vehicles (e.g., Slocum underwater profiling gliders) are a novel technology and have resulted in more cost-effective observational techniques than traditional methods. Slocum gliders allow for targeted high resolution and high-quality oceanographic measurements over large spatial areas, which would not otherwise be possible through ship-board measurements. While glider missions were recently conducted over the ScS, there is a marked absence of along-shore glider observations over the southwestern ScS (e.g., Davis et al., 2016, Dever et al., 2016, Ross et al., 2017, Ruckdeschel et al., 2020). Despite traditional and novel glider campaigns, the cross-shore and along-shore variability in temperature, salinity and especially DO over the inner shelf of the ScS are not well characterized in the literature. Large temporal and spatial scale studies have linked DO variability to water mass changes (Smith, 1978; Petrie and Yeats,

2000; Townsend et al., 2015). In general, Petrie and Yeats (2000) described that a dominance of the Labrador Slope water, emanating from the Western Grand Banks and adjacent shelf slope, results in the transport of oxygen-rich waters to the ScS. Conversely, a dominance of the Warm Slope Water, emanating from the Gulf Stream, results in the transport of oxygen-poor water to the ScS. While this is important as research has shown a retreat of the Labrador current and a shift to a Warm Slope Water dominating regime, there is a lack of detailed, local-scale studies on DO along the inner shelf (Claret et al., 2018). Smaller scale studies allow insight into the dynamics of coastal waters that would otherwise be missed by larger scale studies.

The main objective of this study is to examine the along-shore and cross-shore variability in temperature, salinity and DO over the inner ScS based on glider observations. The secondary objective of this study is to investigate the dynamic interaction between offshore waters and coastal embayments. Since the bays on the ScS could contain aquaculture farms, it is important not only to understand the general circulation and hydrographic distribution over the inner ScS, but also to examine the potential transport of these offshore waters to the bays that could influence aquaculture production. To fulfill the above two objectives, a Slocum glider was used to conduct temperature, salinity and DO measurements using a novel zigzagging method to capture spatial and temporal variations in these parameters in both the along-shore and cross-shore directions over the inner ScS. The glider observations were made between September 25 to October 12 in 2020 during the period just prior to the fall overturning, when surface waters are still warm and DO is relatively low. The fall overturning is defined as the destabilization of the water column as surface waters become cooler and more dense than deeper waters, resulting in vertical mixing (Shadwick and Thomas, 2011). This typically occurs in late October or early November with preceding periods of intermittent overturning events (Benway et al., 1993). Exploring how the intermittent overturning events affect temperature, salinity and especially DO when the surface oxygen is lowest is important for improved knowledge of the ScS and for farm management.

4.3 Materials and Methods

4.3.1 Study Site

The ScS is bounded by the Laurentian Channel and Gulf of St. Lawrence to the northeast, and the Gulf of Maine to the southwest (Figure 4.1).

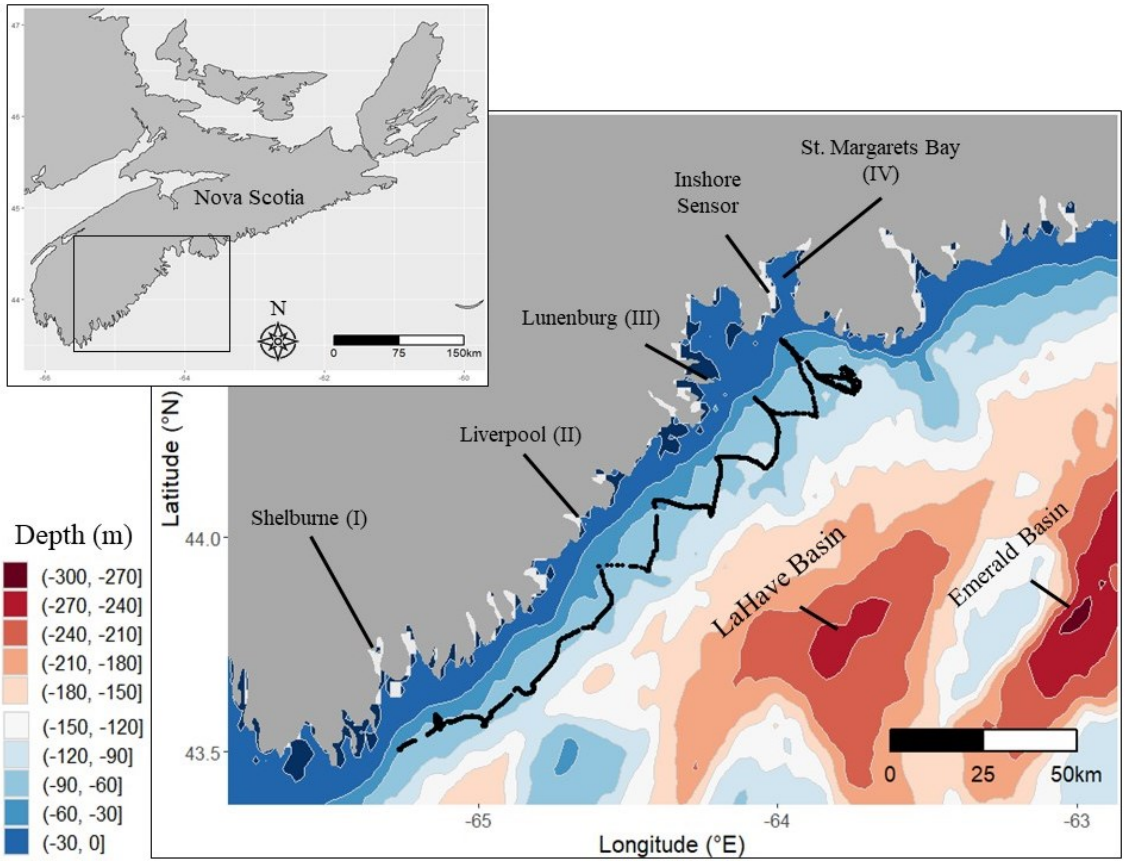

Figure 4.1 Major features of topography over the western Scotian Shelf and the Slocum glider transect (black line) depicting the route from Shelburne Bay (I), past Liverpool (II) and the weather station at Lunenburg (III) to St. Margarets Bay (IV), and an inset map of Nova Scotia.

The ScS has an approximate area of 62 000 km^2 with an average depth of 90 m and is characterized by shallow banks between 25-100 m and deep basins with maximum depths to 300 m (Mills and Fournier, 1979; Sameoto and Herman, 1990). The mean circulation across the ScS is dominated by a southwestward coastal jet, known as the Nova Scotia

Current (NSC), which originates from the major branch of the outflow emanating from the western Gulf of St. Lawrence (GSL) through the Cabot Strait (CBS). Along the shelf break of the ScS, a strong southeastward jet occurs, which is the combination of the inshore branch of the equatorward Labrador Current and a small branch of the outflow from the GSL (Smith and Schwing, 1991; Loder et al., 1997; Dever et al., 2016; Seidov et al., 2021). Over the slope water region beyond the shelf break of the ScS, the slope water jet runs northeastward. It should be noted that the NSC dominates the circulation over the inner ScS (along-shore arrows in Figure 4.2). Over the central ScS, a cross-shelf channel connects the two main basins of Southwest Nova Scotia, LaHave Basin and Emerald Basin to the deep ocean (Shore et al., 2000; cross-shore arrows in Figure 4.2). Additionally, the strength of these currents decreases with depth (length of arrows in each row of Figure 4.2).

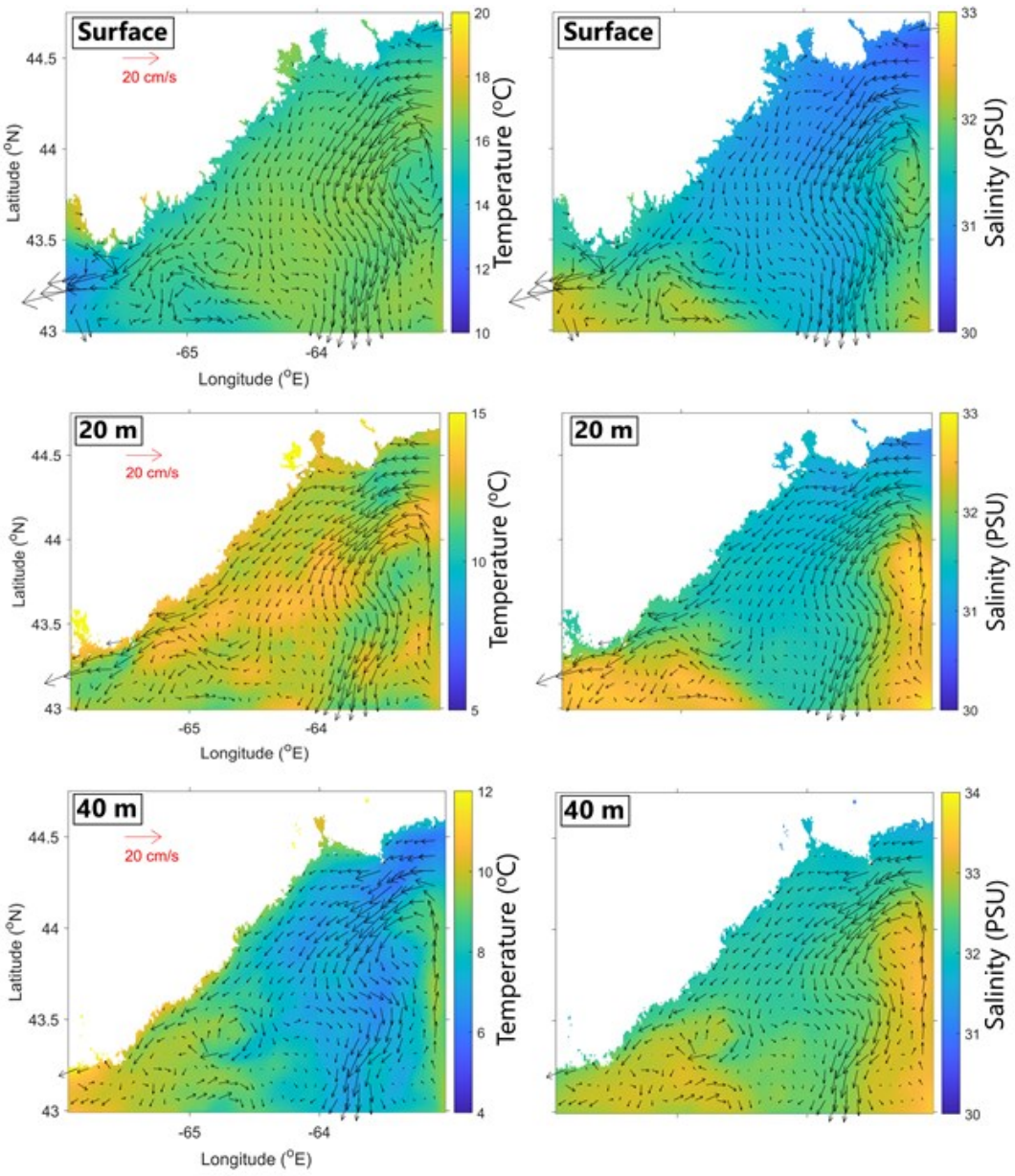

Figure 4.2 Two-month averaged model results of temperature, salinity and currents at three depths (0, 20 m, and 40 m) in September and October 2018 produced by a nested-grid shelf circulation model based on the ROMS (personal communication, Sheng 2022).

Previous studies (e.g., Drinkwater et al., 2003; Dever et al., 2016) demonstrated that there are three main layers of hydrography over the ScS. Sea surface temperature has a typical seasonal cycle with warm surface waters in the late spring and summer (~ 15°C or warmer) and cool from the late autumn to early spring (< 5°C) due to the seasonal changes in the net heat flux at the sea surface. Due mainly to the influence of low-salinity waters from the GSL, the sea surface salinity over the ScS is relatively low and less than

32 (ppt) in comparison with the counterpart in the deep ocean waters beyond the shelf break. Below the surface layer, there is a cold intermediate layer (CIL) composed of waters coming from the Labrador Current and from the Gulf of St. Lawrence, with the average salinity (32-33.5) higher than the surface waters. In the lower layer below the CIL, two water masses can dominate, the Warm Slope Water (WSW), which has a warmer and more saline (> 33.5) signature due to the influence of the Gulf Stream, and a cooler, fresher Labrador Slope Water (LSW) emanating from the Labrador Current. Both deeper waters, WSW and LSW, flow offshore and may penetrate onto the ScS (Gatien, 1976; Smith et al., 1978; Dever et al., 2016). While the three-layer structure of hydrography are normally persistent from spring to autumn over the ScS, winter conditions are characterized by intense vertical convection that collapses the pycnocline and results in a well-mixed water column; this is important as the present study straddles these two seasons (Smith et al., 1978; Hachey, 1942).

4.3.2 Field Measurements

A Teledyne Webb Research Slocum underwater electric glider was deployed between September 25 to October 12 in 2020 over the inner ScS for collecting high-resolution spatial data of hydrography and DO. The wings on the glider convert vertical motion to horizontal movement. The glider can ascend and descend in the water column by altering its density, and make a turn about 2 m from the sea surface and from the seafloor. The Slocum glider was launched from a zodiac outside of Shelburne Bay (43.50°N, 65.26°W) and conducted a zigzag transect roughly 145 km long to St. Margarets Bay (44.36°N, 63.76°W), inshore of the NSC (Figure 4.1). The glider moved at ~1 km h^{-1}, surfacing every 6 h to transmit lower resolution data in real-time via Iridium satellites (full resolution data was downloaded at the end of the mission). The distance of the glider from the shore was calculated and exhibited in Figure 4.3a.

The Slocum glider was equipped with a Seabird unpumped CTD, or Conductivity (accuracy of ± 0.0003 S m^{-1}, resolution of 0.00001 S m^{-1}), Temperature (accuracy of ± 0.002 ℃, resolution of 0.001 ℃), and Depth (accuracy of ± 0.1% of full-scale range, resolution of 0.002% of full-scale range). An Aanderaa optode was also employed to measure DO, with an accuracy of ± 0.03 ℃ and resolution of 0.01 ℃ for temperature

measurements and an accuracy of < 2 µM (or 0.06 mg L^{-1}) and resolution of < 0.1 µM (or 0.003 mg L^{-1}) for DO. Both the CTD and optode sampled continuously in ~ 1 sec intervals. The response of the sensing foils on optical sensors decreases with increasing ambient pressure. Uchida et al. (2008) suggests *in situ* calibration for optodes on profiling moorings or gliders, which compensates for the temperature-dependent delay due to the slow response time. This calibration was performed on the dataset through Python code procured from Uchida et al. (2008).

During the observational period, a real-time optical sensor (AquaMeasure, InnovaSea Systems, Inc., Bedford, Nova Scotia) was deployed at 5 m depth in St. Margarets Bay at Tilley Point (44.57°N, 64.03°W) by the Centre for Marine Applied Research. The sensor recorded temperature and DO in 10-minute intervals within the Bay. Observed wind speeds and directions were acquired through 3 Environment Canada weather stations located at Sandy Point in Shelburne Bay (43.70°N, 65.32°W), Western Head in Liverpool Bay (43.99°N, 64.66°W) and at Lunenburg, NS (44.36°N, 64.30°W), 30 km south of St. Margarets Bay. For highest accuracy, wind stations closest to the associated glider position was used. The weather station at Shelburne is located in Sandy Point which is ~20 km inshore of the glider position, resulting in lower recorded wind speeds, therefore the wind was corrected with the following equation (Hsu, 1980):

$$V_{sea} = 3\, V_{land}^{2/3} \tag{8}$$

where V is the total wind velocity at 10 m from the sea surface.

4.3.3 Wind-Related Parameters and Water Mass Properties

The vertical water movement near the coast generated by wind stress can be estimated from the Ekman transport (I_w) based on the method suggested by Bakun (1973):

$$I_w = \frac{\tau_a}{\rho_w f} = -\frac{\rho_A C_D |u| V}{\rho_w f} \tag{9}$$

where τ_a is along-shore wind stress (Pa), ρ_w is the density of seawater (1025 kg m^{-3}), f is the Coriolis parameters (1.014 x 10^{-4} s^{-1} at 43° latitude), ρ_A is the density of air (1.28 kg m^{-3}), $|u|$ is the along-shore wind speed (m s^{-1}), and V is the total wind speed (at 10 m above sea level, m s^{-1}). Finally, C_D is the dimensionless drag coefficient defined as (Large and Pond, 1981; Powell et al., 2003):

$$C_D = \begin{cases} 1.2 \times 10^{-3} & |\vec{u}| < 11 \text{ m s}^{-1} \\ (0.49 + 0.065\,|\vec{u}|) \times 10^{-3} & 11 \leq |\vec{u}| \leq 27 \text{ m s}^{-1} \\ 2.25 \times 10^{-3} & |\vec{u}| > 27 \text{ m s}^{-1} \end{cases} \quad (10)$$

The intensity of wind-induced coastal upwelling/downwelling is affected by the persistence of the alongshore wind forcing. Following Shan and Sheng (2022), the persistence of along-shore winds was estimated using the wind impulse (I) at a given time (t) defined as the integration of along-shore wind stress during a past period:

$$I(t) = \int_{t-T}^{t} \tau_a(t')\, dt' \quad (11)$$

where τ_a is along-shore wind stress (which is defined as positive in the upwelling-favourable direction, i.e., the ocean water is to the right of the wind direction), and T is set to be a 48 h rolling window. A large and positive (negative) value of $I(t)$ represents a strong upwelling (downwelling) event at time t.

A temperature-salinity diagram (TS-diagram) was used to examine the water mass distribution along the transect based on the glider observations. Only observations below 30 m were used to decrease the effects of short-term variability due to surface heat fluxes. Additionally, cross-correlations were conducted between the temperature and dissolved oxygen observations offshore and inshore (made by the glider and the sensor in St. Margarets Bay, respectively).

4.4 Results

4.4.1 Water Mass Distribution

To examine distributions of observed temperature, salinity and DO over the inner ScS, a TS-diagram was constructed with an overlay of DO values (Figure 4.3). The glider intercepted a warmer (~14-16°C) and fresher (~30-31) surface water mass that had a lower DO signal (7.94 ± 0.12 mg L^{-1}; "surface mixed layer" in Figure 4.3), also consisting of a small offshoot of similar temperatures and DO but more saline (~31-32). The glider also encountered a deeper (intermediate) water mass that was denser than the surface as it was cooler (~3-5°C), and more saline (~31.5-32.5; CBS-CIL in Figure 4.3); this water mass also contained the highest DO signal (9.44 ± 0.30 mg L^{-1}). Lastly, there was a water mass with higher temperatures than the previously described CBS-CIL (5.5-

7.5°C), the highest salinity (33-33.8), and the lowest DO (7.68 ± 0.33 mg L^{-1}; WSW in Figure 4.3), representing the deepest part of the transect. Waters with T,S characteristics in between the CBS-CIL and WSW lie along a major mixing line connecting the two water mass endpoints.

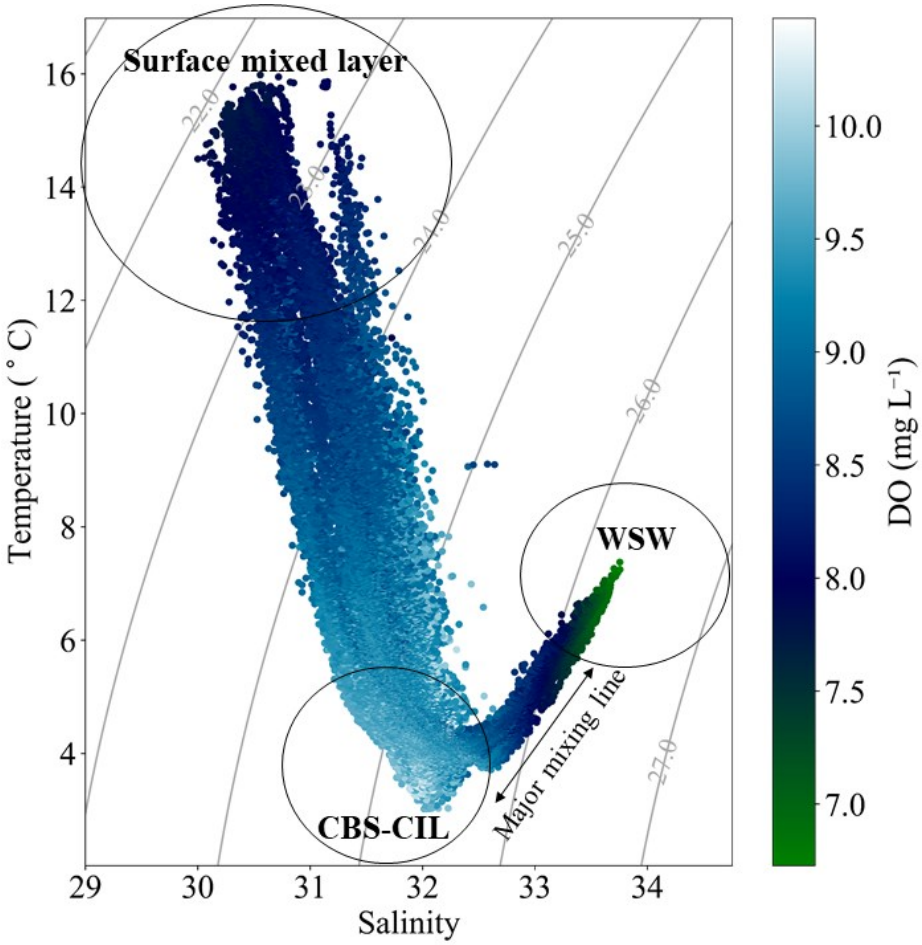

Figure 4.3 Temperature-salinity diagram based on Slocum glider observations along the full transect, including the isopycnals (-1000, kg m^{-3}). The colour scheme corresponds to the DO (mg L^{-1}) distribution, with light blue indicating highest values and green indicating lowest. The relevant water masses are indicated as the surface mixed layer, Cabot Strait – Cold Intermediate Layer (CBS-CIL) and Warm Slope Water (WSW), with the major mixing line between the latter two.

4.4.2 Along-Shore Variability

The vertical stratification of observed hydrography along the glider route over the inner ScS featured a two-layer system, divided by a pycnocline which shallowed from about 60 m near Shelburne Bay (I in Figure 4.4) to about 20 m near St Margarets Bay

(IV) during the observation period. The thermocline delineated a warm surface layer of 15.3 ± 0.73℃ (mean ± SD) from a cold deep layer of 4.72 ± 0.78℃, with some variations in the cross-shelf direction depending on the offshore distance of the glider (Figure 4.4a, b).

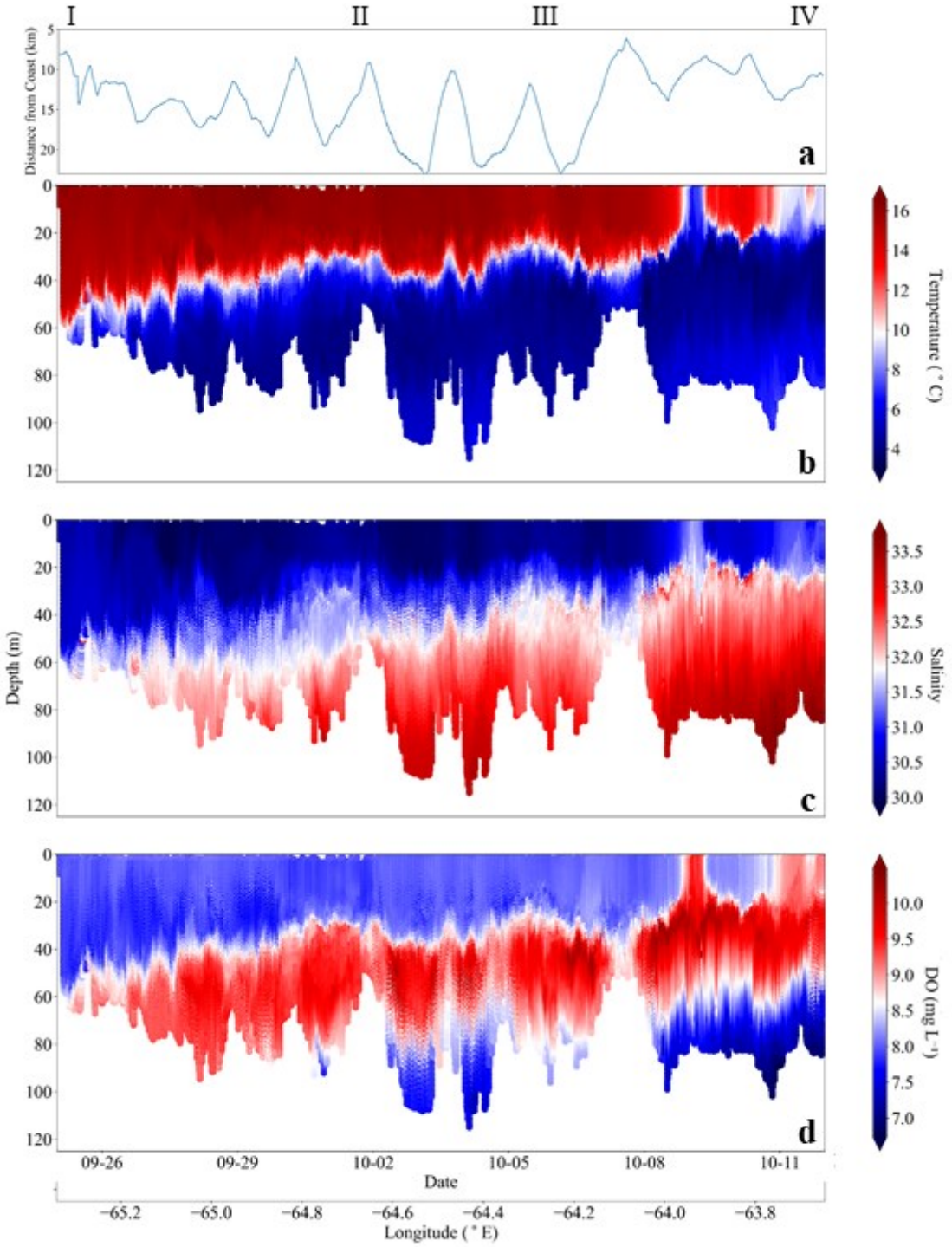

Figure 4.4 The distance to shore along the glider transect (a), the vertical distribution of temperature (°C; b), salinity (c), and dissolved oxygen (DO, mg L^{-1}; d), along the Slocum glider transect (September 25 – October 12 2020). The glider was programmed to turn 2 m above the seafloor, indicated by the white area in each plot. The shoreline waypoints are indicated by roman numerals (Shelburne Bay, I; Liverpool Bay, II; Lunenburg, III; St. Margarets Bay, IV). Dark red colours indicate highest temperature, salinity, oxygen while dark blue colours indicate lowest.

Adjacent to Shelburne Bay (I) on September 26, the thermocline reached nearly to the seafloor, but then shallowed to ~30 m by Liverpool (II) on October 1. The thermocline remained at ~30 m until October 9, between Lunenburg (III) and St. Margarets Bay (IV), when a strong vertical mixing event occurred. This intense mixing event resulted in a collapse of the thermocline and a full cooling of the water column to 5.35 ± 1.14°C through the upwelling of deep water to the surface. This mixing event lasted for ~11 h before the thermocline was re-established at ~20 m. The two-layer system persisted until the end of the transect when there was another but less pronounced upwelling event which lasted ~13 h and lowered surface temperatures to 8.94 ± 0.64°C. After this upwelling event, there was brief surface warming in the upper 10 m to 10.2 ± 0.69°C followed by re-cooling to 9.26 ± 0.61°C for the remaining 10 h of the transect.

The observed halocline had similar characteristics as the thermocline, with lower sea surface salinity of 30.5 ± 0.35 and high sub-surface salinity of 32.6 ± 0.32 (Figure 4.4c). The halocline was less clearly defined compared to the thermocline as it was distributed across 15 m depth at the beginning of the transect and stretching to 30 m deep by October 1, near Liverpool (II). The first vertical mixing event between Lunenburg (III) and St. Margarets Bay (IV) on October 9 upwelled marginally higher saline waters (31.5 ± 0.10) to the surface. The brief upwelling event at the end of the transect also resulted in a slight increase in salinity to 31.2 ± 0.01.

The vertical oxygen distribution consisted of a three-layer system with the oxycline delineating low oxygen surface waters (8.05 ± 0.11 mg L^{-1}) from the high oxygen intermediate waters (9.21 ± 0.50 mg L^{-1}). Below the intermediate waters, the oxygen declined to levels similar to the surface (8.22 ± 0.32 mg L^{-1}). Similar to the thermocline, the observed oxycline shallowed throughout the glider route until the first mixing event on October 9 (Figure 4.4d) when the upwelling event moved the high oxygen waters

(9.57 ± 0.29 mg L^{-1}) from intermediate depths to the surface, rather than low oxygen waters from the deepest regions of the transect. Similarly, at the end of the transect, the second upwelling event resulted in a rise in DO in the surface layer to 9.01 ± 0.14 mg L^{-1}.

4.4.3 Cross-Shore Variability

The physico-chemical conditions over the ScS were found to have significant variability in both the along-shore and cross-shore directions. The zigzag transect by the glider along the inner ScS allowed for the examination of this cross-shore variability (Figure 4.5a). At the beginning of the glider deployment, near Shelburne, the observed vertical profiles of temperature, salinity and DO along the short glider transect approximately in the cross-shelf direction revealed a mixed layer to depth of ~40 m with temperatures of 15.6 ℃, salinity of 30.3 and DO of 7.94 mg L^{-1} (Figure 4.5b). Below the surface mixed layer, noticeable differences occurred in the observed hydrography between the inner and outer profiles. The inner and outer profiles were defined as the vertical profiles of observed hydrography and DO over the inner and outer segments of the short cross-shore transect, respectively. The inner profiles were warmer (12.1 ℃ inner and 9.28 ℃ outer profiles), fresher (30.9 inner and 31.5 outer profiles), and less oxygenated (8.32 mg L^{-1} inner and 8.78 mg L^{-1} outer profiles) than the outer profiles. However, the middle profile (defined as the observed vertical profile at the middle point of the short cross-shore transect) was the warmest, freshest and least oxygenated (13.1℃, 30.8, 8.25 mg L^{-1}, respectively) in comparison with the other profiles. Lastly, there was no clear oxygen maximum zone observed in any of the profiles, as the oxygen increased consistently until the seafloor.

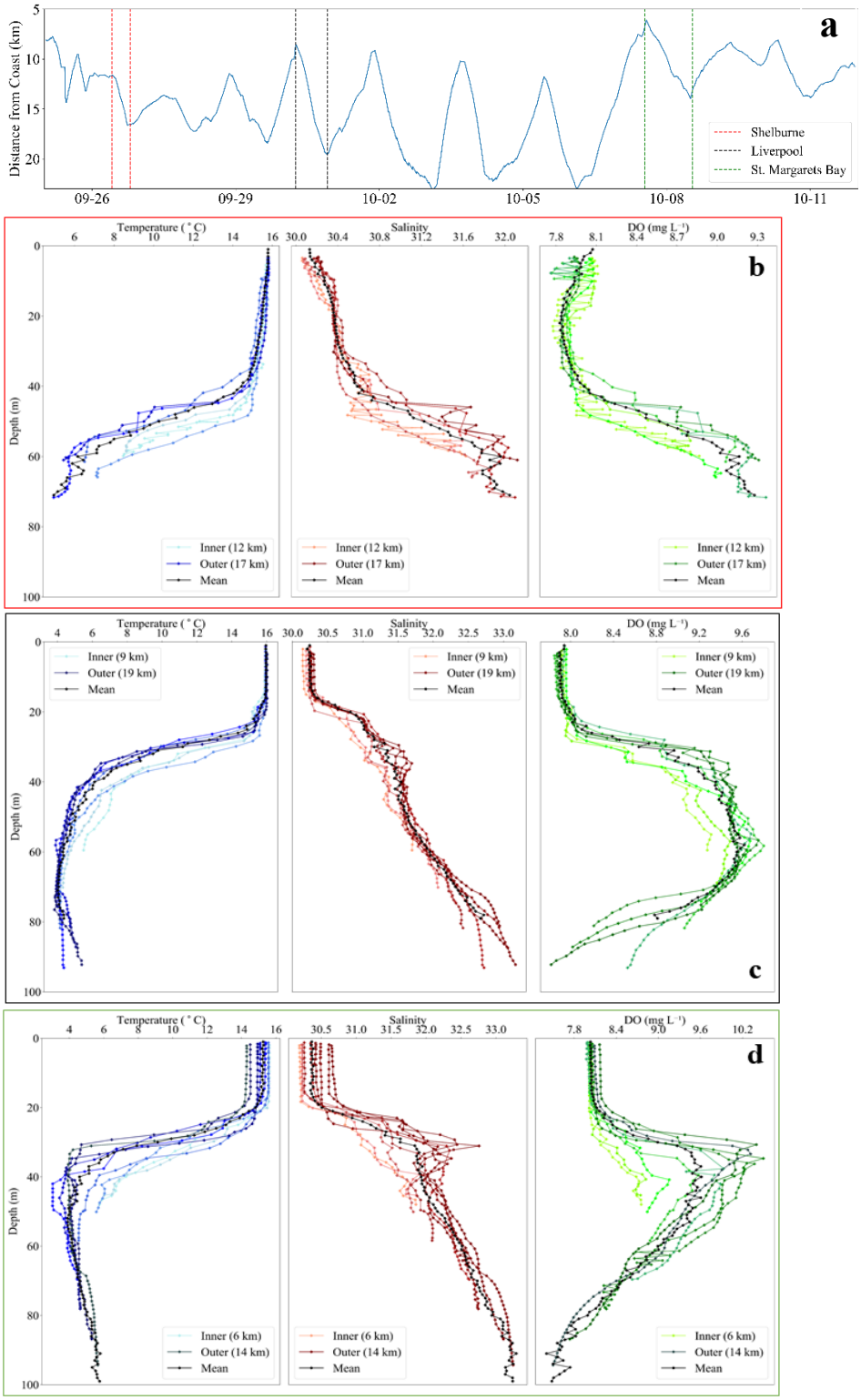

Figure 4.5 Three cross-shore transects selected on the full along-shore glider track (a) and the subsequent temperature (°C; blue), salinity (red) and DO (mg L^{-1}; green) profiles for the transect near Shelburne (b), near to Liverpool (c) and near St. Margarets Bay (d). The lightest colours indicate the profiles closest to shore, while the darker colours indicate those furthest from shore.

As the glider reached Liverpool (II), a similar pattern was observed (Figure 4.5c). The inner and outer profiles were, again, distinct as the inner profile was warmer (8.32°C inner and 6.42°C outer), fresher (31.3 inner and 31.6 outer profiles) and less oxygenated (8.93 mg L^{-1} inner and 9.32 mg L^{-1} outer profiles). However, in this region of the along-shore transect, the mixed layer was only 20 m deep and the oxygen maximum was apparent at ~60 m.

Towards St. Margarets Bay (IV), the mixed layer became more heterogeneous over the cross-shore transect as the inner profile surface waters were warmer (15.5°C inner and 14.2°C outer profiles) and less saline than the outer profiles (30.2 inner and 30.7 outer; Figure 4.5d). Below the surface, the inner profile temperature was more similar to the outer than in the previous cross-shore transects; however, on average, the inner profile was warmer than the outer by 3.16°C. The salinity and DO were lower for the inner profiles compared to the outer profiles by 0.6 and 1 mg L^{-1}, respectively. The DO maximum was observed at 40 m in the outer profiles and the inner profiles never reached a maximum. The DO within the inner profiles increased by an average of 0.9 mg L^{-1} until the glider reached the seafloor.

4.4.4 The Role of Local Wind Forcing

Between Lunenburg (III) and St. Margarets Bay (IV), the glider remained relatively close to the coast, and intercepted an upwelling event (grey bar in Figure 4.6b). This upwelling period was preceded by strong along-shore winds, with a maximum wind speed of 15.3 m s^{-1} and stress of 0.39 Pa to the northeast, and negative cross-shore wind stress of -0.29 Pa (purple bars in Figure 4.6c, d, e).

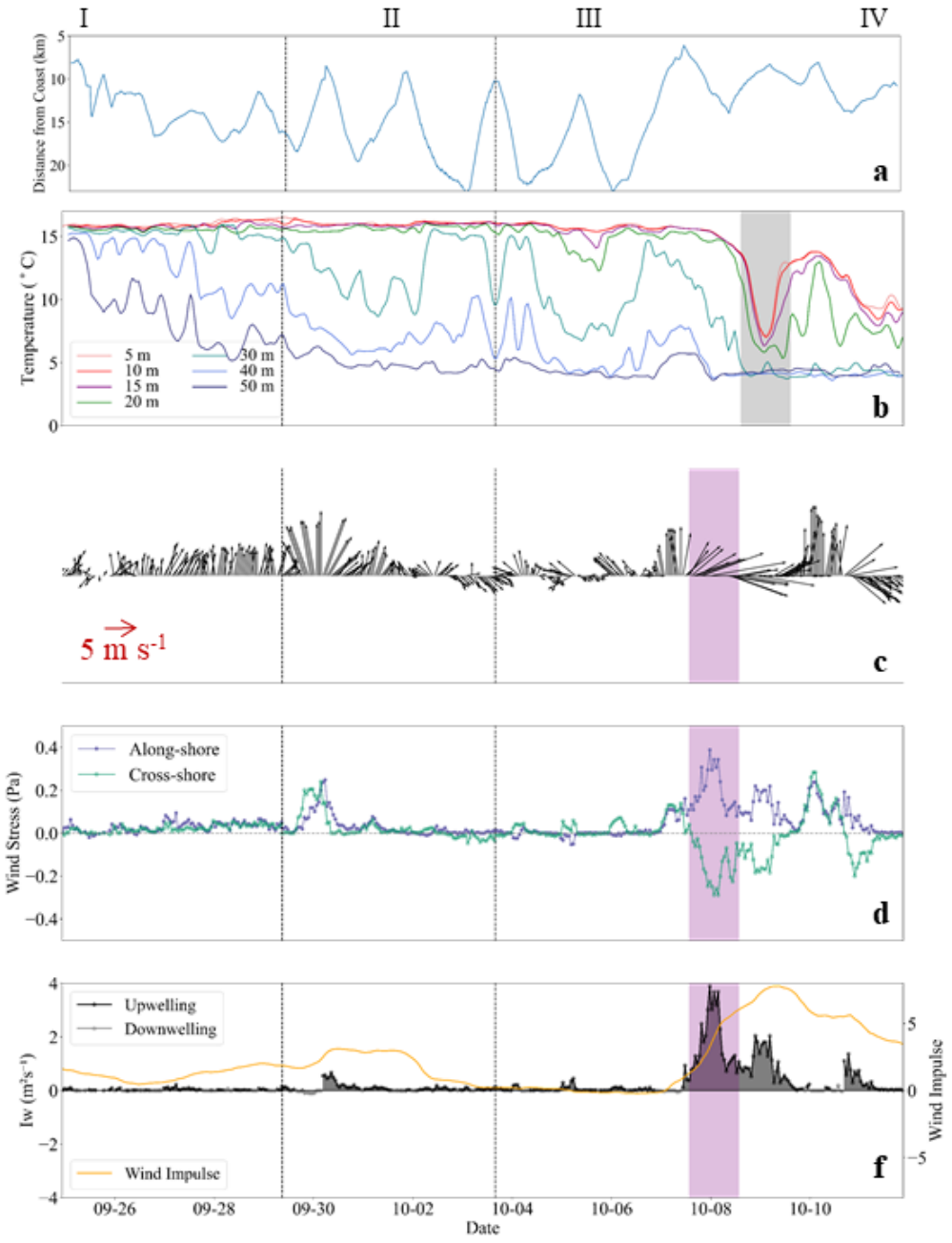

Figure 4.6 The distance to shore along the glider transect (a), temperature observations (°C) from the Slocum glider at 7 depths (5-50 m; b), the associated wind vectors (m s^{-2}; c), and the along-shore (U, m s^{-1}; purple) and cross-shore (V, m s^{-1}; teal) wind components (d) for the duration of the transect. In (f), the Ekman transport (I_w, m^2 s^{-1}) depicting upwelling (black) and downwelling (grey), as well as the wind impulse (orange). Each plot is between September 26 and October 12 2020. The grey bar indicates the strong upwelling event, while the purple bar indicates the wind components 25 h prior to this period. The black dotted lines indicate the transition between winds each of the three stations: Shelburne, Liverpool and Lunenburg; while the roman numerals indicate the coastline waypoints: Shelburne Bay, I; Liverpool Bay, II; Lunenburg, III; St. Margarets Bay, IV.

The along-shore wind driven Ekman Transport (I_w) was relatively low with a slight peak on September 30, followed by low values until a large increase on October 8 reaching 3.9 $m^2 s^{-1}$ (Figure 4.6f). To further quantify this, wind impulse was calculated from the wind stress over the previous 48 h (Figure 4.6f). During the upwelling event, persistent and strong northeastward (along-shore) winds occurred for at least 2 days culminating in a wind impulse of 7.8, ultimately resulting in upward movement of sub-surface waters. Prior to the large upwelling event, at the start of the Liverpool wind section (II) around September 30, along-shore winds were present but upwelling was not observed. This was likely due to low winds prior to this period, with average I_w and wind impulse 0.2 $m^2 s^{-1}$ and 1.5, respectively, creating inconsistent conditions for upwelling.

4.4.5 Offshore-Inshore Interaction

The DO-temperature sensor within St. Margarets Bay was compared with the glider observations when the glider was located offshore, adjacent to the Bay (IV) between October 7-12 (Figure 4.7). Prior to the upwelling period, there was very little variation in the inshore sensor temperature and DO observations (coefficient of variation was 0.97%), resulting in low cross correlation values with glider observations (0.31; Figure 4.7a, b). However, the upwelling event was associated with a similar event observed in the Bay, with a lag time of 30 h. The upwelled waters from further offshore were likely advected inshore resulting in the decreased temperatures observed in the Bay.

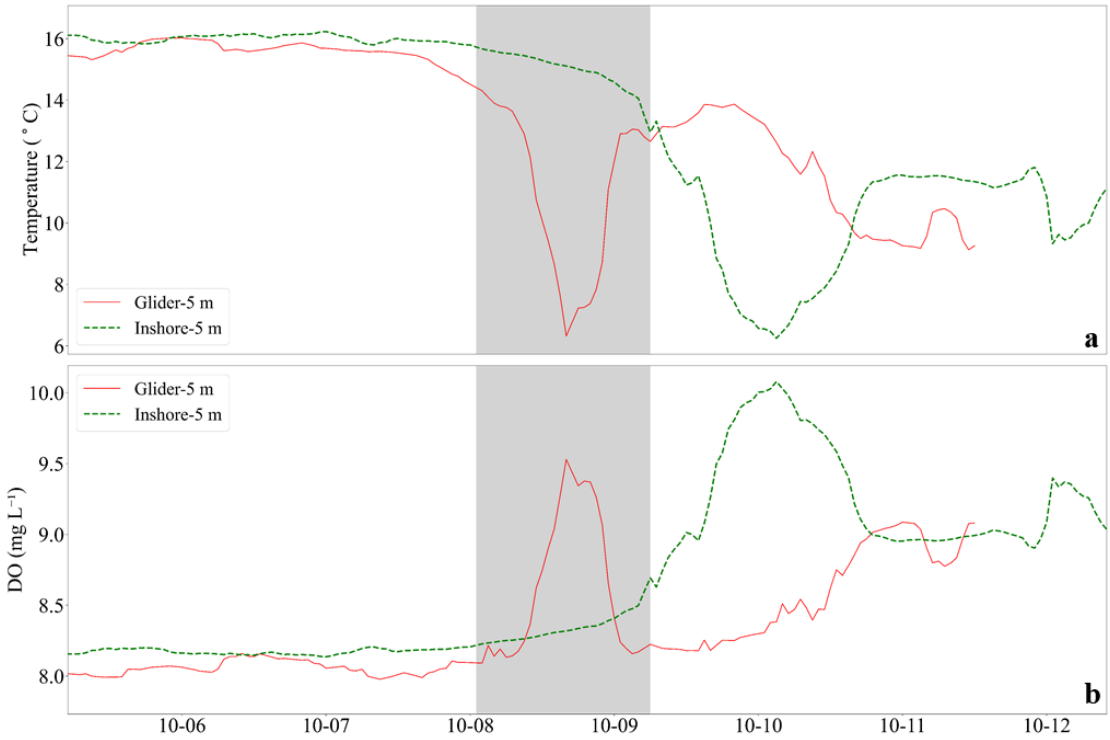

Figure 4.7 Temperature (°C; a) and DO (mg L^{-1}; b) based on the Slocum glider observations at 5 m depth (red) and inshore observations from a sensor placed at 5 m within St. Margarets Bay (green).

The magnitude of the upwelling was comparable between offshore (glider) and inshore (bay sensor), with temperature in the glider observations decreasing from 15.5°C to 6°C while the inshore sensor recorded a decrease from 16°C to 6.3°C. The DO values followed the same pattern that temperature, though the change was slightly higher inshore, from 8.13 mg L^{-1} to 10.1 mg L^{-1}, than at the position of the glider, from 7.98 mg L^{-1} to 9.53 mg L^{-1}. Following the upwelling event, both offshore and inshore values recorded an increase in temperature (decreases in DO), likely due to the advection of replacement surface waters that were warmer and contained less DO.

4.5 Discussion

Cross-shore advection and upwelling over the inner ScS have been described in the past across all seasons, based on satellite remote sensing data, moored observations, and numerical studies (e.g., Petrie et al. 1987; Umoh and Thompson, 1994; Greenan et al.

2004; Chegini et al. 2018). Glider and ship-based measurements have also traditionally been conducted in the cross-shore direction on the ScS. In this study, a Slocum glider was used to collect high resolution spatial data of hydrography and DO in a zigzag route following approximately the coast over the inner ScS, which was the first coastal along-shore transect to be conducted in this area. Analysis of the glider measurements revealed large cross-shelf variations in temperature, salinity and DO, with warmer, fresher and lower oxygenated shoreward waters over the inner ScS. The glider observations also demonstrated that wind forcing significantly affects the local hydrography over the inner ScS, particularly regarding the wind-generated cross-shelf transport of water masses and wind-induced coastal upwelling. Lastly, strong and persistent winds of minimum 2 days were found to generate advection of cold, oxygen-rich upwelled waters into coastal bays.

4.5.1 Water Mass Distribution

The vertical structure of the coastal waters in this study were clearly defined with a warmer, fresher mixed layer above denser waters that were cooler and more saline. The warmer, fresher surface waters also contained relatively low DO. There was an offshoot of the surface waters that were similar in temperature but saltier, which occurred throughout the transect, rather than in one region, indicating that perhaps the glider intercepted intermittent, more saline waters advected in from either off-shore or along-shore. Much of the variability in temperature-salinity-oxygen on the continental slope and shelf is due to the low frequency nature of water mass structure (Petrie and Yeats, 2000). The spatial and temporal circulation structure across the Southwestern ScS is characterized by both the topography, with shallow outer banks, deep inner basins and cross-shelf channels that link these two, and by the dominant currents in the area (Han and Loder, 2003). Partial gyres due to the topography may have resulted in the advection of observed offshore water masses to the coast.

The deeper, cooler waters with high DO had intermediate salinities, which can be associated with the Cabot Strait-Cold Intermediate Waters (CBS-CIL; Dever et al., 2016). Dever et al. (2016) explored the seasonal differences in water masses within the same system and noted that the waters emanating from the inshore Labrador Current have similar T-S characteristics as the CBS-CIL; however, those waters tend to be cooler than the water masses observed in the present study. Additionally, a deep warmer, saltier

water mass with the lowest DO was observed, likely due to Warm Slope Water (WSW) intrusion. This was also described by Dever et al. (2016), although the present study observed lower temperatures and salinities than their study. The former study was conducted cross-shore towards the Slope, while the present study was consistently on the inner shelf and may have observed water mass mixing as the WSW was transported towards the coast. Finally, there was also deep water mixing between the WSW and CBS-CIL (indicated by the major mixing line in Figure 4.5), as there was a region of higher salinities and temperatures than the CBS-CIL but contained lower DO. Although the distribution of water masses described in this study corresponded well to those found in Dever et al. (2016), this study further contributed the DO concentrations for each water mass, increasing our understanding of DO dynamics and variability on the ScS.

4.5.2 Along-Shore Dynamics

Throughout the study period, until the major upwelling event, the vertical profiles of observed temperature and salinity made by the glider were characterized by a well-defined two-layer system. Surface waters were warmer and fresher, while bottom waters were cooler and saltier. This indicates that the glider captured the summer condition of hydrography over the inner ScS during the study period, in contrast to the previously described winter conditions from Dever et al. (2016), as cold surface waters with relatively low salinity above a deeper warm, salty layer.

Prior to the upwelling event, the vertical structure of DO over the inner ScS featured a three-layer structure in the vertical, with low oxygen at the surface ("surface waters"), well-oxygenated intermediate waters ("CBS-CIL"), and oxygen-poor bottom waters ("WSW"). It is important to note that the lowest observed oxygen was 6.73 mg L^{-1} and no hypoxia (typically defined as between 2-5 mg L^{-1}) was found along the glider transect. In the winter/spring, surface cooling results in higher surface DO compared to the summer/autumn, while the intermediate and deep waters remain relatively similar between the two time periods (Zorz et al. 2019). This will then affect the three-layer system, reducing it to two-layers with a high oxygen surface-intermediate layer and a low oxygen deep layer in the winter/spring. Therefore, the vertical structure of temperature-

salinity-DO is highly seasonal, and it is important to understand how these vary throughout the year to improve knowledge of the system dynamics.

4.5.3. Cross-Shore Dynamics

The along-shore current is dominant on the inner shelf with a mean speed of 0.13 m s^{-1} consistent with the southwest flow of the NSC; cross-shore currents are documented as much lower at 0.031 m s^{-1} (Greenan et al., 2004). Therefore, cross-shore advection is mainly due to wind-induced currents and small-scale eddy-type currents associated with the NSC. Cross-shelf vertical structure has been observed along the Halifax line (Umoh and Thompson, 1994; Dever et al., 2016; Shen and Shang, 2022); however, the method employed in this study allowed for a more detailed analysis in both temporal and spatial resolution of the cross-shore structure. In general, there was a common cross-shelf structure to the profiles observed. The inner regions of the transects were warmer, fresher and lower in DO compared to the outer regions. In contrast, Umoh and Thompson (1994) explored the long-term mean of temperature and salinity across the ScS and found that temperatures decreased shoreward, however there were lower salinities at the coast, consistent with the present results. As water mass structure is highly seasonal, using a monthly-mean averaged over several years may not capture the same dynamics as described in the present study.

The first cross-shore transect, near Shelburne, contained a deeper surface mixed layer compared to the following two cross-shore transects. This is likely due to the strong tidal regime near the southwestern-most part of the domain (Clark's Harbour and Yarmouth), mixing the waters to 40 m. The effects of tides on the hydrography were weaker as the glider moved northeast to the subsequent two transects, away from the strong tidal regime. Moreover, the surface mixed layer was homogenous across the shelf in each of the first two cross-shore transects; however, the surface mixed layers of the inner and outer profiles differed in the third cross-shore transect. The winds during the first two transects were predominantly in the cross-shore direction, resulting in cross-shore mixing of the surface water masses and creating homogeneity between the inner and outer profiles. Conversely, the third transect near St. Margarets Bay coincided with strong along-shore winds, potentially resulting in more mixing in the along-shore direction and

causing disparity between the inner and outer profiles. Furthermore, the third transect was located offshore of St. Margarets Bay, a bay that due to the irregular coastline has different physical properties compared to the adjacent coastal waters (Shan and Sheng 2022). This suggests that the irregular coastline could have enhanced the differences in profiles observed at this transect compared to the previous two.

This was the first study on observed along-shore and cross-shore variability in DO profiles over the inner ScS, since most previous observational studies focused on temperature and salinity (e.g., McLellan et al., 1957; Umoh and Thompson, 1994; Townsend et al., 2015; Wang et al., 2022). There was strong variability in DO, both in the cross-shore and along-shore directions, highlighting the importance of this type of sampling regime. Higher DO was associated with lower temperatures observed in the outer region of the transect, as lower water temperatures increase oxygen solubility. In the third transect, the DO in the outermost profiles were almost 2 mg L^{-1} higher than the DO maxima of the 3 innermost profiles. The temperature-salinity-DO in the outer profiles coincide with the coldest-highest DO proportion of CBS-CIL water mass. However, the innermost profiles which are relatively shallow, more resemble a mixture of CBS-CIL and surface water. Therefore, water mass mixing combined with the shallow nature of the coastal zone can affect the cross-shore variability in hydrography and DO of this system.

4.5.4 The Role of Local Wind Forcing

Winds play a salient role in the circulation of near-surface water masses, and highly influence coastal shelf ecosystems (Petrie et al., 1987). Around September 30, near the Liverpool weather station, winds were predominantly directed in both the cross- and along-shore directions, and although there was cooling of the subsurface waters, the winds were not sufficient to cause a similar upwelling event as observed on October 9. The strong upwelling event on October 9 was triggered by persistent winds to the northeast (along-shore) for 2 days prior. However, the event seemed to have stemmed from the intermediate waters as the deepest oxycline did not change over the course of the upwelling event and the salinities were not raised to the highest values. This likely means that the winds would need to be stronger or for a longer period to raise the deepest

waters to the surface. It is important to note that winds are not the only driver of onshore advection. Cyclonic (anticyclonic) mesoscale eddies over basins (banks) further offshore can entrain and transport water with certain temperature, salinity, and DO properties to the coast (visible in Figure 4.2; Loder et al., 1997; Combes et al., 2013). These mesoscale eddies are primarily generated by larger scale upwelling and alongshore currents or Rossby waves (Marchesiello et al., 2003; LaCasce and Pedlosky, 2004; Combes et al., 2013).

During the upwelling events, oxygen-rich waters were upwelled from the intermediate layer, resulting in increased surface oxygen. This could have impacts on the biota living in this area, supplying them with high oxygen waters. This contrasts with other studies that found upwelling had raised oxygen-poor waters from depth, decreasing surface concentrations, though these studies were conducted on the ScS (Lewis, 1981; Blanco et al., 2001; Chavez et al., 2018; Largier, 2020). Yu et al. (2015) developed a model for the Gulf of Mexico describing the effects of wind forcing on hypoxia and found that upwelling-favourable winds resulted in hypoxia while downwelling winds simulated no hypoxia. There would likely be upwelling of oxygen-poor waters in the winter/spring when the surface-intermediate layers are relatively homogenous and higher in DO than at depth; though further studies are needed to explore these seasonal differences in DO dynamics.

4.5.5 Offshore-Inshore Interaction

Bay-ocean interactions have not been widely documented in the literature. The flushing rates of nutrients in coastal embayments have been examined in the past (Heath, 1973; Petrie and Drinkwater 1978; Lewis and Platt, 1981), though the connection to the physical properties of the adjacent coastal shelf is lacking. Local processes such as freshwater discharge and eutrophication are important factors affecting DO in coastal areas (Xia et al. 2011; Coffin et al. 2018); however, it is crucial to understand whether external oxygen dynamics on the shelf also play a role. For example, ocean-bay stratification (and thus, density) differences will be important in the circulation and baroclinic exchange of water masses between the two (Barton et al., 2015). Also, depending on the size of the bay, outer areas of coastal embayments will likely

experience more of the wind-driven transport than inner areas, while the inner areas will be more influenced by tidal-driven circulation (Barton et al., 2015; Burke et al., 2021).

Tides have been examined in the past as a source DO renewal of semi-enclosed bays and estuaries, primarily where the prevalent tidal cycle is semi-diurnal (e.g., Santana et al., 2018; Burke et al., 2021). It is unclear whether shelf circulation in this region of Nova Scotia would influence oxygen concentrations as well. Barton et al. (2015) found that upwelling and downwelling events on the coast can influence circulation within a semi-enclosed bay, though their study occurred in an intense upwelling system of the Iberian peninsula. The lag between upwelled waters observed by the glider and recorded by the sensor in St. Margarets Bay was ~30 h. According to Narella and Vankatesh (1989), there is a dominant tidal cross-shore current close to St. Margarets Bay and away from the influence of the strong tidal regime of the southwestern-most part of the domain (Yarmouth and Clark's Harbour), with a speed of 0.05-0.2 m s^{-1}. The distance between the inshore sensor and the glider was about 26 km, thus it would take between 35-144 h for the water to travel that distance. The observed lag of ~30 h for the transport of water is around this range, indicating it is possible that the upwelled waters travelled into the bay via this cross-shore current combined with the strong cross-shore winds observed shortly after the upwelling event.

This study also determined that low wind impulse, or winds that are relaxed or inconsistent, did not lead temperature or DO exchange in St. Margarets Bay. The calculated wind impulse determined that 2 days of persistent winds was required to transport upwelled waters to the Bay. This is congruent with the findings from De Young et al. (1993) on a coastal embayment in Newfoundland that found a correlation between wind and temperatures within the bay with a lag time on the order of 2-10 days. Lastly, the upwelling caused an increase in DO to the bay; however, the transport of low oxygen cannot be disregarded. Multiple studies (e.g., Rodriguez et al., 1991; Takahashi et al., 2009; Rixen et al., 2012; Coogan et al., 2019) found that there can be transport of low oxygen to coastal embayments in highly productive regions of the world due to oxygen minimum zones found in the subsurface. This may also be possible on the ScS if intense upwelling transports low oxygen up from the deepest depths. Additionally, though at much larger scales than measured in this study, warm and cold core rings emanating from

the Gulf Stream may transport oxygen to the shelf and could then influence the embayments. Rings are eddies that entrap a core water mass from a different origin than the Gulf Stream. Rings forming to the south or east entrap cold waters of Labrador Slope origin (cold core), while rings that form from the north or west entrap warm waters from the Sargasso Sea (warm core; Wiebe et al., 1976, Bishop et al., 1990). The properties of these rings are then conserved as they are advected to the ScS, potentially influencing the temperature, salinity and DO present along the coast.

4.6 Conclusion

The present study demonstrates the efficiency of glider observations using a zigzag protocol for temporal, along-shore and cross-shore variability of hydrography and DO. Additionally, having access to high spatial and temporal resolution around coastal embayments helps to quantify the role that the inner shelf may play in bay-wide circulation. Better understanding of this interaction can lead to improved aquaculture farm management. For instance, advection of oxygen-rich waters to bays due to upwelling, especially in the summer when oxygen levels are relatively low in coastal surface waters, decreases fish stress and improves fish growth and welfare (Abdel-Tawwab et al., 2019).

This study documented a strong upwelling event in mid-October on the inner ScS, though upwelling occurs more frequently during the summer when winds are predominantly blowing from the southwest and west. Moreover, the high wind impulse, due to along-shore winds persisting on the order of 2 days, was dominant in controlling the intrusion of cooler, higher oxygenated waters to St. Margarets Bay. It is important to note that many upwelling zones upwell low oxygen to the surface instead, which may also occur in this system if there were either higher winds for a more prolonged period, or in the spring when warmer waters at depth may upwell low oxygen to the surface. Understanding the intricacies of along- and cross-shore variability in temperature, salinity and DO is increasingly important as climate change progresses and aquaculture farmers seek to adapt management practices.

CHAPTER 5 PROJECTIONS OF DISSOLVED OXYGEN VARIABILITY UNDER CLIMATE CHANGE SCENARIOS ON THE SOUTHWESTERN SCOTIAN SHELF

5.1 Abstract

Climate change is projected to cause a 3-4% decline in the ocean oxygen inventory by the year 2100. This is expected to cause profound changes to marine ecosystems, through shifts in biodiversity, habitats and ecological interactions. The main contributor to this decline is increased sea temperatures, as it causes reduced oxygen solubility while increasing biological metabolism. Moreover, increased temperatures are projected to be highest (0.5°C decade^{-1}) on the Scotian Shelf. There are many consequences of climate change expected to impact dissolved oxygen on the Scotian Shelf, including: increased temperatures, weakened Gulf Stream and Labrador Current, increased storm events, and decreased general wind forcing. Numerical experiments using an oxygen model were conducted for the southwest Scotian Shelf. The effect of the four aforementioned potential stressors on oxygen dynamics were examined, along with a combined experiment which accounted for the interacting effects of increased temperature, weakened Gulf Stream-Labrador Current, and weakened wind forcing. Weakened Gulf Stream-Labrador Current resulted in the most significant decrease in oxygen on the inner Scotian Shelf, while increased winds (due to stronger storm events) resulted in the highest decreases in oxygen on the mid-outer Scotian Shelf. Increased knowledge of the drivers of oxygen dynamics within aquaculture farms and the adjacent waters is important for the management of the region as well as for the future of aquaculture production and management of coastal economies.

5.2 Introduction

Increasing atmospheric greenhouse gas emissions are warming the oceans at a rapid rate (Johnson and Lyman, 2020). There is evidence that ~3/4 of global coastal areas have increased in sea surface temperature (SST) between 1982 and 2010 (Lima and Wethey, 2012). On the Northwest Atlantic shelf in particular, over the past 50 years, there has been a linear increase in SST of 0.37 ± 0.06 °C decade^{-1} (Chen et al., 2020). Future SST changes are projected to be greatest on the Scotian Shelf (ScS); warming of

0.5°C decade^{-1} is predicted to occur based on the representative concentration pathway (RCP) 8.5 from the Coupled Model Intercomparison Project phase 5 (CMIP5; Alexander et al., 2018). Increased temperatures also affect the ocean oxygen inventory. This can occur through: increased metabolic rate, net primary production and subsequent oxygen consumption (Tait and Schiel, 2013; Rabalais et al., 2014; Brennan et al., 2016); decreased oxygen solubility (Hildebrand, 1916; Emerson et al., 2002; Shaffer et al., 2009; Oschlies, 2019); decreased ventilation to the ocean interior via increased stratification (Breitburg et al., 2018; Stramma and Schmidtko, 2019); and lastly, a weakening of the Atlantic Meridional Overturning Circulation (AMOC; Yamamoto et al., 2015; Schmidtko et al., 2017). These changes to temperature and DO can significantly impact biodiversity, species habitats and ultimately, ecosystem functioning (Khan et al., 2013; Nunez et al., 2019). Moreover, the potential effects on fisheries and coastal economies, including net pen aquaculture production, have not been widely examined. The metabolism and consequent respiration of ectothermic organisms increase with temperature, increasing the amount of oxygen needed for growth and survival. Fish within net pen aquaculture farms have the added challenge of containment, having to withstand the conditions in which they are placed. Thus, there are limitations for growing aquaculture production in coastal embayments due to carrying capacity and potential environmental and welfare issues. A possible solution to this problem is to move net pen farms offshore to more exposed locations. However, it is important to understand how oxygen concentrations may shift with a changing climate, so that farmers can choose adequate locations and improve farm management.

Large scale deoxygenation trends have been documented on the Northwest Atlantic shelf, outpacing the global rate (Claret et al., 2018). A leading cause of this deoxygenation is a weakening of the AMOC by about 15% since the mid-20th century, while numerical models predict a further decrease in the AMOC of 25% by 2100 (Saba et al., 2016; Claret et al., 2018; Caesar et al., 2018). The result of this weakening is a retreat in the oxygen-rich Labrador Current (LC) and subsequent replacement with oxygen-poor subtropical waters emanating from the Gulf Stream (GS) off the shelf. Deep water winter convection in the Labrador Sea homogenizes the water column in the top 1000-2000 m and mixes undersaturated deep waters to the surface for oxygen renewal. The LC then

advects these well oxygenated waters southward ultimately aerating the Scotian Shelf (Yashayaev and Loder, 2016; Lavoie et al., 2017; Koelling et al., 2022). In contrast, the stratified GS has relatively high oxygenated surface waters above oxygen-poor bottom waters. The GS is also expected to slow down as the AMOC weakens (Chen et al., 2019; Chi et al., 2021), and it is unclear how the combination of a weakening in the LC and GS will affect DO on the Scotian Shelf.

Winds also play a salient role in ocean oxygen dynamics, through air-sea oxygen flux, advection of oxygen-rich (oxygen-poor) waters to oxygen-poor (oxygen-rich) areas through wind driven currents, or by generating upwelling of subsurface waters with oxygen properties differing those at the surface. Over the last 40 years, there has been a reported 5-15% decline in surface wind speeds in the northern mid-latitudes, with further decreases projected, due partly to changes in atmospheric circulation as the Earth warms (Vautard et al., 2010; Karnauskas et al., 2018). In contrast, increased latent heat due to climate change is projected to increase severe storms, including thunderstorms, extratropical rain or snowstorms, tropical cyclones and hurricanes (Trenberth 2018). Both weakened wind speeds and increased storm activity will likely result in changes to the oxygen dynamics on the shelf through changes to the air-sea flux, wind driven currents and upwelling.

The simulation and prediction of regional hydrodynamics to investigate the effect that climate change may have on DO in the future require the use of numerical models. Numerical models are idealized representations of a process or concept and are valuable tools for predicting future states of a system. While climate change simulations have been conducted in the Northwest Atlantic (e,g. Belkin, 2009, Saba et al., 2016, Seidov et al., 2016, Alexander et al., 2020; Lavoie et al., 2020), these studies have focused primarily on pH, temperature and salinity, while the effects on DO are less well understood. Additionally, previous model simulations have relatively coarse resolutions (10-50 km), which cannot resolve smaller scale hydrodynamics along the inner Scotian Shelf (e.g. Paiva et al., 1999, Smith et al., 2000, Bryan et al., 2007, Winton et al., 2014, Pereira et al., 2022). The overall goal of this study is to explore the potential effects of climate change on oxygen dynamics on the ScS. A suite of simulations were carried out using a high-resolution (1/108°) numerical oxygen model for the Southwestern ScS. The effect of

the major drivers of change in DO were simulated over a series of scenarios: increased temperature, weakened Gulf Stream/Labrador Current (GSLC), increased local winds for "storm" conditions, and weakened local winds. A final experiment was run with increased temperature, weakened GSLC, and weakened winds together, to represent the full climate change scenario. As the response to climate change can be seasonally dependent (Alexander et al., 2018), this study will also explore these four drivers in the "summer" (August) and the "autumn" (November). The climate change scenarios are compared to a control scenario that represents the conditions in 2018. Exploring how these climate change stressors may impact DO dynamics is important for the management of the region as well as for the future of aquaculture production and coastal economies.

5.3 Methods

5.3.1 Study Domain

The ScS is a 700 km long portion of the Continental Shelf off Nova Scotia (Canada), varying in width from 120-240 km (Hannah et al., 1997; Figure 5.1). The Southwestern section of the ScS (bounded between 43°-45°N, and 63°-66°W) has depths ranging from 30 m at the coast to 300 m within the two large basins (LaHave and Emerald); the average depth is approximately 90 m. The western ScS is unique in its bathymetry, characterized by the two deep basins (LaHave and Emerald) connected by a shallow bank (Sambro) at the midshelf, and three shallow outer banks (Roseway, Baccaro and LaHave).

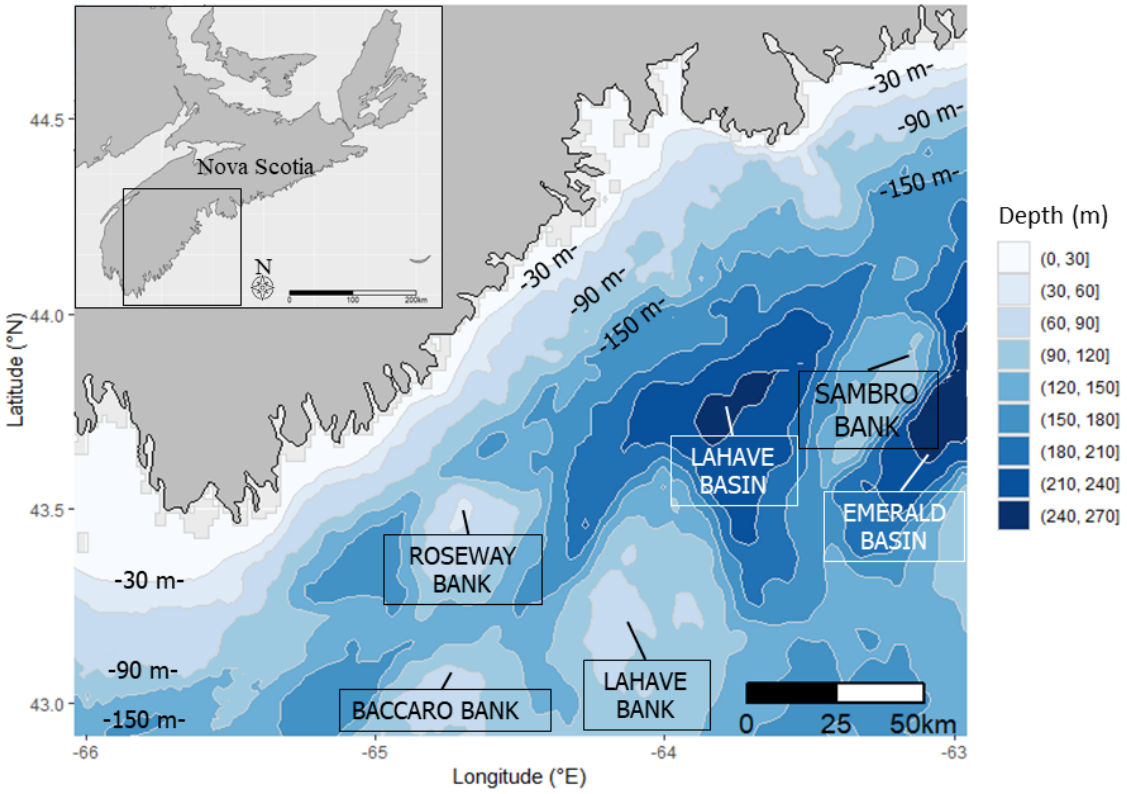

Figure 5.1 Major features of topography over the western Scotian Shelf, including the basins (LaHave, Emerald) and banks (Roseway, Baccaro, LaHave, Sambro) and the isobaths at 30 m, 90 m, and 150 m relevant for the results, and an inset map of Nova Scotia.

On the shelf and shelf break, the mean circulation is dominated by a coastally trapped southwestward jet known as the Nova Scotia Current (NSC; an outflow from the Gulf of St Lawrence that exits the Gulf through the Cabot Strait), and an extension of the Labrador Current from the Newfoundland Shelf (Han et al., 1997; Loder et al., 1997). The NSC meanders offshore around the LaHave Basin, with a weaker branch located closer to shore, most apparent in the summer (Figure 5.2).

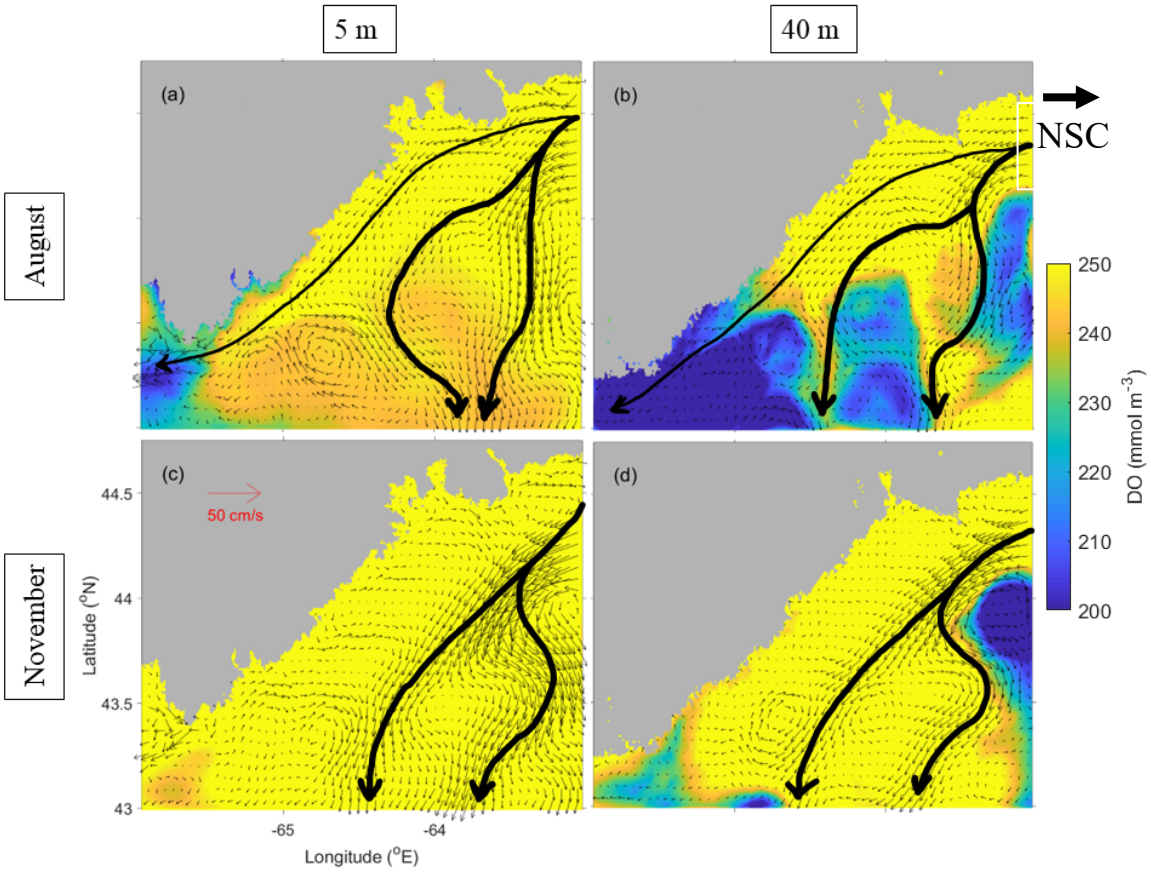

Figure 5.2 Model results of the control scenario (representing the conditions in 2018) with an overlay of the currents at 5 m (a, c) and 40 m (b, d) in August (a, b) and November (c, d). The black arrows indicate the path of the Nova Scotia Current (NSC).

Over the central region, a cross-shelf channel also connects the LaHave and Emerald Basins, and results in water transport from the coast towards the shelf break (Shore et al., 2000). To the southwest of the basins, there is a partial gyre that circulates between the three banks due to the topography, tidal rectification and local circulation (Hannah et al., 2000). On the southwestern region of the ScS there is a strong semi-diurnal tidal regime, influenced by the Fundy-Maine tidal system (Greenberg, 1979). The tidal effects then dissipate up the coast and towards the outer shelf (Hannah et al., 2000). At the slope of the ScS, beyond the shelf break, there is a northeastward jet influenced by the Gulf Stream (Han et al., 1997).

5.3.2 Model Setup

A numerical oxygen model developed by Qiantong Pei (MSc Thesis, Dalhousie University, 2022) and based off Yu et al., (2015) was coupled with a circulation (Regional Ocean Modelling System, ROMS)-ice (Sea Ice Model, CICE) modelling system over Southwest ScS. ROMS is a 3D free-surface, terrain-following ocean model that uses accurate and efficient physical and numerical algorithms for biogeochemical, bio-optical, sediment, and sea ice applications. More details about ROMS are available at https://www.myroms.org/.

The basic governing equations of the ROMS in the Cartesian coordinates are:

$$\frac{\partial u}{\partial t} + V \cdot \nabla u - fv = -\frac{\partial \emptyset}{\partial x} - \frac{\partial}{\partial z}\left(\overline{u'w'} - \nu \frac{\partial u}{\partial z}\right) + F_u + D_u \quad (12)$$

$$\frac{\partial v}{\partial t} + V \cdot \nabla u + fu = -\frac{\partial \emptyset}{\partial y} - \frac{\partial}{\partial z}\left(\overline{v'w'} - \nu \frac{\partial v}{\partial z}\right) + F_v + D_v \quad (13)$$

$$\frac{\partial \emptyset}{\partial z} = \frac{\rho g}{\rho_0} \quad (14)$$

$$\frac{\partial c}{\partial t} + V \cdot \nabla C = -\frac{\partial}{\partial z}\left(\overline{C'w'} - v_\theta \frac{\partial C}{\partial z}\right) + F_C + D_C \quad (15)$$

with the continuity equation:

$$\frac{\partial u}{\partial x} + \frac{\partial v}{\partial y} + \frac{\partial w}{\partial z} = 0 \quad (16)$$

where u, v, and w are the x, y, and z components, respectively, of the velocity vector, V. $f(x, y)$ is the Coriolis parameter, while $\emptyset(x, y, z, t)$ is the dynamic pressure corresponding to:

$$\emptyset(x, y, z, t) = \frac{P}{\rho_0} \quad (17)$$

C is the concentration of the observed tracer (e.g. DO), $\overline{u'w'}, \overline{v'w'}$ are the Reynolds stresses and $\overline{C'w'}$ is the tracer flux. v and v_θ represent the molecular viscosity and diffusivity, F is the term for forcing (u, v) and source/sink for the tracer (C), D is the horizontal diffusive terms.

The oxygen model has a fine horizontal resolution of 1/108° (~700 m east-west, 1 km north-south) and 40 sigma levels in the vertical. The sigma vertical coordinate used is defined as:

$$\sigma = \frac{z-\eta}{H+\eta} \quad (18)$$

Where z is the cartesian vertical coordinate, z = 0 for the equilibrium position of the sea surface, $\eta(x, y, t)$ is the displacement of sea surface from z=0, and H(x,y) is the water depth.

The oxygen model consists of oxygen advection (driven by the ROMS-CICE modelling system), oxygen diffusion, net water respiration (NWR), air-sea oxygen flux, and sediment oxygen consumption (SOC). More information about the oxygen model and the validation and ground truthing of the model is explored in Appendix D.2.

According to Pei and Sheng (in prep.), the governing equations for DO in the cartesian coordinates are:

$$\frac{\partial O_2}{\partial t} = -\left(\mathrm{u}\frac{\partial O_2}{\partial x} + v\frac{\partial O_2}{\partial y} + w\frac{\partial O_2}{\partial z}\right) + \frac{\partial}{\partial x}\left(K_h\frac{\partial O_2}{\partial x}\right) + \frac{\partial}{\partial y}\left(K_h\frac{\partial O_2}{\partial y}\right) + \frac{\partial}{\partial z}\left(K_v\frac{\partial O_2}{\partial z}\right) + NWR \quad (19)$$

where u, v, and w represent the eastward, northward, and upward components of ocean currents, respectively, and O_2 denotes DO concentrations in the study area. K_h and K_v are the horizontal and vertical molecular diffusion coefficients for DO, respectively. NWR is determined through two processes: primary production (PP) and respiration (R), where,

$$NWR = PP - R \quad (20)$$

Respiration rate is linearly dependent on chlorophyll concentration (chl; Packard and Christensen, 2004) such that:

$$R = a(chl) + b \quad (21)$$

Where a and b are coefficients estimated from observations over the southwestern ScS and outlined in Pei (MSc thesis, Dalhousie University, 2022). The chlorophyll and primary production rate were extracted from the Global Ocean Biogeochemistry Hindcast dataset (details provided in Pei MSc thesis, Dalhousie University, 2022).

A previous sensitivity analysis showed that removing NWR only resulted in a 3% change in DO (Pei MSc Thesis, Dalhousie University, 2022). Accordingly, and for the sake of parsimony, this current parameterization of NWR was deemed appropriate for the

simulation of the climate change scenarios. The boundary conditions of DO at the sea surface and sea bottom are defined according to Yu et al., (2005) as:

$$K_v \frac{\partial O_2}{\partial z} = 6 \cdot 2^{T/10} \cdot \left(1 - exp\left(-\frac{O_2}{30}\right)\right), \text{at } z = -h(x,y) \quad (22)$$

$$K_v \frac{\partial O_2}{\partial z} = \frac{Vk_{O2}}{\Delta z}(O_{2sat} - O_2), \text{at } z = \eta \quad (23)$$

where T is ocean temperature, $h(x,y)$ represents local water depths, $z = -h(x,y)$ represents the vertical Cartesian coordinates of the sea bottom. $\eta(x,y)$ represents sea surface elevations, while $z = \eta$ indicates the vertical Cartesian coordinates of the sea surface, Δz is the thickness of the respective grid box, and O_{2sat} indicates the saturated DO, which is a function of temperature and salinity. The gas transfer velocity (Vk_{O2}) is defined as:

$$Vk_{O2} = 0.31 \cdot {u_{10}}^2 \cdot \left(\frac{660}{Sc_{ox}}\right)^{\frac{1}{2}} \quad (24)$$

where u_{10} represents the wind speed at 10 m above sea surface, while Sc_{ox} is the Schmidt number for oxygen provided by Wanninkhof (1992). According to Hetland and DiMarco (2008), the SOC, defined as the biological sink of DO by the benthos, is calculated by:

$$SOC = K_v \frac{\partial O_2}{\partial z} = 6 \cdot 2^{T/10} \cdot \left(1 - exp\left(-\frac{O_2}{30}\right)\right) \quad (25)$$

5.3.3 Numerical Experiments

To assess the sensitivity of DO to four climate change stressors, numerical experiments were run for each month between July and November. The baseline scenario (hereafter control) was run as a representation of the ScS conditions in 2018. The percent changes were chosen to depict severe perturbations from climate change stressors (numerical experiments summarized in Table 5.1). As it remains unclear exactly how temperature, GSLC and wind forcing will change in the future, this study chose extreme cases to examine the individual effects of these stressors on DO.

Table 5.1 Summary of numerical experiments. NARR: North American Regional Reanalysis; GSLC: Gulf Stream/Labrador Current.

	Experiment	Methodology	Magnitude of change	Spectral Nudging/Semi-Prognostic Method
1.	Temperature increased	Increased lateral boundary condition and increased net heat flux	+ 30 % (of boundary condition); air temperature + 5°C	Yes
2.	GSLC weakened	Weakened open boundary conditions of both currents	- 40 %	No
3.	Wind forcing - Increased	Magnitude of default wind velocity field (from NARR) increased	+ 20 %	No
4.	Wind forcing - Decreased	Magnitude of default wind velocity field (from NARR) decreased	- 20%	No
5.	Combined	Same methodology used for 1,2,4	Same change used for 1,2,4	No

Finally, as these stressors are not likely to occur individually, a last experiment was run with the increased temperature, weakened GSLC, and weakened winds together. The increased temperature simulation was run with spectral nudging and semi-prognostic method to reduce the systematic model drifts and model errors in the large-scale circulation. However, these methods smooth the model results and tend to underestimate the effects that wind stress and currents may have, thus these methods were turned off to investigate the effects of wind forcing and the GSLC. To determine the magnitude of the effects that the four stressors may have on the hydrodynamics and DO, the anomaly between the simulation and the control was determined through the percent difference of the monthly-means where:

$$\%\, difference = \frac{simulation - control}{control} \times 100\% \qquad (26)$$

5.4 Results and Discussion

5.4.1 Baseline Conditions

The reference scenario was run in August and November of 2018. In August at 5 m depth, simulated DO was relatively high throughout the study domain, particularly in the northeast region (Figure 5.2a). The lowest simulated DO concentrations were located in the southwest region, where DO was 40-50 mmol m^{-3}[3] lower than the rest of the domain. This was most apparent at 40 m depth, as the lower DO extended out to the banks (Figure 5.2b). This decrease in simulated DO was likely due to the strong tidal regime in this area, causing mixing and subduction of low oxygen to the subsurface. Studies have shown that there is lower oxygen in the surface mixed layer during the summer compared to the subsurface waters (Zorz et al., 2019). At 40 m depth, there were also lower DO concentrations on the banks and the shallower areas of the two basins simulated in the model. Higher oxygen values followed the path of the NSC, likely as it transported cool, oxygen-rich waters to the area.

The modelled thermocline was well established in August (Figure 5.3). A vertical transect from the eastern region of the domain over the LaHave Basin revealed a stable thermocline at ~ 8-12 m, shoaling to ~2-5 m as the transect approached the coastline (44.2ºN). The modelled thermocline remained consistent horizontally along the shelf at ~8-12 m.

[3] mmol m^{-3} was used for this model as it was created for use by all ocean scientists and thus a SI unit was preferred. The conversion to mg L^{-1} is: $mg\ L^{-1} = \frac{(mmol\ m^{-3})}{31.262}$

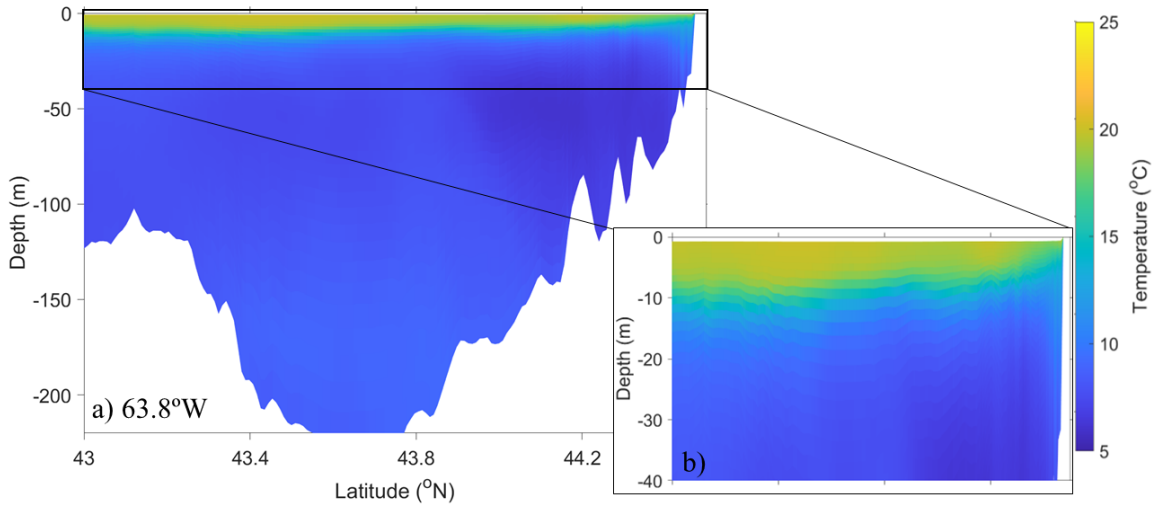

Figure 5.3 Temperature profile along a vertical transect over the full study domain at 63.8ºW longitude (a), and an inset figure with a focus on the top 40 m depth (b).

The modelled oxycline, however, exhibited differences between transects located along the coast, and closer to shore (Figure 5.4). Each of the transects exhibited an oxycline at ~10-20 m with a distinct oxygen maximum between 10 and 35 m depth. The oxygen maximum is likely the result of the shoreward advection of oxygen-rich water masses (Burke et al., in prep.). The transect located towards the west of the model domain, intersecting the shore at 43.8ºN, contained a lower oxygen maximum (~ 275 mmol m^{-3}; Figure 5.4a) compared to the transects in the center (~ 325 mmol m^{-3}; Figure 5.4b) and towards the east (350 mmol m^{-3}; Figure 5.4c,d). The transect located in the center of the domain over the LaHave Basin contained the highest simulate DO likely as tidal energy dissipates north of Yarmouth, stratifying the water column and isolating the oxygen maximum (Pei MSc thesis, Dalhousie University, 2022).

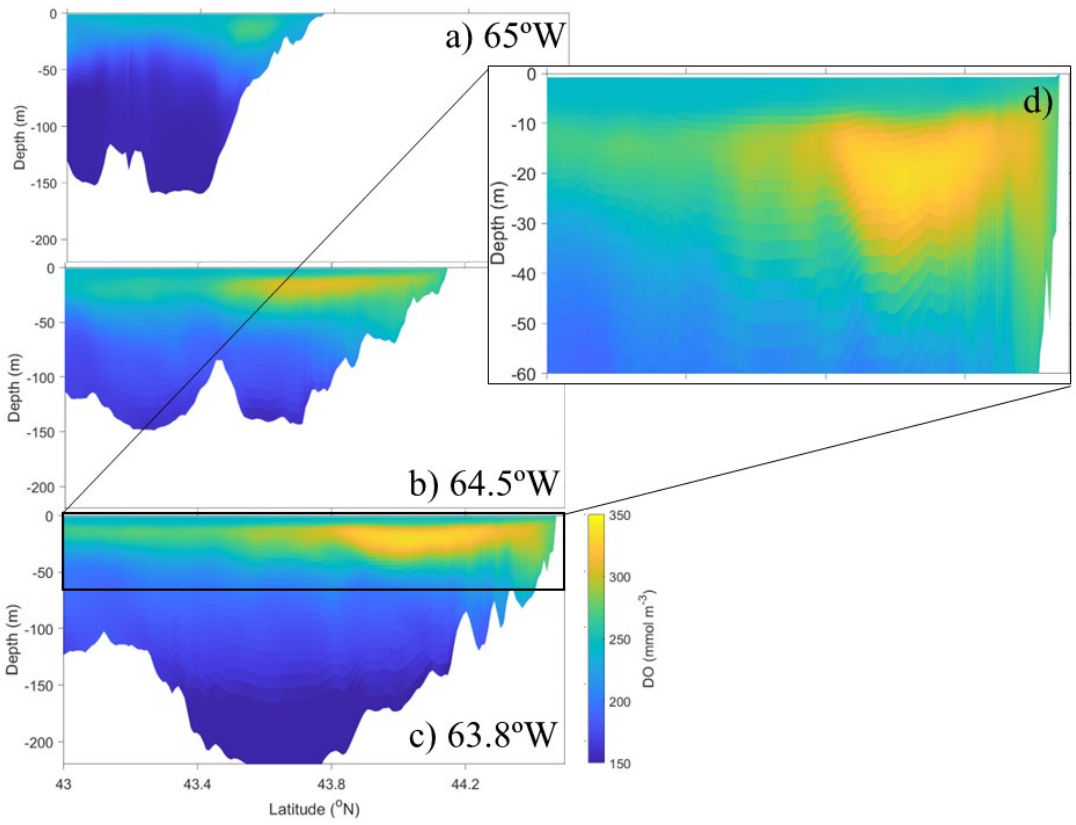

Figure 5.4 Oxygen profiles along 3 vertical transects over the full study domain; (a) at 65ºW longitude; (b) at 64.5ºW longitude; and (c) 63.8ºW longitude. The inset figure depicts the top 60 m of the profile along the 63.8ºW transect (d).

In November, the entire model domain depicted well oxygenated waters, with only minor decreases in the southwest region (235-240 mmol m^{-3}; Figure 5.2c). At 40 m, similar to august conditions, there were lower levels of DO simulated in the southwest region, though the lowest values were located in the Emerald Basin (~200 mmol m^{-3}; Figure 5.2d). As the domain was rich in oxygen due to the cool nature of November waters, the effects of the strong tidal regime were less apparent in the southwest region. Low oxygen appears to have been advected into the Emerald Basin from offshore waters influenced by the oxygen-poor Gulf Stream.

5.4.2 Temperature Increased

Increased temperature forcing at the boundary resulted in non-uniform spatial distribution in temperature across the domain and between August and November (Appendix D.1.1). In August, the lowest percent change was located from the coast to the

30 m isobath (~10% increase) and around the Roseway, Baccaro and LaHave Banks (15-20% increase). In contrast, within the outer LaHave Basin, there was a 35% increase in temperature. In November, the pattern differed, with the least amount of change in the northern region of the LaHave Basin (10-15%), extending to Roseway Bank, while the largest increase was located around the LaHave Bank (30-35%).

The comparison between the control scenario and the increased temperature simulation revealed similar patterns in DO anomalies between the two depths (5 m and 40 m), though they differed between August and November (Figure 5.5). In August, on average, there were lower concentrations of DO in the simulation across the full study domain. This decrease was most apparent in the LaHave Basin, with decreases in DO of between 20-30%. The exception was in the shallower regions along the 10-20 m isobath and on the three banks, where there were minor increases in DO in the simulation (+ 5-15% increase).

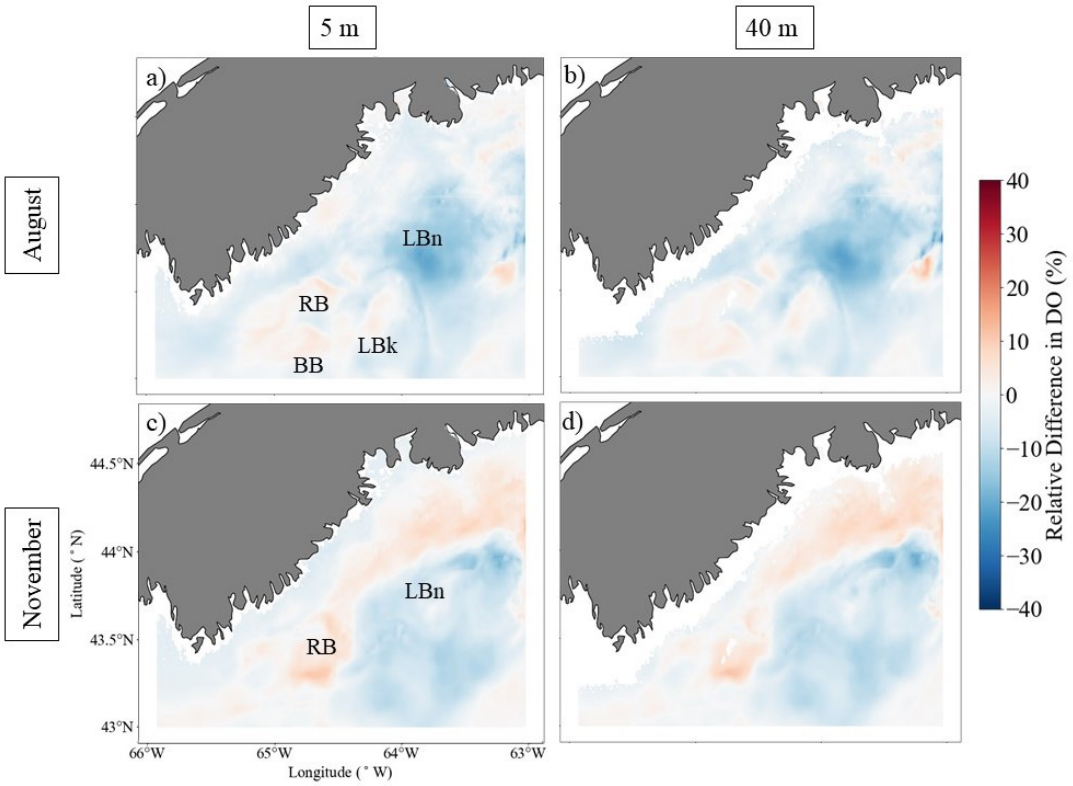

Figure 5.5 The relative difference (%) in DO between the monthly-means of the control and the increased temperature numerical experiment along southwest Nova Scotia (Canada). The results are presented for August at 5 m (a) and 40 m (b) depth, and November at 5 m (c) and 40 m (d) depth. The banks/basins relevant for the results are indicated as LBn (LaHave Basin), RB (Roseway Bank), BB (Baccaro Bank), and LBk (LaHave Bank).

On average over the full study domain, higher temperatures resulted in lower DO in the simulation. This was expected as higher temperatures lower oxygen solubility, while increasing biological metabolism and subsequent respiration (Breitburg et al., 2018). Schmidtko et al., (2017) found that within the top 1000 m of the ocean, 50% of the observed decrease in oxygen over time is due to changes in solubility, and that percentage is even higher in shallower depths. In August, the simulated water temperatures were highest in the LaHave Basin (Appendix D.1.1) and the DO concentrations reflect this (Figure5. 3a,b). LaHave Basin waters warmed about 10% more in the simulation than the surrounding shelf waters, leading to lower oxygen values. Warm Slope Water, influenced by the Gulf Stream, fills the inner basins through the Scotian Gulf at depth resulting in warm basin water year-round compared to the surrounding shelf waters (Williamson et al., 1984; Beazley et al., 2018). At the southern boundary, the Warm Slope Waters increased in temperature by the tested model forcing, leading to even warmer basin waters.

At the southwestern boundary and along the coast, there was a lower negative DO anomaly in the simulation compared to the surrounding domain, likely as a result of the tidal regime. At the shallow coastline, tidal energy is stronger than it is offshore (Zeng et al., 2021). Tides enhance mixing and result in less warming than the surrounding shelf (Pingree and Maddock 1979; Sutherland and O'Neill 2016). Additionally, there is an eddy that circulates around the region between the three banks to the southwest of LaHave Basin. The spatial structure of the eddy is characterized by vorticity-dominated inner cores with different properties than the deformation-dominated outer regions (Isern-Fontanet et al., 2004). This results in cooler waters around the eddy and warmer waters within the eddy. This temperature contrast between the inner and outer regions corresponds to a similar pattern in DO, with a positive DO anomaly around the eddy and a negative anomaly within.

In November, from the coast to the 30 m isobath, there were little to no differences between the control and the increased temperature simulation (Figure 5.5b,c). Further offshore, between the 30 m isobath and the basins, there was a moderately positive DO anomaly (+10-20%). The negative DO anomalies in the LaHave basin were present though less pronounced than in the August simulation. Lastly, in the southwestern

region of the domain, there were smaller differences between the control and simulation (− 5-10%) compared to the central and western regions (− 10-25%), likely again due to the strong tidal regime.

It appears that the non-uniform distribution in simulated DO depended largely on the bathymetry and circulation of the area. The region shallower than the 150 m isobath warmed more than the deeper areas, due to the effects of shallowness and coastal dynamics (Sanchez-Cabeza et al., 2022). The region that warmed the least, to the north of the LaHave Basin and down southwest to Roseway Bank, and the eddy surrounding the banks, showed a positive DO anomaly. As the NSC also flows in this direction, there was likely a larger inflow of cold, oxygen-rich waters compared to the rest of the domain. Within the center of the LaHave Basin and the immediate surroundings to the south, there was a negative DO anomaly which corresponds to the areas of most intense warming. This was likely again due to the intrusion of Warm Slope Water to the region that was warmed at the southern boundary.

5.4.3 GSLC Weakened

Weakening both the GS and the LC resulted in a pronounced decrease in simulated DO (− 40%) at the coast to approximately the 90 m isobath in August (Figure 5.6a,b). Much of this decrease was between the northeastern boundary and extending towards Shelburne Harbour (43.5°N, 65°W). This negative DO anomaly was present in the LaHave Basin, while the Emerald Basin, and Roseway, Baccaro, and LaHave Banks largely consisted of higher oxygenated waters (+10-20%). In November, a negative DO anomaly at the coast was also apparent; however, it was on average only −20% difference compared to the −40% in August (Figure 5.6c,d). More offshore, at approximately the 120 m isobath, there were higher oxygen concentrations across the domain. In both August and November, the positive DO anomalies at 40 m depth were more pronounced (maximum +40%) compared to the 5 m depth (maximum +25%).

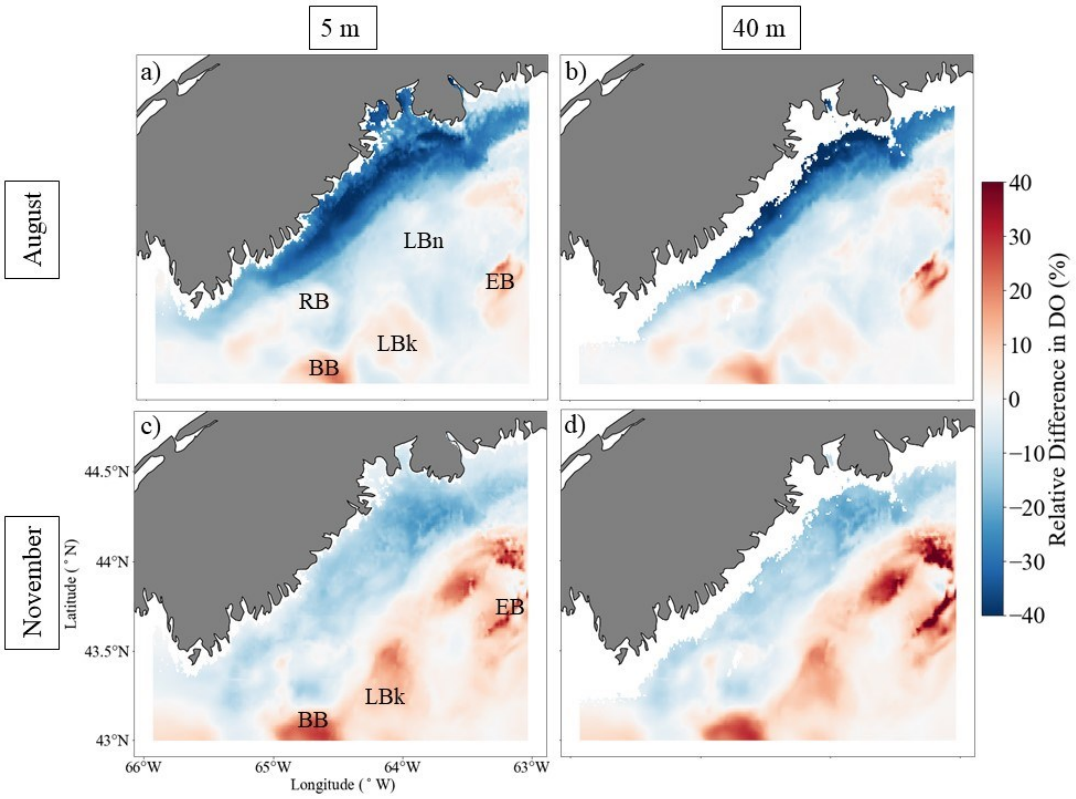

Figure 5.6 The relative difference (%) in DO between the monthly-means of the control and the weakened Gulf Stream/Labrador Current numerical experiment along southwest Nova Scotia (Canada). The results are presented for August at 5 m (a) and 40 m (b) depth, and November at 5 m (c) and 40 m (d) depth. The banks/basins relevant for the results are indicated as LBn (LaHave Basin), EB (Emerald Basin), RB (Roseway Bank), BB (Baccaro Bank), and LBk (LaHave Bank).

Weakening the LC resulted in low oxygen at the coast, with the strongest change occurring in August. The LC transports in cold, oxygen-rich waters via the NSC, but when it was weakened, this renewal was no longer present. This is consistent with past studies that have indicated the primary role of the LC in transporting oxygen-rich waters to the region (Claret et al., 2018; Jutras et al., 2020). In November, however, there was less of an effect from slowing of the LC, likely as the water was already cold and higher in oxygen, so the effect of the LC was less apparent. The significant decrease at the coast due to the weakened LC may also impact the adjacent coastal embayments, and associated cultured or wild biota, through bay-shelf interaction (Burke et al., *in prep*). Conversely, most notably in November, weaking of the GS resulted in a positive DO anomaly on the outer shelf, on the Baccaro and LaHave banks, as well as in Emerald

Basin. This was likely due to the lesser effect the GS had on the slope waters that were circulating on the outer shelf. The positive DO anomaly was stronger at 40 m, since the water mass that contains the warm, oxygen-poor waters with the GS properties is transported in at depth (Dever et al., 2016) resulting in a higher positive DO anomaly compared to at 5 m depth.

5.4.4 Wind Increased

In the August simulation, there was an overall decrease in DO in the northeastern portion of the domain after increasing winds (Figure 5.7a,b). The strongest negative DO anomaly (on average −30%) surrounded the Sambro Bank, within much of the LaHave and Emerald Basins; this anomaly was most apparent at 40 m depth (on average −40%). Along the southwestern region, there were positive DO anomalies that were most pronounced on the three banks (+10%). As wind forcing was increased in August there was a notable decrease in oxygen towards the eastern boundary. This low oxygen patch was located within the LaHave and Emerald Basins indicating that increased winds may cause stronger diapycnal mixing, raising lower oxygenated waters up from these deeper locations. As these basins are the deepest regions of the shelf, stratification results in lower oxygen concentrations at depth. Moreover, the winds altered the paths of the currents in the area, creating an eddy surrounding the Sambro Bank (Appendix D.1.2) and likely resulted in low oxygen on the outskirts of the eddy, and higher oxygen within the core. The southwest region of the domain differs from the northeast region and has moderately positive DO anomalies, likely due to the strong tidal regime present as explored in previous sections.

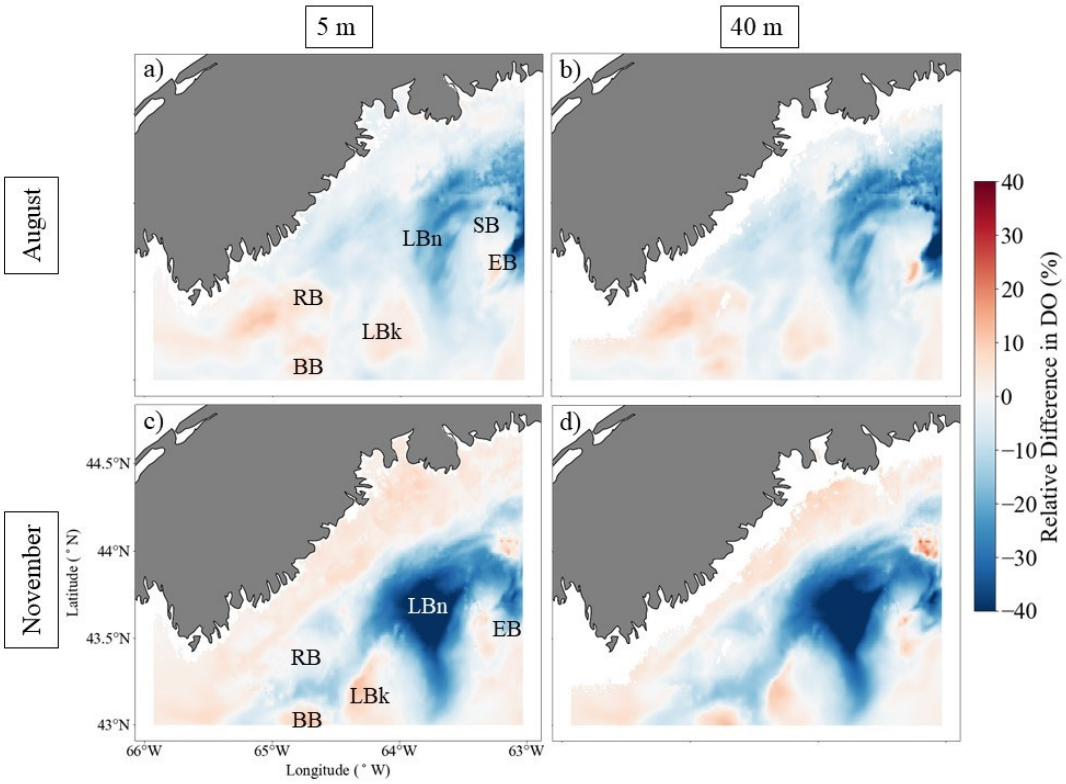

Figure 5.7 The relative difference (%) in DO between the monthly-means of the control and the increased wind forcing numerical experiment along southwest Nova Scotia (Canada). The results are presented for August at 5 m (a) and 40 m (b) depth, and November at 5 m (c) and 40 m (d) depth. The banks/basins relevant for the results are indicated as LBn (LaHave Basin), EB (Emerald Basin), SB (Sambro Bank), RB (Roseway Bank), BB (Baccaro Bank), and LBk (LaHave Bank).

In the November simulation, there was a positive DO anomaly (on average +10%) along the coastline to approximately the 120 m isobath (Figure 5.7c,d). This positive difference extended the full length of the domain from the northeast to the southwest. The shallow coastal zone and the banks contain positive DO anomalies. It is likely that, as the waters are cooler in November, oxygen solubility is highest, allowing for more oxygen to be transferred across the air-sea interface with increased winds.

Further offshore, there was a pronounced region with a negative DO anomaly (−40%) within the LaHave and Emerald Basins. The banks, however, to the southwest of the LaHave Basin contained positive DO anomalies (+10-20%), similar to the results in August. The patterns between 5 m and 40 m were very similar, though the negative DO anomaly in the basins were slightly more pronounced. The large negative DO anomaly

within the LaHave Basin, and extending between the three banks, coincided with the NSC that travels between these. Additionally, the increased wind forcing altered the currents in this region, creating an eddy surrounding the LaHave Basin. These currents and the intense mixing from the winds likely resulted in vertical mixing in the Basin, transporting lower oxygen up from the depths which the NSC then transported towards the Banks. Increased winds in the along-shore direction will cause changes to the upwelling regime, potentially increasing the upwelling of lower oxygenated deep waters to the surface (Burke et al., in prep.). Similarly, increasing cross-shore winds will increase the advection of water masses with differing properties to the coast, transporting in lower (or higher) oxygenated waters from offshore, depending on the characteristics and origin of the water mass (Burke et al., in prep.).

5.4.5 Wind Weakened

Weakening the winds in the August simulation, resulted in, on average, a positive DO anomaly throughout the full study domain of approximately the same magnitude (+10-20%; Figure 5.8a,b). However, at around the 30 m isobath, there was a negative DO anomaly (on average – 10%) which extended the length of the coastline and meandered offshore around the Roseway Bank and between the Baccaro and LaHave Banks. There was also a negative DO anomaly within the LaHave Basin (on average – 10%). The pattern at 40 m was the same as 5 m, though with marginally higher positive DO anomalies.

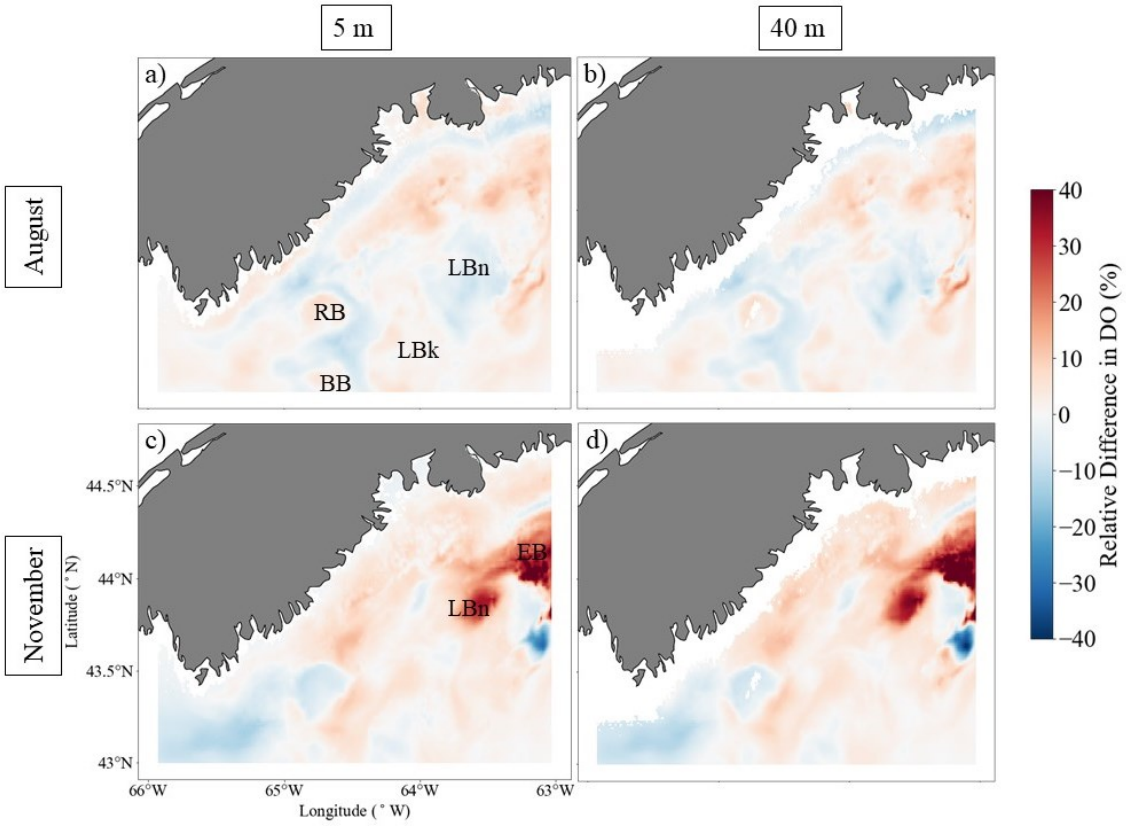

Figure 5.8 The relative difference (%) in DO between the monthly-means of the control and the decreased wind forcing numerical experiment along southwest Nova Scotia (Canada). The results are presented for August at 5 m (a) and 40 m (b) depth, and November at 5 m (c) and 40 m (d) depth. The banks/basins relevant for the results are indicated as LBn (LaHave Basin), RB (Roseway Bank), BB (Baccaro Bank), and LBk (LaHave Bank).

The simulated negative DO anomaly along-shore and around the eddy southwest of the basins, closely resembles the local circulation patterns. The currents may transport in lower oxygen from outside of the domain due to the open boundary conditions and leading to negative DO anomalies. Overall, however, weakened winds resulted in low-moderate increases in DO throughout the study domain. This is corroborated by a past study using a numerical model that decreased wind stress in the lower latitudes and discovered that weakened winds led to a more oxygenated ocean (Ridder and England, 2014). The authors revealed that weakened winds reduced the upwelling of nutrients and primary production (thus subsequent oxygen consumption) and led to changes in ocean circulation. For the present study, due to the shorter time scale, the effects on ocean circulation appeared to be the dominating result. Weaker winds increased stratification, in

turn increasing surface oxygen values and reducing the air-sea flux if the waters became supersaturated (Turner et al., 1987; Schmidtko et al., 2017). Though it is important to note the shallow nature of the Scotian Shelf. The waters may be saturated in DO in the upper depths with weakened winds, however a reduction in ventilation of deep waters can result in low average DO in the global ocean. In fact, the majority of the global oxygen decrease can be explained by decreased exchange between the surface and deep waters (Helm et al., 2011).

In November, on the northeastern boundary, there was a positive DO anomaly that was higher in magnitude than in the August simulation (+30%; Figure c,d). This positive anomaly was located just north of a small area with a negative DO anomaly (−35%). These patterns were similar at 40 m, however the strong positive/negative DO anomalies were more pronounced compared to 5 m (+/- 40%). Overall, in the weakened winds simulation, the central and eastern areas of the domain were higher in DO, while the southwestern boundary contained lower DO concentrations.

The highest positive DO anomaly within the Emerald Basin and the northeast region of the LaHave Basin was likely due to the increased stratification and isolation of cooler and more highly oxygenated surface waters compared to in August. There was a small patch of water with a negative DO anomaly within the deepest area of the Emerald Basin. The weakened winds affected the circulation of the eddy in this area and resulted in transportation of waters from outside of the domain, likely bringing lower oxygen in (Appendix D.1.3). Lastly, in the southwest region of the domain, negative DO anomalies were present again likely from the strong tidal regime promoting mixing of DO.

5.4.6 Combined Simulation

When temperatures were increased, and GSLC/wind forcing decreased, the effect of the weakened LC on the inner shelf was apparent in both August and November. In the August simulation, along the inner shelf until 90 m isobath, there was a highly negative DO anomaly (− 40%; Figure 5.9a,b). The remainder of the domain was moderately negative (− 10-20%), with an exception in the Emerald Basin, where there were low-moderately positive DO anomalies (+ 10-15%). This positive anomaly was stronger at 40

m (+ 25%). There was also a low positive DO anomaly on the Baccaro Bank, apparent at both 5 m and 40 m (+ 10%).

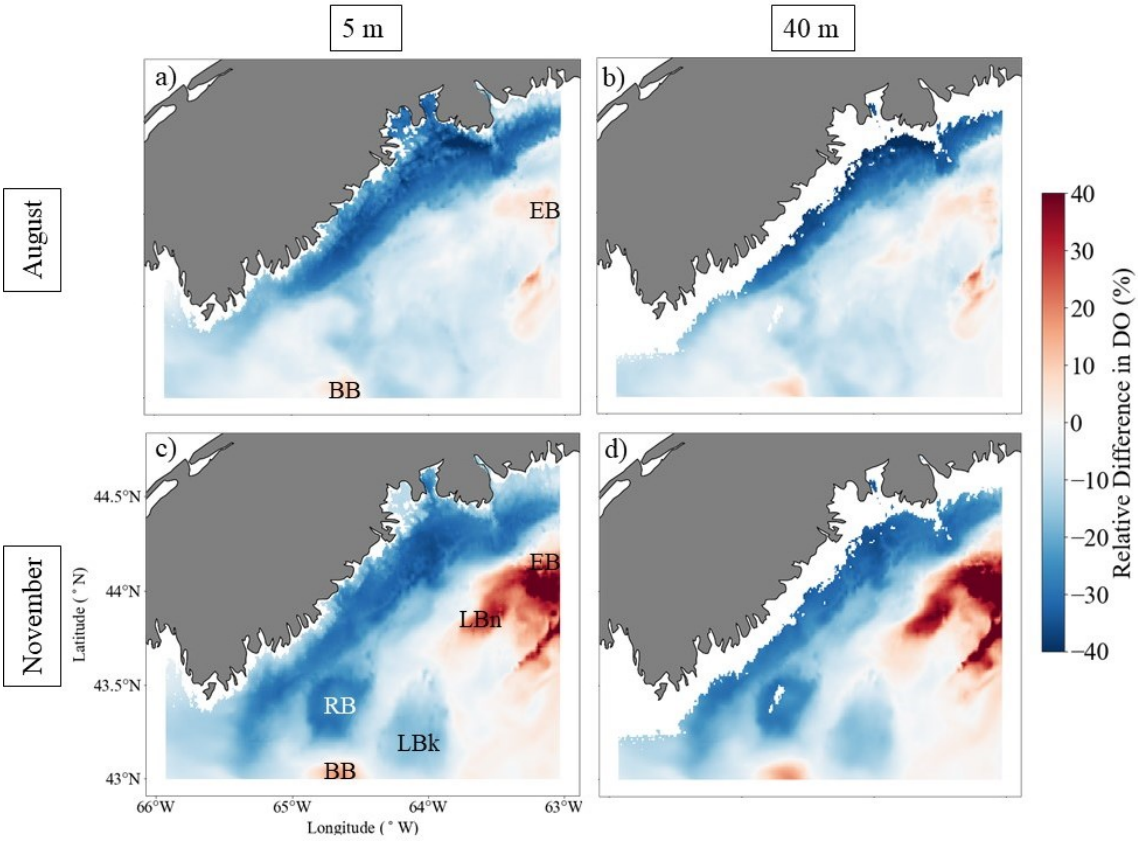

Figure 5.9 The relative difference (%) in DO between the monthly-means of the control and the combined numerical experiment of increased winds, weakened GSLC, and weakened wind forcing along southwest Nova Scotia (Canada). The results are presented for August at 5 m (a) and 40 m (b) depth, and November at 5 m (c) and 40 m (d) depth. The banks/basins relevant for the results are indicated as LBn (LaHave Basin), EB (Emerald Basin), RB (Roseway Bank), BB (Baccaro Bank), and LBk (LaHave Bank).

In the November simulation, the effects of the experimental stressors were intensified compared to August (Figure 5.9b,c). The negative DO due to the weakened LC was again apparent at the coast until approximately the 90 m isobath, however there was a strong negative DO anomaly on the Roseway Bank (− 35%). Additionally, there was a stronger positive DO anomaly in the LaHave and Emerald Basins (+ 35%) compared to in August. This positive DO anomaly in Emerald Basin was even stronger at 40 m depth (+ 40%).

Labrador current has the largest effect on the coast to mid-shelf. In the basins, particularly in Emerald Basin in November, weakened winds appear to have the largest influence as it corresponds to the positive DO anomaly found in the individual scenario. The high resolution of this model allows the distinguishing of this non-uniform spatial distribution in oxygen with future climate change. This is the first study to provide information at this scale, to observe the positive DO anomaly around the basins and a negative DO anomaly through the remainder of the domain, and how these vary with the season. Past studies have focused on the implications of climate change on the biology of the area at larger, shelf-wide spatial scales (e.g. Guénette et al., 2014, Lavoie et al., 2020, McGinty et al. 2021). The present study allows a more comprehensive view of the region and how currents and bathymetry play a role in the distribution of oxygen with future climate change stressors.

5.5 Conclusion

Predictive numerical models have been used to assess the effects of climate change stressors on the Scotian Shelf, though primarily through the lens of ecosystem change and focused on changes to temperature and salinity (Ji et al., 2008; Guénette et al., 2014; Stortini et al., 2015; Brennan et al., 2016). The response of DO to climate change has not been well established, especially at the high-resolution presented here. It is important to understand how DO is likely to change in the future, to better manage the Scotian Shelf and coastal economies. It is also important as there is speculation that variations in DO on the shelf can be an indicator of dynamical shifts in DO offshore (Claret et al., 2018).

Previous studies have indicated that physical forcing of DO, including mixing, advection and air-sea flux play the most important roles (e.g. Sarma et al., 2013, Du and Shen, 2014, Huang et al., 2019). The present study did not explore the role that temperature had on the NWR term in the governing equation, nor explicitly how primary production may influence DO dynamics. However, biology cannot be discounted, thus future studies may incorporate biology into the model for a more holistic approach. For example, when comparing the results of the model to *in situ* observations (Figure D.2.6), two of the profiles were incongruent between 50 and 90 m depth. This was likely due to

error in the parametrization of NWR. The chlorophyll and primary production data from the GRB29 dataset are based on numerical model results without data assimilation, leading to significant differences compared to the true values (Pei MSc thesis, Dalhousie University, 2022).

In the present study, the weakening of the Labrador Current had the largest effect on declining DO at the coast, while increased wind forcing decreased the DO significantly at the mid-outer shelf, and weakened wind forcing increased DO in the basins. The scenario that combined the stressors revealed that while the overall DO is projected to decrease, there will be pockets of increased oxygen in the basins. However, the individual wind increased scenario determined that strong storm events will decrease oxygen in those basins. Thus, there is this interplay between the stressors that are important to understand for this region.

CHAPTER 6 CONCLUSION

6.1 Summary of Thesis

The central objective of this thesis was to explore the distribution and variability of dissolved oxygen within coastal embayments and on the shelf of southwestern Nova Scotia. The first goal was to determine the oxygen dynamics within bays that contain aquaculture farms. This is important for farm management as it relates to site selection and feeding regimes. The second goal was to describe oxygen variability on the southwestern Scotian Shelf and subsequently forecast oxygen changes due to climate change-related stressors. The Scotian Shelf is rich with marine life, communities, and habitats, while also providing essential ecological resources for coastal economies, such as aquaculture production. As climate change threatens the Scotian Shelf ecosystem, it is crucial to understand oxygen dynamics and how these may change in the future, to adapt management plans (e.g. marine spatial planning) and prioritize research efforts in more vulnerable areas. The summary and major findings of each research chapter is as follows:

The objective of chapter 2 was to establish baseline oxygen variability through an aquaculture farm, using an extensive array of real-time oxygen sensors. Previous research has focused on temporal and spatial variations in oxygen within sea cages (e.g. Stehfest et al. 2017; Oldham et al. 2018; Solstorm et al. 2018), with limited knowledge of how oxygen conditions vary between cages and the drivers of this variability. DO is affected primarily by physical transport (winds, currents) and secondarily through fish physiology (respiration, metabolism). The results of this chapter revealed that tidal forcing, seasonality, and cage infrastructure are the most important factors governing the oxygen dynamics between cages in aquaculture farms. Oxygen concentrations were out of phase on opposite ends of the farm. During flood (ebb) tide, the cages located towards the outer (inner) bay were inundated with oxygen-rich waters, while subsequent fish behaviour, physiology, and flow restriction from cage infrastructure reduced oxygen in the cages downstream. Tides transport oxygenated waters to the oxygen-depleted cages, with the outermost cages on either end of the farm experiencing the highest levels of exchange. This is most important during the summer and early autumn, when temperatures are highest and oxygen is lowest.

The objectives of chapter 3 were to assess the effectiveness of an oxygen supplementation system on increasing DO concentrations within sea cages and explore how the system will affect the local baseline oxygen variability. As sea temperatures increase and oxygen continues to decline, it may become necessary to implement oxygenation or aeration systems to enrich oxygen depleted farms (Berillis et al. 2016). While oxygenation and aeration have been studied in ponds and recirculating aquaculture systems (Vinci and Summerfelt 2015; Boyd et al. 2018), their use in the open ocean is still in its infancy. The results of this chapter revealed that oxygenation likely upwelled cooler water from depth, lowering cage temperatures, increasing oxygen solubility and decreasing fish metabolism. These factors ultimately led to increased DO within the cages, likely reducing fish stress and mortality.

The two objectives of chapter 4 were first, to use a Slocum glider to quantify the along- and cross-shore distribution of oxygen, temperature and salinity on the inner Scotian Shelf, and second, to explore the onshore advection of offshore waters to coastal embayments. As climate change is projected to cause further deoxygenation of coastal regions (Breitburg et al., 2018), it is important to understand the present oxygen variability and the interaction between the coastal zones and adjacent bays. Additionally, many coastal economies rely on adequate water quality, such as local fisheries and aquaculture. The results of this chapter revealed that wind direction had a significant effect on the variability of hydrography and DO on the inner Scotian Shelf. Strong and persistent along-shore winds caused coastal upwelling of cold, oxygen-rich waters from the subsurface. Alternatively, strong cross-shore winds advected offshore transient water masses to the coast, creating heterogeneity in the cross-shore glider profiles, and generally warmer, fresher, and less oxygenated shoreward waters. Lastly, there was a strong upwelling event adjacent to St. Margaret's Bay, which was then observed within the Bay 30 h later, illustrating potential offshore-inshore interaction.

The objective of chapter 5 was to use numerical experiments to explore the effect of climate change-related stressors on oxygen dynamics along the inner southwestern Scotian Shelf. Climate change will produce a variety of consequences, some of which are already discernable, such as: increased ocean temperatures, which reduces oxygen solubility and increases biological metabolism (Brennan et al., 2016; Oschlies, 2019);

decreased Atlantic Meridional Overturning Circulation (AMOC), which weakens the oxygen-rich Labrador Current and oxygen-poor Gulf Stream (Yamamoto et al., 2015; Schmidtko et al., 2017; Claret et al., 2018); weakened wind forcing due to changes in the atmospheric circulation with a warming planet (Vautard et al., 2010; Karnauskas et al., 2018); and increased storm events due to increased latent heat (Trenberth, 2018). These four climate-related scenarios were simulated with a numerical oxygen model for the southwestern Scotian Shelf. A final experiment was conducted to simulate the most probable scenario where stressors will interact, which combined increased temperature, weakened Gulf Stream-Labrador Current, and weakened wind forcing. The results of this chapter predict a predominant decrease in DO over the domain, with the weakened Labrador Current causing the most significant decrease, both individually and when combined with other stressors. The Labrador Sea is a site of intense downwelling, oxygenating deep waters which are then transported via the Labrador Current to the Scotian Shelf. With the weakening of the AMOC and subsequently the Labrador Current, there will likely be a lower influx of well-oxygenated waters to the region. On an individual level, stronger winds are also projected to cause a large decrease in oxygen, particularly in August on the mid-shelf, due to stronger diapycnal mixing and vertical exchange with oxygen-poor bottom waters. Conversely, within the basins, weakened winds are projected to increase DO concentrations. Weakened winds may increase stratification, trapping well-oxygenated surface waters and ultimately increasing DO within the basins.

6.2 Research Contributions

This thesis sought to understand, describe (chapter 2-4) and forecast (chapter 5) dissolved oxygen variability on the Scotian Shelf. The research chapters explored oxygen dynamics within aquaculture farms and on the southwestern Scotian Shelf, both of which were not previously reported. Previous studies on dissolved oxygen in salmon farms were located in areas with differing conditions to Nova Scotia (e.g. Newfoundland, Norway, and Australia; Cheshuk et al., 2003, Johansson et al., 2006, Monsour et al., 2008, Burt et al., 2012, Stehfast et al. 2017, Oldham et al., 2018, Solstorm et al., 2018). As oxygen dynamics can be very site specific, observations in Nova Scotia are essential for accurate

monitoring of the area and marine spatial planning. Chapter 2 also revealed that inadequate monitoring may result in a failure to capture the spatial distribution in oxygen. This is important, as the feeding regime for fish is dependent on the oxygen conditions within cages, thus without sufficient monitoring, farmers may assume fish are experiencing similar oxygen concentrations across the farm and feed accordingly. This study can contribute to more informed decision making on the farms, ultimately improving fish welfare and production.

The assessment of an oxygenation system undertaken in chapter 3 was novel for open ocean aquaculture farms. Previous studies were conducted in pond or recirculating aquaculture systems, without the added challenges of the adjacent open ocean. As sea cages (as with the water column) are prone to stratification in the summer, when oxygen is lowest and oxygen supplementation is most needed, vertical mixing is paramount to improve oxygen conditions. This research suggests that farmers may use a cheaper alternative such as aeration to create the same upwelling effect, considering stripping oxygen from air and transporting it to remote aquaculture sites is not cost effective.

While there are numerous studies focused on the Scotian Shelf, they are often directed at temperature/salinity (e.g. Sutcliffe et al., 1976; Petrie and Drinkwater, 1993; Loder et al., 1996; Dever et al. 2016; Brickman et al., 2018) and CO_2 (e.g. Shadwick et al., 2010, 2011, 2014; Rutherford et al., 2021), without considering oxygen. This research expanded the literature of the Scotian Shelf to include oxygen dynamics, both at present and with added climate-related stressors. Additionally, the study in chapter 4 presented a novel approach for collecting hydrographic and DO data on the inner Scotian Shelf. This study utilized a novel zig-zagging glider sampling technique to collect both along- and cross-shore data, while previous studies mainly provided observations from a moored buoy or through a single cross-shelf track (e.g. Atlantic Zone Monitoring Program; Dever et al., 2016, Wu et al., 2016, Galbraith et al., 2017). Lastly, the numerical experiments were novel in their approach to projecting dissolved oxygen response to various climate change stressors. These experiments enhance the collective knowledge of oxygen processes on the Scotian Shelf under climate change. While dissolved oxygen on the Scotian Shelf has been projected to decline, the spatial distribution of the change had not previously been documented. The knowledge gained in this thesis, by describing the

distribution and drivers of oxygen, is essential for the development of bay- and shelf-scale management.

6.3 Limitations and Research Opportunities

This thesis provides a baseline for future research into oxygen dynamics both within aquaculture farms and on the Scotian Shelf. As oceanographic processes are location dependent, it is essential to monitor each aquaculture farm to determine the individual drivers affecting these sites specifically. This is necessary to inform management in the future for all farms, leading to improved fish welfare and aquaculture production.

Oxygenation is also in its infancy within open ocean farms. While the study presented in chapter 3 determined that oxygen supplementation may indirectly raise oxygen levels to adequate concentrations, farmers are still interested in the idea of using these systems to increase oxygen concentrations to near 100% saturation in the oxygen-depleted summer months. There are many companies attempting to create an effective oxygenation system, thus further studies are required to ensure their success. Additionally, the study design was not able to incorporate a control cage for comparison (for the health of the fish), thus the conclusions are not as robust as they might have been with a control.

The continued monitoring of the oxygen on the entire Scotian Shelf is essential to understand where there are vulnerabilities to the ecosystem, however it is also critical to expand the surveys to multiple times a year in order to capture seasonality and the entire spatial and temporal variability. This thesis revealed the highly variable nature of oxygen dynamics (chapter 2, 4), thus only sampling in one location is not sufficient for effective monitoring. Furthermore, additional sensors within the coastal embayments would have provided more compelling evidence of the shelf-bay interaction.

Lastly, the numerical model used in chapter 5 can continue to be modified and updated, to ensure that the responses to climate change are properly represented. It may also prove useful to include the biological component of oxygen dynamics in the equations for the model. While the biological component is empirical, the physical processes currently used in the model are mechanistic in nature. Therefore, adding the

biology to the mechanistic approach would likely improve the accuracy and value of the model. Lastly, projecting the effects of climate change for each season is critical to understanding the future of oxygen on the Scotian Shelf, and how biodiversity and suitable habitats are likely to change.

Appendix A.1

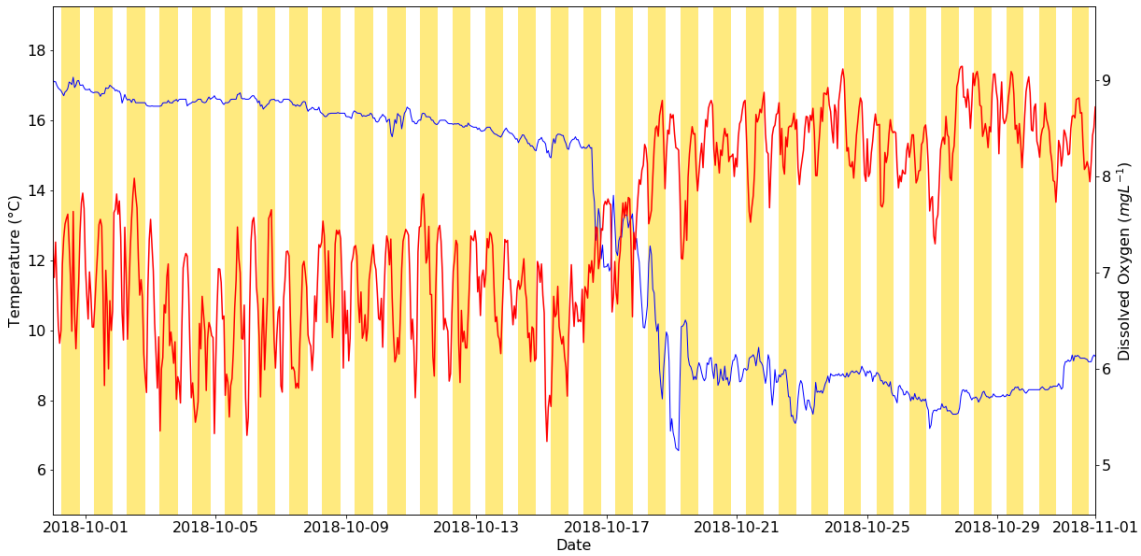

Figure A.1 The relationship between temperature (blue), dissolved oxygen (red) and photoperiod (yellow bars indicating daylight).

Appendix A.2

The InnovaSea optical sensors were calibrated prior to deployment using a 2-point calibration (0% and 100%). Previous studies have reported high stability (within a few tenths of a percent per year) for optodes during deployment, thus the relatively short nature of the study (5 months) allowed us to assume no drift was occurring (Bittig et al., 2018). Despite calibration, some sensors reported inaccurate readings and consequently were not included in the study. The criterium to remove these sensors was based on differences of +/-0.5 mg L^{-1} compared to those located in the adjacent cage or within the same cage at the same depth. With the experience gained during this thesis, I worked with InnovaSea to create a quality control program that checks several sensors within each batch with a 20-point calibration to ensure the sensors are performing accurately and precisely.

The sensors were deployed by an engineer associated with Cooke Aquaculture, using a standard operating procedure (SOP) developed by Burke, M. The SOP indicated the exact locations and depths the sensors were to be placed. Additionally, they were cleaned once a week by the farm staff, as per the SOP. Deploying a month prior to the

study period ensured that the SOP was being followed, that proper cleaning practices were in place, and allowed for elimination of sensors that were not recording accurately.

Appendix B

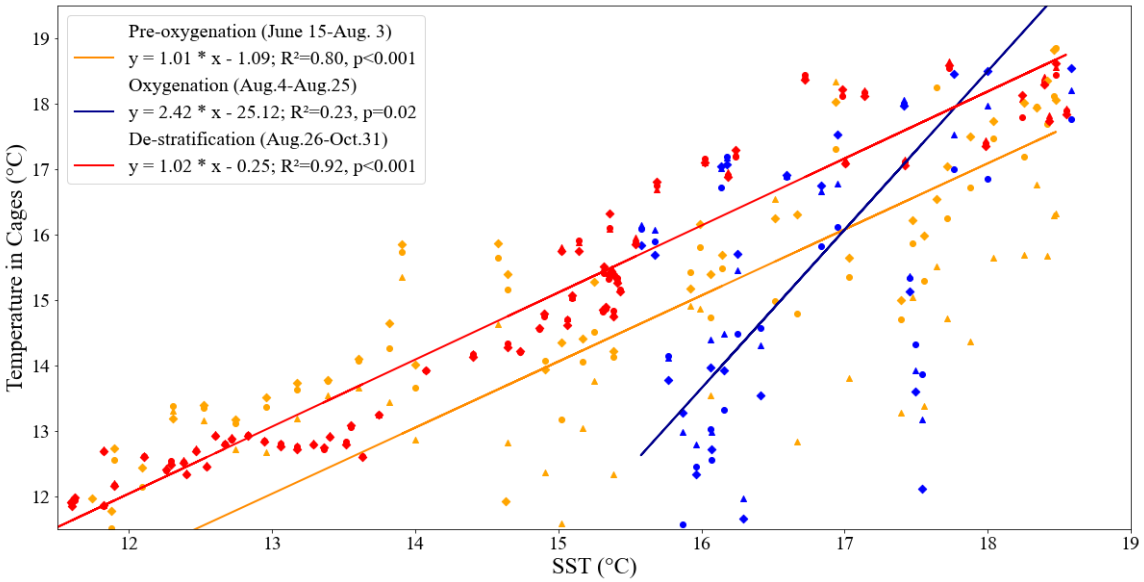

Figure B.1 The relationship between satellite derived sea surface temperature (SST) and temperature in cages 1 (circles), 2 (triangles) and 5 (diamonds) during pre-oxygenation (orange), oxygenation (blue), and de-stratification (red).

Appendix C

Given that Ekman transport is affected by the shoreline and as Nova Scotia is orientated ~60° clockwise from true North, the I_w must be in reference to this orientation (Scrosati and Ellrich 2020). Using equation 2.3 from Kämpf and Chapman (2016), the new I'_w is calculated as:

$$I'_w = I_w \times \cos(\alpha) \tag{27}$$

where angle α is the difference between the average orientation of the Nova Scotian coast (60°) and the angle associated with wind direction where the origin is situated above the glider position. Therefore, southwesterly winds blowing parallel up the coastline will give a cos (0) = 1, and will result in positive values of I'_w describing upwelling-favourable scenarios, while winds from the northeast result in negative values, describing downwelling-favourable Ekman transport (Petrie et al. 1987; Alvarez-Salgado et al. 2008).

Wind vectors were created by determining the u and v wind components by:

$$u = -(V \times \sin(\theta)) \tag{28}$$

$$v = -(V \times \cos(\theta)) \tag{29}$$

where V is wind speed (10 m above sea level, m s^{-2}) and θ is wind direction (radians). Along-shore and cross-shore wind components were determined by rotating the coordinate system with the following equations:

$$U' = U\cos(\alpha) - V\sin(\alpha) \tag{30}$$

$$V' = U\sin(\alpha) + V\cos(\alpha) \tag{31}$$

where angle α is the difference between the average orientation of the Nova Scotian coast (60°) and the angle associated with wind direction, as stated above.

Appendix D.1

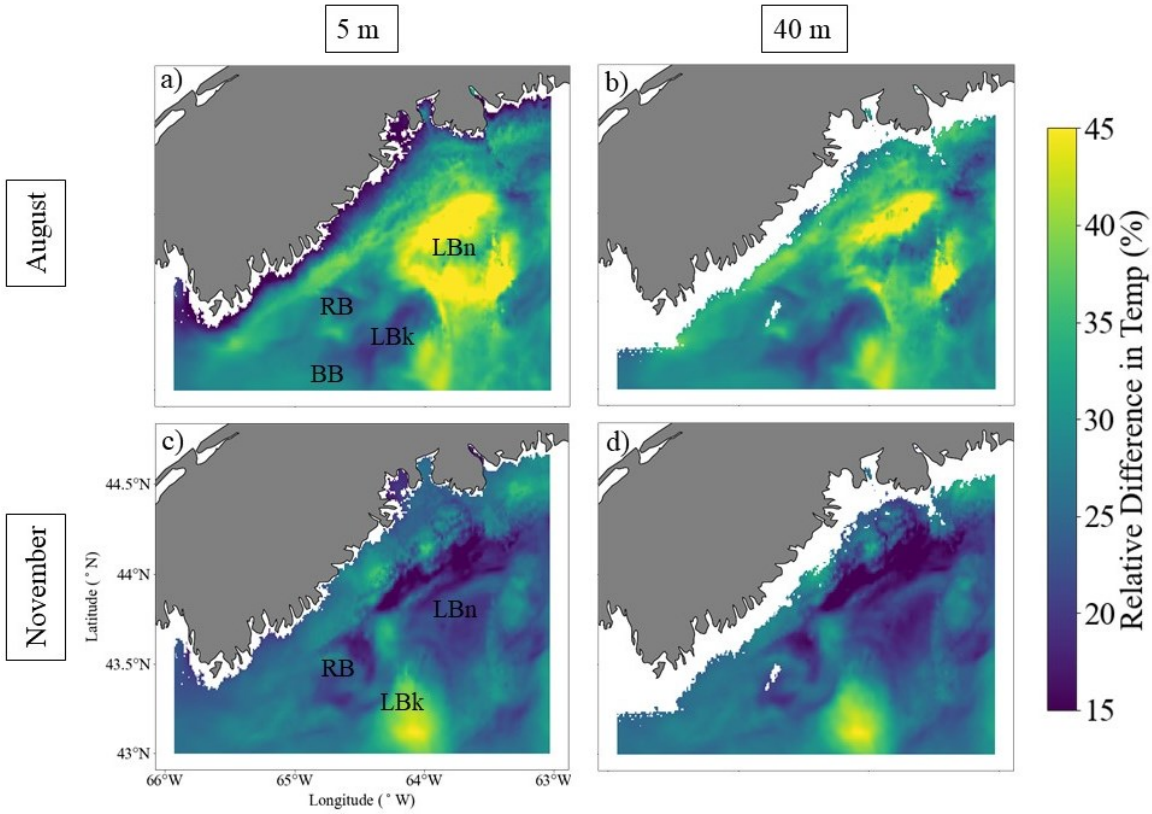

Figure D.1.1 The relative difference (%) in ocean temperature between the monthly-means of the control and the increased temperature numerical experiment along southwest Nova Scotia (Canada). The results are presented for August at 5 m (a) and 40 m (b) depth, and November at 5 m (c) and 40 m (d) depth. The banks/basins relevant for the results are indicated as LBn (LaHave Basin), Roseway Bank (RB), BB (Baccaro Bank), and LBk (LaHave Bank).

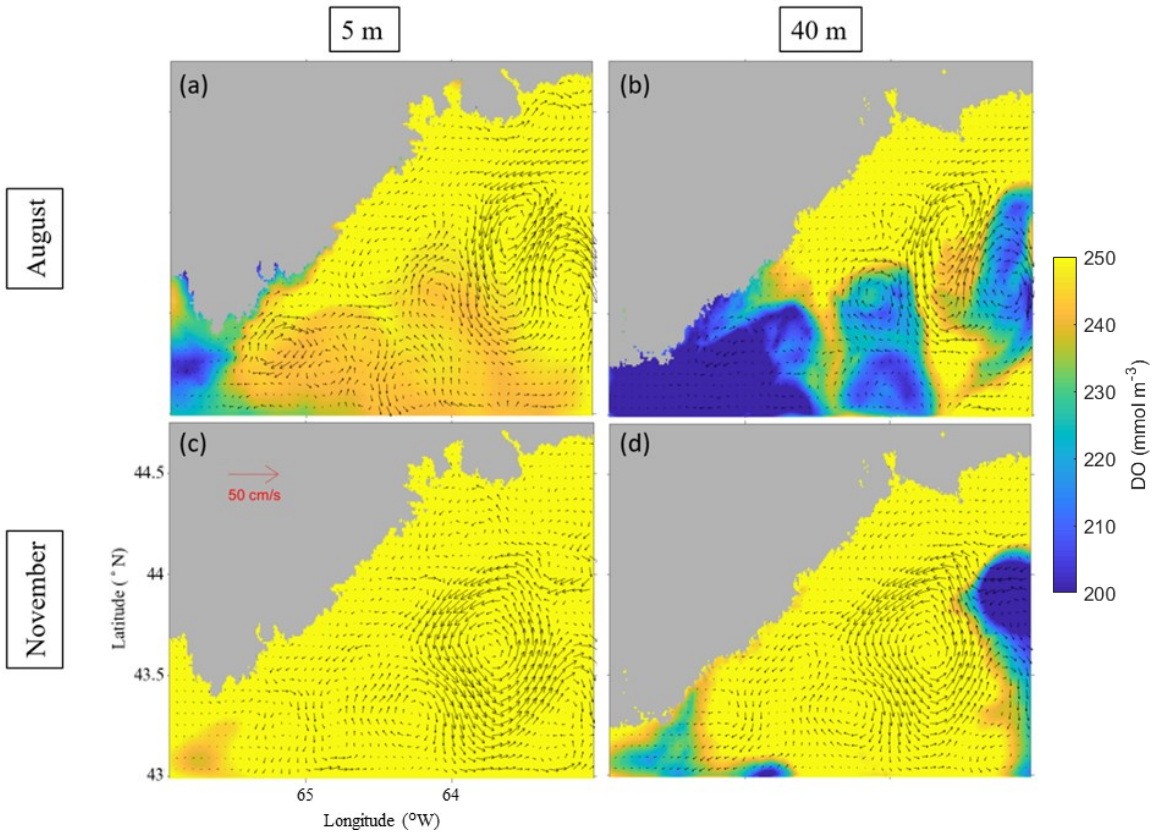

Figure D.1.2 Model results of the control scenario (representing the conditions in 2018) with an overlay of the difference in currents between the control and the increased wind forcing simulation at 5 m (a, c) and 40 m (b, d) in August (a, b) and November (c, d).

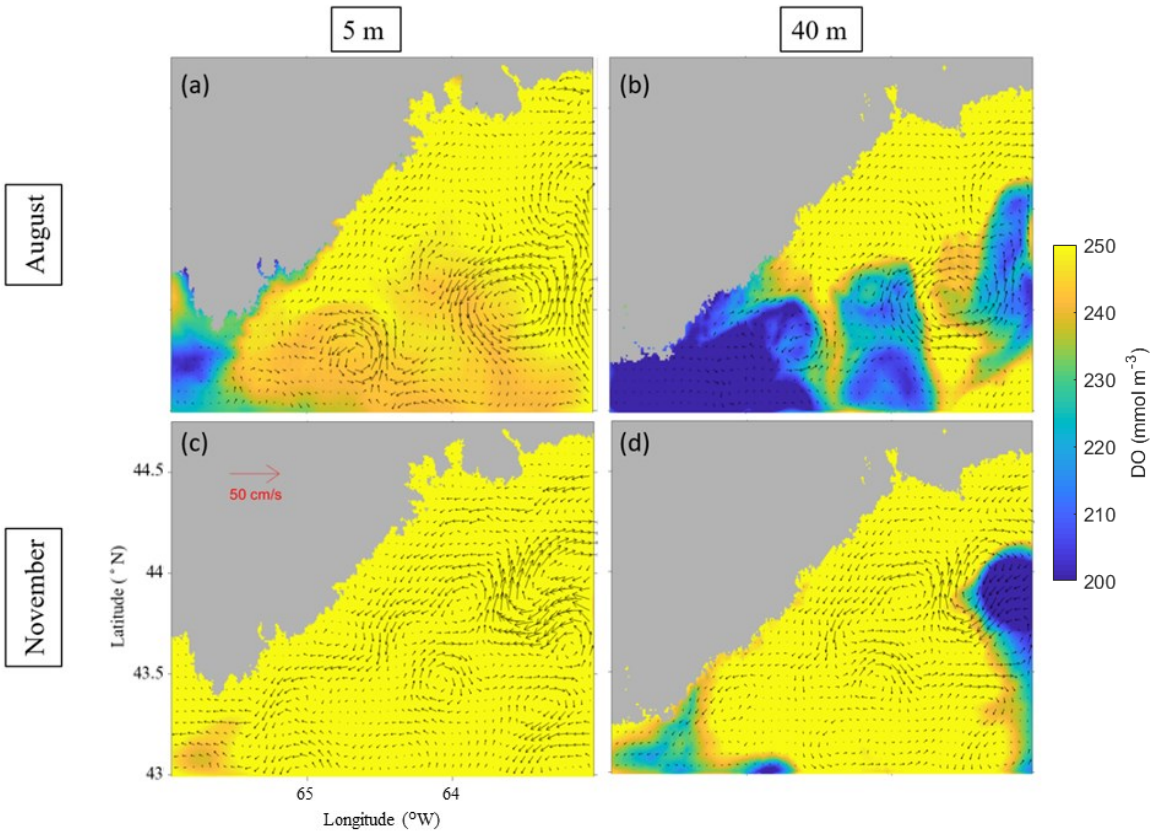

Figure D.1.3 Model results of the control scenario (representing the conditions in 2018) with an overlay of the difference in currents between the control and the weakened wind forcing simulation at 5 m (a, c) and 40 m (b, d) in August (a, b) and November (c, d).

Appendix D.2

The coupled circulation-ice modelling system was based on the Regional Ocean Modelling System (ROMS) and the Los Alamos Sea Ice Model (CICE) for the southwestern Canadian Shelf. This modelling system has 3 sub-models within nested domains of successively small areas. The domain of level 1 (L1) sub-model contained 1/12° horizontal resolution, level 2 (L2) contained 1/36° resolution, while the level 3 (L3) sub-model was centered on the southwestern Scotian Shelf with 1/108° horizontal resolution (Figure D.2.1). The oxygen model was coupled to the L3 sub-model, and using a one-way nesting technique, information from the upper level sub-models was transferred to the lower levels. Results of sea surface elevations, currents, temperature, salinity, and sea ice conditions produced in L1 was used to specify boundary conditions for L2, and L2 results specified conditions for L3. Additionally, in each sub-model, the

Smagorinsky scheme (Smagorinsky, 1963) and the level 2.5 Mellor-Yamada turbulence closure (Mellor and Yamada, 1982) were used for the horizontal and vertical eddy mixing coefficients, respectively.

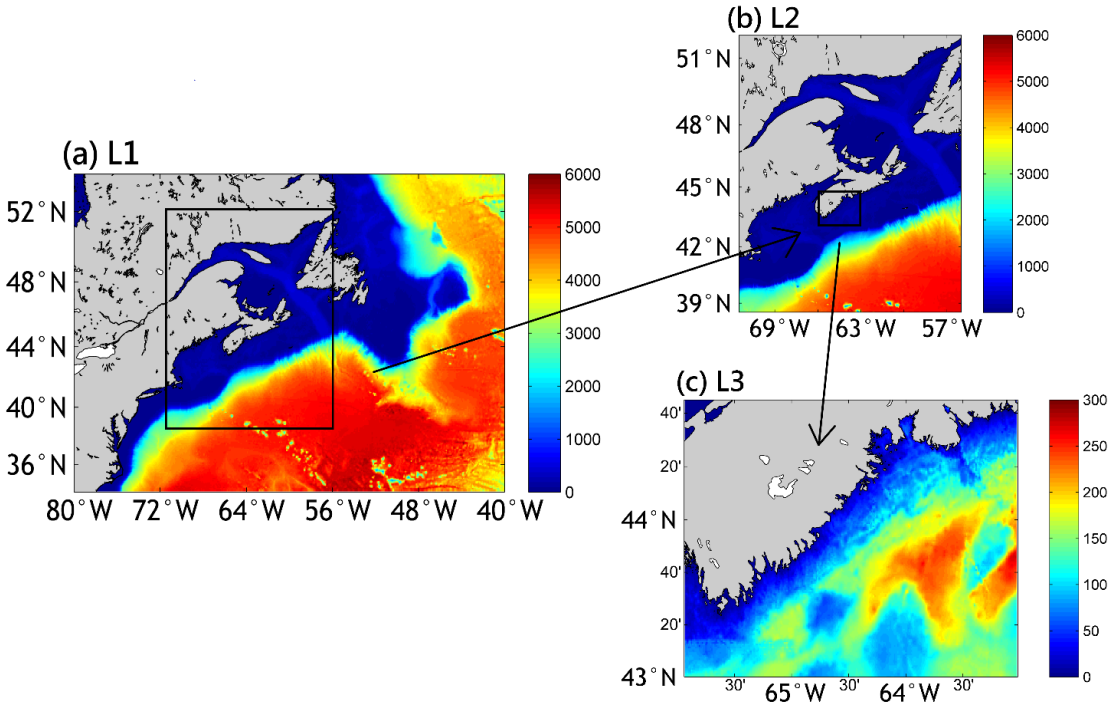

Figure D.2.1. Major topographic features and domains of three submodels for a nested-grid coupled circulation-ice modelling system for the southeastern Canadian shelf and adjacent deep ocean waters of the northwestern Atlantic Ocean. The horizontal resolutions of submodels (a) L1, (b) L2, and (c) L3 are respectively 1/12°, 1/36° and 1/108°. The color image in each subplot represents water depths (from Pei MSc thesis, Dalhousie University, 2022).

Tidal gauges were used to assess the physical model performance in simulating sea surface elevations. The observed and simulated tidal heights agreed well, as shown in Figure D.2.2 for the results from Yarmouth. Specifically, γ^2 was used to assess the model performance based on the definition given by Thompson and Sheng (1997):

$$\gamma^2 = \frac{Var(X_O - X_S)}{Var(X_O)} \tag{32}$$

where X_S and X_O represent respectively the simulated and observed value of variable X at the same observation time. Smaller values of γ^2 indicate better model performances in simulating variable X. The γ^2 values for simulating the total, tidal, and non-tidal sea

surface elevations at Yarmouth during this period are ~0.02, ~0.01 and ~0.32 respectively.

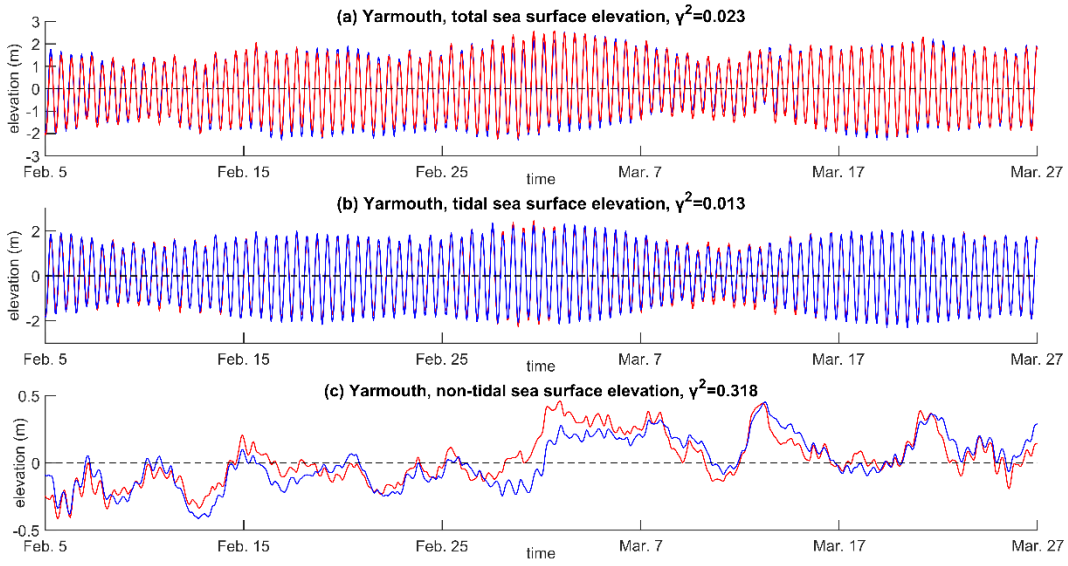

Figure D.2.2 Time series of observed (red) and simulated (blue) (a) total, (b) tidal and (c) non-tidal surface elevations at Yarmouth tidal gauge station from 5 February to 27 March 2018. The simulated results are produced by submodel L1 (from Pei MSc thesis, Dalhousie University, 2022).

To validate the model further, the co-phases (black contour lines) and co-amplitudes (red contour lines) of the M_2 tidal frequency computed from the L1 model were compared with the results from the Oregon State University Tidal Inversion System (OTIS) tidal model (Figure D.2.3). The OTIS is a data-assimilative tidal model that uses various satellite altimetric data (including data collected by TOPEX Poseidon, TOPEX Tandem, European Remote Sensing, and Geosat Follow-On Satellites) and in-situ observations made by tide gauges and ship born acoustic Doppler current profilers. The smaller-scale variations in the L1 model indicate internal waves that were not captured by the OTIS model. The L1 sub-model successfully reproduces the positions of two M_2 amphidromic points. One M_2 amphidromic point is close to the eastern boundary of L1 domain, and another is over the central area of the Gulf of St. Lawrence. Furthermore, the positions of M_2 amphidromic points, rotations of M_2 tidal elevations, and distribution of M_2 co-amplitudes produced by submodel L1 are consistent with previous model results made by Han et al. (2010) and Wang et al. (2020).

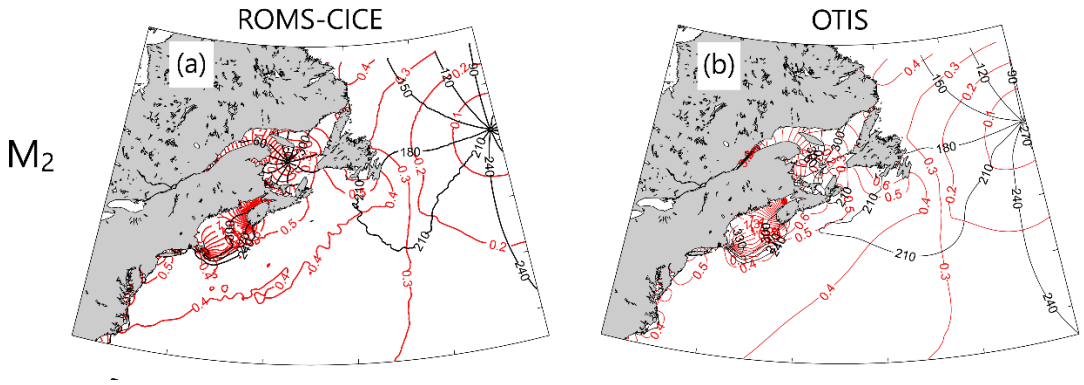

Figure D.2.3 Co-phases (black contour lines) and co-amplitudes (red contour lines) of the M_2 tidal elevations calculated from results produced by submodel L1 using t_tide (a) and taken from OTIS dataset (b; from Pei MSc thesis, Dalhousie University, 2022). The ground truth data are from m_map Matlab program (Pawlowicz, 2020).

To assess the model's performance in simulating temperature and salinity, the simulated results were compared to satellite remote sensing data and global ocean reanalysis. The satellite remote sensing data of SST used here were extracted from the daily GHRSST Level 4 CMC0.1deg Global Foundation Sea Surface Temperature Analysis (GDS version 2) dataset, provided by the Physical Oceanography Distributed Active Archive Center (PODAAC). The satellite remote sensing data of SSS was extracted from the Sea Surface Salinity Essential Climate Variable (ECV) dataset (version 1.8) produced by the European Space Agency's (ESA) Climate Change Initiative (CCI).

The submodel L1 successfully reproduced the general features of observed monthly-mean SST (as shown for March 2018 in Figure D.2.4). Specifically, the submodel L1 reproduced well the cold areas over the Gulf of St. Lawrence, Grant Banks, the coastal/shelf waters of the Scotian Shelf, Newfoundland Shelf, and Labrador Shelf. It also reproduced the warm SST in the deep ocean off the southern Eastern Canadian Shelf (ECS).

The submodel L2 also successfully reproduced the general large-scale features of monthly-mean SSS ove the model domain (as shown for March 2018 in Figure D.2.4). Submodel L1 reproduced the observed high SSS over the deep ocean waters off the ECS and the observed low SSS over the coastal and shelf waters of the ECS.

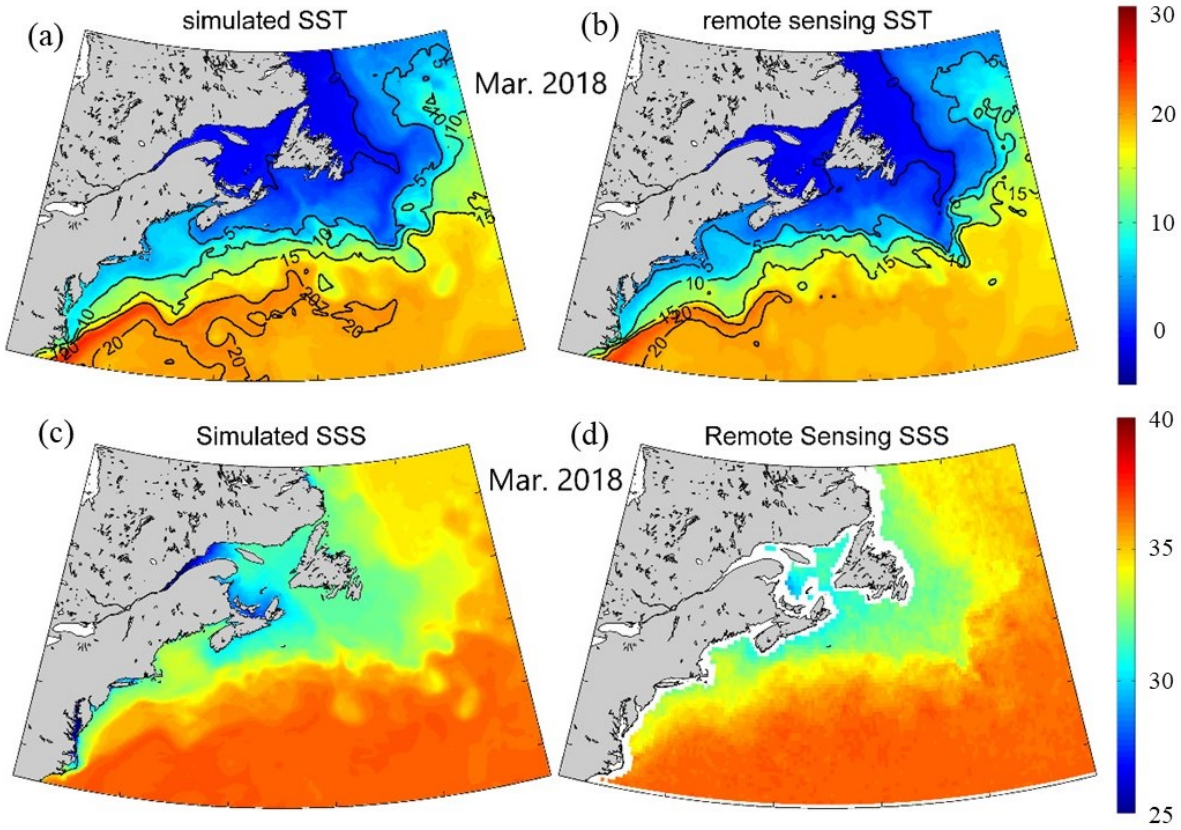

Figure D.2.4 Monthly-mean SST (a,b) and SSS (c,d) over the domain of submodel L1 in March 2018 calculated respectively from (a,c) results produced by submodel L1 and (b) satellite remote sensing SST data, and (d) extracted from the Sea Surface Salinity Essential Climate Variable (ECV) dataset (version 1.8) produced by the European Space Agency's (ESA) Climate Change Initiative (CCI; adapted from Pei MSc thesis, Dalhousie University, 2022).

To assess the validity of coupled circulation-oxygen model, the performance in simulating DO over the L3 domain and compared it to model results with the Global_Reanalysis_BIO_001_029 (GRB29) dataset (Pei MSc thesis, Dalhousie University, 2022). Figure D.2.5 compares the simulated DO with the GRB29 DO at 2 depths. While the L3 model is higher in resolution (1/108° compared to the 1/4° resolution of GRB29), the pattern simulated by GRB29 is preserved. Both model results show the relatively high DO over the inner shelf and relatively low DO over offshore waters adjacent to the eastern and southern open boundaries.

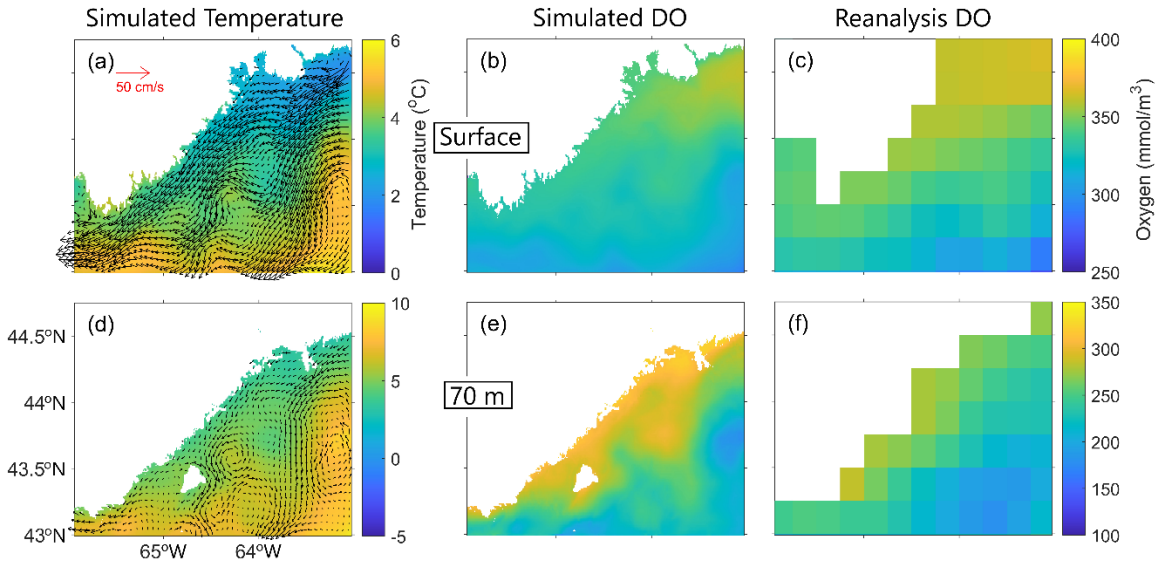

Figure D.2.5 Monthly-mean temperature (a,d), currents (arrows in a,d), and DO (b,e) produced by L3COM at (a,b) the surface and (d,e) 70 m over the L3 domain in March 2018. For clarity, velocity vectors are plotted at every 6th model grid point. Figure 4.3c,f presents the March-mean DO in 2018 at the sea surface and 70 m over the L3 domain calculated from the daily-mean product of the GRB29 dataset (from Pei MSc thesis, Dalhousie University, 2022).

Lastly, the performance of the oxygen L3 model in simulating the vertical structure of DO was assessed by comparing the model results to *in situ* observations of DO (Figure D.2.6). Vertical profiles of DO observations were compared to the simulated DO from the oxygen model at 3 points on the southwestern Scotian Shelf in July 2018: Point B (63.9 °W, 43.7 °N), Point C (63.7 °W, 43.6 °N), and Point D (63.5 °W, 43.9 °N). Overall, the two profiles agree well and indicate that the L3 model can reproduce the general vertical structure of observed DO.

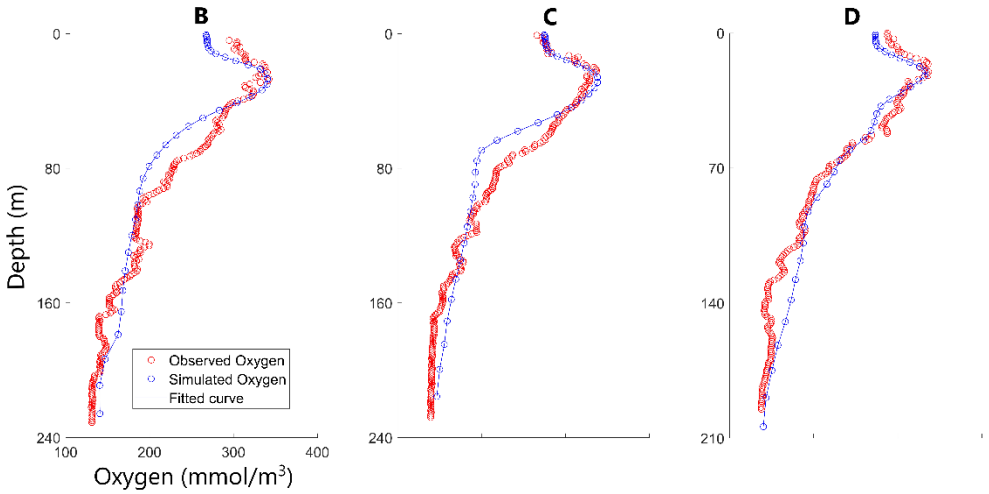

Figure D.2.6 Vertical profiles of observed (red dots) and simulated (blue lines) DO at Points B, C, and D over the southwestern Scotian Shelf in July 2018. The blue line in each subplot represents the daily-mean DO by averaging model results at four grid points around each observation point (from Pei MSc thesis, Dalhousie University, 2022).

REFERENCES

Abdel-Tawwab, M., Monier, M.N., Hoseinifar, S.H., Faggio, C., 2019. Fish response to hypoxia stress: growth, physiological, and immunological biomarkers. Fish Physiol Biochem 45, 997–1013. https://doi.org/10.1007/s10695-019-00614-9

Alexander, M.A., Scott, J.D., Friedland, K.D., Mills, K.E., Nye, J.A., Pershing, A.J., Thomas, A.C., 2018. Projected sea surface temperatures over the 21st century: Changes in the mean, variability and extremes for large marine ecosystem regions of Northern Oceans. Elementa: Science of the Anthropocene 6, 9. https://doi.org/10.1525/elementa.191

Alexander, M.A., Shin, S., Scott, J.D., Curchitser, E., Stock, C., 2020. The Response of the Northwest Atlantic Ocean to Climate Change. J Clim 33, 405–428. https://doi.org/10.1175/JCLI-D-19-0117.1

Altieri, A.H., Gedan, K.B., 2015. Climate change and dead zones. Glob Chang Biol. 21, 1395–1406. https://doi.org/10.1111/gcb.12754

Andrade, Y., 1991. Upwelling on the Scotian Shelf inferred from satellite and coastal measurements. Ph.D. thesis, Dalhousie University.

Aure, J., Strand, Ø., Erge, S.R., Strohmeier, T., 2007. Primary production enhancement by artificial upwelling in a western Norwegian fjord. Mar Ecol Prog Ser 352, 39–52.

Axler, R. P., Tikkanen, C., McDonald, M., Larsen, C, Host, G., 1993. Fish bioenergetics modeling to estimate waste loads from a net pen aquaculture operation. In Techniques for Modern Aquacultur:. Proceedings of an Aquacultural Engineering Conference.

Bakun, A., 1973. Coastal upwelling indices, west coast of North America, 1946-71. NOAA Tech. Rep. NMFS SSRF-671. U.S. Dep. of Commer., NOAA.

Barnes, R. K., King, H., Carter, C.G., 2011. Hypoxia tolerance and oxygen regulation in Atlantic salmon, Salmo salar from a Tasmanian population. Aquaculture 318, 397–401. https://doi.org/10.1016/j.aquaculture.2011.06.003

Barton, E.D., Largier, J.L., Sheridan, M., Trasviña, A., Souza, A., Pazos, Y., Valle-Levinson, A., 2015. Coastal upwelling and downwelling forcing of circulation in a semi-enclosed bay: Ria de Vigo. Prog Oceanogr 134, 173–189. https://doi.org/10.1016/j.pocean.2015.01.014

Beazley, L., Wang, Z., Kenchington, E., Yashayaev, I., Rapp, H.T., Xavier, J.R., Murillo, F.J., Fenton, D., Fuller, S., 2018. Predicted distribution of the glass sponge Vazella pourtalesi on the Scotian Shelf and its persistence in the face of climatic variability. PLOS ONE 13, e0205505. https://doi.org/10.1371/journal.pone.0205505

Berg, A., Danielsberg, A., Seland, A., 1993. Oxygen demand for postsmolt Atlantic salmon (Salmo salar L.), in: Fish Farming Technology. CRC Press, 297–300.

Benway, R. L., Thomas, K.P., Jossi, J.W. 1993. Water column thermal structure in the Middle Atlantic Bight and Gulf of Maine during 1978-92, NOAA Tech. Memo. NMFS fluorescence/NEC-97, U.S. Dep. of Commer., Woods Hole, Mass.

Bergheim, A., Gausen, M., Naess, A., Holland, P.M., Krogedal,. P., Crampton, V., 2006. A newly developed oxygen injection system for cage farms. Aquac Eng 34, 40-46. https://doi.org/10.1016/j.aquaeng.2005.04.003

Berillis, P., Mente, E., Nikouli, E., Makridis, P., Grundvig, H., Bergheim, A., Gausen, M., 2016. Improving aeration for efficient oxygenation in sea bass sea cages. Blood, brain and gill histology. Open Life Sci 11, 270–279. https://doi.org/10.1515/biol-2016-0028

Beveridge, M.C.M., 2008. Cage Aquaculture. John Wiley & Sons.

Bi, C.-W., Zhao, Y.-P., Dong, G.-H., Xu, T.-J., Gui, F.-K., 2013. Experimental investigation of the reduction in flow velocity downstream from a fishing net. Aquac Eng 57, 71–81. https://doi.org/10.1016/j.aquaeng.2013.08.002

Bianchi, T.S., Johansson, B., Elmgren, R., 2000. Breakdown of phytoplankton pigments in Baltic sediments: effects of anoxia and loss of deposit-feeding macrofauna. J Exp Mar Biol Ecol 251, 161–183. https://doi.org/10.1016/S0022-0981(00)00212-4

Bishop, C., De Young, B., Bachmayer, R., 2009. Autonomous Underwater Glider Research at Memorial University. Underw Interv 4, 7–15.

Bishop, J.K.B., Smith, R.C., Baker, K.S., 1992. Springtime distributions and variability of biogenic particulate matter in Gulf Stream warm-core ring 82B and surrounding N.W. Atlantic waters. Deep-Sea Res I: Oceanogr Res Pap 39, S295–S325. https://doi.org/10.1016/S0198-0149(11)80017-8

Bittig, H.C., Kortzinger, A., Neill, C., van Ooijen, E., Plant, J.N., Hahn, J., Johnson, K.S., Yang, B., Emerson, S.R., 2018. Oxygen Optode Sensors: Principle, Characterization, Calibration, and Application in the Ocean | Marine Science. Front Mar Sci 24. https://doi.org/10.3389/fmars.2017.00429

Blanco, J.L., Thomas, A.C., Carr, M.-E., Strub, P.T., 2001. Seasonal climatology of hydrographic conditions in the upwelling region off northern Chile. J Geophys Res-Oceans 106, 11451–11467. https://doi.org/10.1029/2000JC000540

Bögner, D., Bögner, M., Schmachtl, F., Bill, N., Halfer, J., Slater, M.J., 2021. Hydrogen peroxide oxygenation and disinfection capacity in recirculating aquaculture systems. Aquac Eng 92, 102140. https://doi.org/10.1016/j.aquaeng.2020.102140

Bonsdorff, E., Blomqvist, E.M., Mattila, J., Norkko, A., 1997. Coastal eutrophication: Causes, consequences and perspectives in the Archipelago areas of the northern Baltic Sea. Estuar Coast Shelf Sci 44, 63–72. https://doi.org/10.1016/S0272-7714(97)80008-X

Bopp, L., Le Quére, C., Heimann, M., Manning A. C., 2002. Climate-induced oceanic oxygen fluxes: implications for the contemporary carbon budget. Global Biogeochem Cycles 16, 1022. https://doi.org/10.1029/2001GB001445

Boyd, C.E., 1982. Water quality management for pond fish culture. Water quality management for pond fish culture.

Boyd, C.E., Torrans, E.L., Tucker, C.S., 2018. Dissolved Oxygen and Aeration in Ictalurid Catfish Aquaculture. J World Aquac Soc 49, 7–70. https://doi.org/10.1111/jwas.12469

Boyd, C.E., Tucker, C.S., 2019. Water quality, in: Aquaculture: Farming Aquatic Animals and Plants. John Wiley & Sons, 63–92.

Breitburg, D., L.A. Levin, Oschlies, A., Gregoire, M., Chavez, F.P., Conley, D.J., Garcon, V., Gilbert, D., Gutierrez, D., Isensee, K., Jacinto, G.S., Limburg, K.E., Montes, I., Naqvi, S.W.A., Pitcher, G.C., Rabalais, N.N., Roman, M.R., Rose, K.A., Seibel, B.A., Telszewski, M., Yasuhara, M., Zhang J., 2018. Declining oxygen in the global ocean and coastal waters. Science 359, eaam7240. https://doi.org/10.1126/science.aam7240

Burke, M., Grant, J., Filgueira, R., Stone, T., 2021. Oceanographic processes control dissolved oxygen variability at a commercial Atlantic salmon farm: Application of a real-time sensor network. Aquaculture 533, 736143. https://doi.org/10.1016/j.aquaculture.2020.736143

Brennan, C.E., Blanchard, H., Fennel, K., 2016. Putting temperature and oxygen thresholds of marine animals in context of environmental change: A regional perspective for the Scotian Shelf and Gulf of St. Lawrence. PLOS ONE 11(12): e0167411. https://doi.org/10.1371/journal.pone.0167411

Brett, J.R., 1972. The metabolic demand for oxygen in fish, particularly salmonids, and a comparison with other vertebrates. Respir Physiol 14, 151–170. https://doi.org/10.1016/0034-5687(72)90025-4

Brickman, D., Hebert, D., Wang, Z., 2018. Mechanism for the recent ocean warming events on the Scotian Shelf of eastern Canada. Cont Shelf Res 156, 11–22. https://doi.org/10.1016/j.csr.2018.01.001

Burt, K., Hamoutene, D., Mabrouk, G., Lang, C., Puestow, T., Drover, D., Losier, R., Page, F., 2012. Environmental conditions and occurrence of hypoxia within production cages of Atlantic salmon on the south coast of Newfoundland. Aquac Res 43, 607–620. https://doi.org/10.1111/j.1365-2109.2011.02867.x

Burt, K., Hamoutene, D., Perez-Casanova, J., Gamperl, A.K., Volkoff, H., 2014. The effect of intermittent hypoxia on growth, appetite and some aspects of the immune response of Atlantic salmon (*Salmo salar*). Aquac Res 45, 124-137. Doi:10.1111/j.1365-2109.2012.03211.x

Burt, W.J., Thomas, H., Auclair, J.-P., 2013. Short-lived radium isotopes on the Scotian Shelf: Unique distribution and tracers of cross-shelf CO2 and nutrient transport. Mar Chem 156, 120–129. https://doi.org/10.1016/j.marchem.2013.05.007

Caesar, L., Rahmstorf, S., Robinson, A., Feulner, G., Saba, V., 2018. Observed fingerprint of a weakening Atlantic Ocean overturning circulation. Nature 556, 191–196. https://doi.org/10.1038/s41586-018-0006-5

Chavez, F.P., Sevadjian, J., Wahl, C., Friederich, J., Friederich, G.E., 2018. Measurements of pCO2 and pH from an autonomous surface vehicle in a coastal upwelling system. Deep Sea Res Part II: Top Stud Oceanogr 151, 137–146. https://doi.org/10.1016/j.dsr2.2017.01.001

Chegini, F., Lu, Y., Katavouta, A., Ritchie, H., 2018. Coastal Upwelling Off Southwest Nova Scotia Simulated With a High-Resolution Baroclinic Ocean Model. J Geophys Res- Oceans 123, 2318–2331. https://doi.org/10.1002/2017JC013431

Chen, C., Wang, G., Xie, S.-P., Liu, W., 2019. Why Does Global Warming Weaken the Gulf Stream but Intensify the Kuroshio? J Clim 32, 7437–7451. https://doi.org/10.1175/JCLI-D-18-0895.1

Chen, Z., Kwon, Y.-O., Chen, K., Fratantoni, P., Gawarkiewicz, G., Joyce, T.M., 2020. Long-Term SST Variability on the Northwest Atlantic Continental Shelf and Slope. Geophys Res Lett 47, e2019GL085455. https://doi.org/10.1029/2019GL085455

Cheshuk, B.W., Purser, G.J., Quintana, R. 2003. Integrated open-water mussel (*Mytilus planulatus*) and Atlantic salmon (*Salmo salar*) culture in Tasmania, Australia. Aquaculture 218, 357-378. Doi:10.1016/S0044-8486(02)00640-3

Chi, L., Wolfe, C.L.P., Hameed, S., 2021. Has the Gulf Stream Slowed or Shifted in the Altimetry Era? Geophys Res Lett 48, e2021GL093113. https://doi.org/10.1029/2021GL093113

Claireaux, G., Lagardere, J.-P., 1999. Influence of temperature, oxygen and salinity on the metabolism of the European sea bass. J Sea Res 42, 157–168. https://doi.org/10.1016/S1385-1101(99)00019-2

Claret, M., Galbraith, E.D., Palter, J.B., Bianchi, D., Fennel, K., Gilbert, D., Dunne, J.P., 2018. Rapid coastal deoxygenation due to ocean circulation shift in the NW Atlantic. Nat Clim Change 8, 866–872. https://doi.org/10.1038/s41558-018-0263-1

Coffin, M.R.S., Courtenay, S.C., Pater, C.C., van den Heuvel, M.R., 2018. An empirical model using dissolved oxygen as an indicator for eutrophication at a regional scale. Mar Pollut Bull 133, 261–270. https://doi.org/10.1016/j.marpolbul.2018.05.041

Combes, V., Chenillat, F., Di Lorenzo, E., Rivière, P., Ohman, M.D., Bograd, S.J., 2013. Cross-shore transport variability in the California Current: Ekman upwelling vs. eddy dynamics. Prog Oceanogr 109, 78–89. https://doi.org/10.1016/j.pocean.2012.10.001

Coogan, J., Dzwonkowski, B., Lehrter, J., 2019. Effects of coastal upwelling and downwelling on hydrographic variability and dissolved oxygen in Mobile Bay. J Geophys Res- Oceans 124, 791–806. https://doi.org/10.1029/2018JC014592

Cronin, E.R., Cheshire, A.C., Clarke, S.M., Melville, A.J., 1999. An investigation into the composition, biomass and oxygen budget of the fouling community on a tuna aquaculture farm. Biofouling 13, 279–299. https://doi.org/10.1080/08927019909378386

Davies, S.M., Sáchez-Valesco, L., Beier, E., Godínez, V.M., Barton, E.D., Tamayo, A., 2015. Three-dimensional distribution of larval fish habitats in the shallow oxygen minimum zone in the eastern tropical Pacific Ocean off Mexico. Deep-Sea Res I: Oceanogr Res Pap 101, 118–129. https://doi.org/10.1016/j.dsr.2015.04.003

Davis, J.C., 1975. Minimal dissolved oxygen requirements of aquatic life with emphasis on Canadian species: A review. J Fish Res Board Can 32, 2295–2332. https://doi.org/10.1139/f75-268

Davis, R.E., 2010. On the coastal-upwelling overturning cell. J Mar Res 68, 369–385. https://doi.org/10.1357/002224010794657173

Davis, R., Baumgartner, M., Comeau, A., Cunningham, D., Davies, K., Furlong, A., Johnson, H., L'Orsa, S., Ross, T., Taggart, C., Whoriskey, F., 2016. Tracking whales on the Scotian Shelf using passive acoustic monitoring on ocean gliders. In: Oceans 2016 MTS/IEEE Monterey, (Piscataway, NJ: IEEE), 1–4. https://doi.org/10.1109/OCEANS.2016.7761461

Dever, M., Hebert, D., Greenan, B.J.W., Sheng, J., Smith, P.C., 2016. Hydrography and Coastal Circulation along the Halifax Line and the Connections with the Gulf of St. Lawrence. Atmos Ocean 54, 199–217. https://doi.org/10.1080/07055900.2016.1189397

De Young, B., Otterson, T., Greatbatch, R.J., 1993. The local and nonlocal response of Conception Bay to wind forcing. J Phys Oceanogr 23, 2636-2649.

Diaz, R.J., 2001. Overview of Hypoxia around the World. J Environ Qual 30, 275– 281. https://doi.org/10.2134/jeq2001.302275x

Dittmar, W. 1884. Report on researches into the composition of ocean-water, collected by HMS Challenger: During the years 1873-1876. *HM Stationery Office.*

Doelle, M., Saunders, P., 2015. Aquaculture Governance in Canada: A Patchwork of Approaches. SSRN Electronic Journal. https://doi.org/10.2139/ssrn.2659079

Doglioli, A.M., Magaldi, M.G., Vezzulli, L., Tucci, S., 2004. Development of a numerical model to study the dispersion of wastes coming from a marine fish farm in the Ligurian Sea (Western Mediterranean). Aquaculture 231, 215–235. https://doi.org/10.1016/j.aquaculture.2003.09.030

Drinkwater, K. F., Petrie, B., Smith, P. C., 2003. Climate variability on the Scotian Shelf during the 1990s. ICES Mar Sci Symp 219, 40-49.

Du, J., Shen, J., 2015. Decoupling the influence of biological and physical processes on the dissolved oxygen in the Chesapeake Bay. J Geophys Res- Oceans 120, 78–93. https://doi.org/10.1002/2014JC010422

Edwards, P.N., 2011. History of climate modeling. WIREs Climate Change 2, 128–139. https://doi.org/10.1002/wcc.95

Ekman, V.W. 1905. On the influence of earth's rotation on ocean-currents. Ark Mat Astron Fys 2, 52

Emerson, S., Stump, C., Johnson, B., Karl, D.M., 2002. In situ determination of oxygen and nitrogen dynamics in the upper ocean. Deep-Sea Res I: Oceanogr Res Pap 49, 941–952. https://doi.org/10.1016/S0967-0637(02)00004-3

Endo, A., Srithongouthai, S., Nashiki, H., Teshiba, I., Iwasaki, T., Hama, D., Tsutsumi, H., 2008. DO-increasing effects of a microscopic bubble generating system in a fish farm. Mar Pollut Bull, EMECS 7/ECSA 40, Caen (France), May 2006 57, 78–85. https://doi.org/10.1016/j.marpolbul.2007.10.014

Engle, C.R., 1989. An economic comparison of aeration devices for aquaculture ponds. Aquac Eng 8, 193–207. https://doi.org/10.1016/0144-8609(89)90028-9

Feng, T., Stanley, R.R.E., Wu, Y., Kenchington, E., Xu, J., Horne, E., 2022. A High-Resolution 3-D Circulation Model in a Complex Archipelago on the Coastal Scotian Shelf. J Geophys Res- Oceans 127, e2021JC017791. https://doi.org/10.1029/2021JC017791

Fore, M., Frank, K., Norton, T., Svendsen, E., Alfredsen J.A., Dempster, T., Eguiraun, H., Watson, W., Stahl, A., Sunde, L.M., Schellewald, C., Skoien, K.R., Alver, M.O., Berckmans, D., 2018. Precision fish farming: A new framework to improve production in aquaculture. Biosyst Eng 173, 176-193. https://doi.org/10.1016/j.biosystemseng.2017.10.014

Fournier, R.O., Ernst, R., Hargreaves, N.B., Det, M.V., Douglas, D., 1984. Variability of Chlorophyll a off Southwestern Nova Scotia in Late Fall and Its Relationship to Water Column Stability. Can J Fish Aquat Sci 41, 1730–1738. https://doi.org/10.1139/f84-213

Galbraith, P., Chassé, J., Gilbert, D., Larouche, P., Caverhill, C., Lefaivre, D., Brickman, D., Pettigrew, B., Devine, L., Lafleur, C., 2014. Physical Oceanographic Conditions in the Gulf of St. Lawrence in 2013. DFO Can Sci Advis Sec Res Doc 2014/062, vi + 84 p.

Galbraith, P.S., Chassé, J., Nicot, P., Caverhill, C., Gilbert, D., Pettigrew, B., Lefaivre, D., Brickman, D., Devine, L., Lafleur, C., 2015. Physical Oceanographic Conditions in the Gulf of St. Lawrence in 2014. DFO Can Sci Advis Sec Res Doc Doc. 2015/032. v + 82 p.

Gatien, M.G., 1976. A study in the Slope Water region south of Halifax. J Fish Res Board Can 33: 2213-2217. https://doi.org/10.1139/f76-270

Gilbert, D., Rabalais, N.N., Díaz, R.J., Zhang, J., 2010. Evidence for greater oxygen decline rates in the coastal ocean than in the open ocean. Biogeosciences 7, 2283–2296. https://doi.org/10.5194/bg-7-2283-2010

Gould, J., Sloyan, B., Visbeck, M., 2013. Chapter 3 - In Situ ocean observations: a brief history, present status, and future directions. Int Geophys 103, 59-81.

Greenan, B.J.W., Petrie, B.D., Harrison, W.G., Oakey, N.S., 2004. Are the spring and fall blooms on the Scotian Shelf related to short-term physical events? Cont Shelf Res 24, 603–625. https://doi.org/10.1016/j.csr.2003.11.006

Greenan, B.J.W., James, T.S., Loder, J.W., Pepin, P., Azetsu-Scott, K., Ianson, D., Hamme, R.C., Gilbert, D., Tremblay, J-E., Wang, X.L. and Perrie, W. (2018): Changes in oceans surrounding Canada; Chapter 7 in (eds.) Bush and Lemmen, Canada's Changing Climate Report; Government of Canada, Ottawa, Ontario, p. 343–423.

Greenberg, D.A., 1979. A numerical model investigation of tidal phenomena in the Bay of Fundy and Gulf of Maine. null 2, 161–187. https://doi.org/10.1080/15210607909379345

Griffies, S.M., Gnanadesikan, A., Dixon, K.W., Dunne, J.P., Gerdes, R., Harrison, M.J., Rosati, A., Russell, J.L., Samuels, B.L., Spelman, M.J., Winton, M., Zhang, R., 2005. Formulation of an ocean model for global climate simulations. Ocean Sci 35.

Gruber, N., S.C. Doney, S.R. Emerson, D. Gilbert, T. Kobayashi, A. Körtzinger, G.C. Johnson, K.S. Johnson, S.C. Riser, O. Ulloa., 2010. Adding oxygen to Argo: Developing a global in-situ observatory for ocean deoxygenation and biogeochemistry. In: Proceedings of OceanObs'09: Sustained Ocean Observations and Information for Society, Vol. 2, Venice, Italy, 21-25 September 2009, (eds Hall, J., Harrison, D.E. & Stammer, D.). Paris, France, European Sace Agency, 12pp (ESA Publication WPP-306). doi:10.5270/OceanObs09.cwp.39

Gruber, N., 2011. Warming up, turning sour, losing breath: ocean biogeochemistry under global change. Philos Trans A Math Phys Eng Sci 369, 1980–1996. https://doi.org/10.1098/rsta.2011.0003

Guénette, S., Araújo, J.N., Bundy, A., 2014. Exploring the potential effects of climate change on the Western Scotian Shelf ecosystem, Canada. J Mar Syst 134, 89–100. https://doi.org/10.1016/j.jmarsys.2014.03.001

Hachey, H.B., 1937. The submarine physiography and oceanographical problems of the Scotian Shelf. Trans Am Fish Soc 66, 237–241. https://doi.org/10.1577/1548-8659(1936)66[237:TSPAOP]2.0.CO;2

Hachey, H.B., 1942. The waters of the Scotian Shelf. J Fish Res Board Canada 5: 377-397.

Han, G., Hannah, C.G., Loder, J.W., Smith, P.C., 1997. Seasonal variation of the three-dimensional mean circulation over the Scotian Shelf. J Geophys Res- Oceans 102, 1011–1025. https://doi.org/10.1029/96JC03285

Han, G., Loder, J. W., 2003. Three-dimensional modeling of seasonal mean and tidal currents over the eastern Scotian Shelf. J Geophys Res 108, 3136. doi:10.1029/2002JC001463.

Han, G., Paturi, S., De Young, B., Yi, Y., Shum, C. K., 2010. A 3-D data-assimilative tidal model of the northwest Atlantic. Atmos Ocean 48, 39-57.

Handå, A., McClimans, T.A., Reitan, K.I., Knutsen, Ø., Tangen, K., Olsen, Y., 2014. Artificial upwelling to stimulate growth of non-toxic algae in a habitat for mussel farming. Aquac Res 45, 1798–1809. https://doi.org/10.1111/are.12127

Hannah, C.G., Shore, J.A., Loder, J.W., Naimie, C.E., 2001. Seasonal Circulation on the Western and Central Scotian Shelf. J Phys Oceanogr 31, 591–615. https://doi.org/10.1175/1520-0485(2001)031<0591:SCOTWA>2.0.CO;2

Hargreaves, J.A., Kakocy, J.E., Bailey, D.S., 1991. Effects of Diffused Aeration and Stocking Density on Growth, Feed Conversion, and Production of Florida Red Tilapia in Cages. J World Aquac Soc 22, 24–29. https://doi.org/10.1111/j.1749-7345.1991.tb00712.x

Hayton, W.L., Barron, M.G., 1990. Rate-limiting barriers to xenobiotic uptake by the gill. Environ Toxicol Chem 9, 151–157. https://doi.org/10.1002/etc.5620090204

Heath, R.A., 1973. Flushing of coastal embayments by changes in atmospheric conditions. Limnol Oceanogr 849–862.

Helm, K.P., N.L. Bindoff, and J.A. Church. 2011. Observed decreases in oxygen content of the global ocean. Geophys Res Lett 38. doi:10.1029/2011GL049513.

Hetland, R.D., DiMarco, S.F., 2008. How does the character of oxygen demand control the structure of hypoxia on the Texas–Louisiana continental shelf? J Mar Syst 70, 49–62. https://doi.org/10.1016/j.jmarsys.2007.03.002

Hildebrand, J.H., 1916. Solubility. J Am Chem Soc 1452–1473.

Hsu, S.A., 1980. On the correction of land-based wind measurements for oceanographic applications. Am Soc Civ Eng 1, 708-724.

Huang, J., Hu, J., Li, S., Wang, B., Xu, Y., Liang, B., Liu, D., 2019. Effects of physical forcing on summertime hypoxia and oxygen dynamics in the Pearl River Estuary. Water 11, 2080. https://doi.org/10.3390/w11102080

Hvas, M., Folkedal, O., Imsland, A., Oppedal, F., 2017. The effect of thermal acclimation on aerobic scope and critical swimming speed in Atlantic salmon, *Salmo salar*. J Exp Biol 220, 2757-2764. Doi:10.1242/jeb.154021

Ikeda, M., 1987. Wind effects on the buoyancy-driven general circulation in a closed basin using a two-level model. J Phys Oceanogr 17, 1707–1723. https://doi.org/10.1175/1520-0485(1987)017<1707:WEOTBD>2.0.CO;2

Isern-Fontanet, J., Font, J., García-Ladona, E., Emelianov, M., Millot, C., Taupier-Letage, I., 2004. Spatial structure of anticyclonic eddies in the Algerian basin (Mediterranean Sea) analyzed using the Okubo–Weiss parameter. Deep Sea Res Part II Top Stud Oceanogr 51, 3009–3028. https://doi.org/10.1016/j.dsr2.2004.09.013

Ji, R., Davis, C.S., Chen, C., Townsend, D.W., Mountain, D.G., Beardsley, R.C., 2008. Modeling the influence of low-salinity water inflow on winter-spring phytoplankton dynamics in the Nova Scotian Shelf–Gulf of Maine region. J Plankton Res 30, 1399–1416.

Johansson, D., Ruohonen, K., Kiessling, A., Oppedal, F., Stiansen, J.-E., Kelly, M., Juell, J.-E., 2006. Effect of environmental factors on swimming depth preferences of Atlantic salmon (Salmo salar L.) and temporal and spatial variations in oxygen levels in sea cages at a fjord site. Aquaculture 254, 594–605. https://doi.org/10.1016/j.aquaculture.2005.10.029

Johansson, D., Juell, J.-E., Oppedal, F., Stiansen, J.-E., Ruohonen, K., 2007. The influence of the pycnocline and cage resistance on current flow, oxygen flux and swimming behaviour of Atlantic salmon (Salmo salar L.) in production cages. Aquaculture 265, 271–287. https://doi.org/10.1016/j.aquaculture.2006.12.047

Jutras, M., Dufour, C.O., Mucci, A., Cyr, F., Gilbert, D., 2020. Temporal Changes in the Causes of the Observed Oxygen Decline in the St. Lawrence Estuary. J Geophys Res- Oceans 125, e2020JC016577. https://doi.org/10.1029/2020JC016577

Kanwisher, J. 1959. Polarographic oxygen electrode. Limnol Oceanogr 4, 210-217. doi:10.4319/lo.1959.4.2.0210

Karnauskas, K.B., Lundquist, J.K., Zhang, L., 2018. Southward shift of the global wind energy resource under high carbon dioxide emissions. Nature Geosci 11, 38–43. https://doi.org/10.1038/s41561-017-0029-9

Keeling, R.F., A. Körtzinger, and N. Gruber. 2009. Ocean deoxygenation in a warming world. Ann Rev Mar Sci 2, 199-229. doi:10.1146/annurev.marine.010908.

Kepenyes, J., Váradi, L., n.d. Chapter 21 Aeration and Oxygenation in Aquaculture. Fish Culture Research Institute.

Khan, A.H., Levac, E., Chmura, G.L., 2013. Future sea surface temperatures in Large Marine Ecosystems of the Northwest Atlantic. ICES Journal of Marine Science 70, 915–921. https://doi.org/10.1093/icesjms/fst002

Klebert, P., Lader, P., Gansel, L., Oppedal, F., 2013. Hydrodynamic interactions on net panel and aquaculture fish cages: A review. Ocean Eng 58, 260–274. https://doi.org/10.1016/j.oceaneng.2012.11.006

Klebert, P., Su, B., 2020. Turbulence and flow field alterations inside a fish sea cage and its wake. Appl Ocean Res 98, 102113. https://doi.org/10.1016/j.apor.2020.102113

Koelling, J., Atamanchuk, D., Karstensen, J., Handmann, P., Wallace, D.W.R., 2022. Oxygen export to the deep ocean following Labrador Sea Water formation. Biogeosciences 19, 437–454. https://doi.org/10.5194/bg-19-437-2022

Kumar, G., Engle, C., 2017. Economics of Intensively Aerated Catfish Ponds. J World Aquac Soc 48, 320–332. https://doi.org/10.1111/jwas.12385

Lagos, M.E., White, C.R., Marshall, D.J., 2015. Avoiding low-oxygen environments: Oxytaxis as a mechanism of habitat selection in a marine invertebrate. Mar Ecol Prog 540, 99-107. doi: 10.3354/meps11509

LaCasce, J.H., Pedlosky, J., 2004. The Instability of Rossby Basin Modes and the Oceanic Eddy Field. J Phys Oceanogr 34, 2027–2041. https://doi.org/10.1175/1520-0485(2004)034<2027:TIORBM>2.0.CO;2

Laffoley, D., Baxter, J.M., 2019. Ocean deoxygenation: Everyone's problem - Causes, impacts, consequences and solutions. Gland, Switzerland: IUCN.

Large, W.G., Pond, S., 1981. Open ocean momentum flux measurements in moderate to strong winds. J Phys Oceanogr 11, 324–336. https://doi.org/10.1175/1520-0485(1981)011<0324:OOMFMI>2.0.CO;2

Largier, J.L., 2020. Upwelling bays: How coastal upwelling controls circulation, habitat, and productivity in Bays. Ann Rev Mar Sci 12, 415–447. https://doi.org/10.1146/annurev-marine-010419-011020

Lavoie, D., Lambert, N., Gilbert, D., 2019. Projections of Future Trends in Biogeochemical Conditions in the Northwest Atlantic Using CMIP5 Earth System Models. Atmos Ocean 57, 18–40. https://doi.org/10.1080/07055900.2017.1401973

Lavoie, D., Lambert, N., Rousseau, S., Dumas, J., Chassé, J., Long, Z., Perrie, W., Starr, M., Brickman, D., Azetsu-Scott, K., 2020. Projections of future physical and biochemical conditions in the Gulf of St. Lawrence, on the Scotian Shelf and in the Gulf of Maine using a regional climate model. Canadian Technical Report of Hydrography and Ocean Sciences 334.

Lawson, T.B., 1995. Oxygen and Aeration, in: Lawson, T.B. (Ed.), Fundamentals of Aquacultural Engineering. Springer US, Boston, MA, pp. 248–310. https://doi.org/10.1007/978-1-4615-7047-9_11

Lekang, O.-I., 2007. Aquaculture engineering. Blackwell Pub, Oxford ; Ames, Iowa

Levin, L.A., 2003. Oxygen minimum zone benthos: Adaptation and community response to hypoxia. Gibson, R.N., Atkinson, R.J.A. (Eds.), Oceanogr Mar Biol 41. CRC Press, pp. 9–9. https://doi.org/10.1201/9780203180570-3

Lewis, R., 1981. Seasonal upwelling along the south-eastern coastline of South Australia. Mar Fresh Res 32, 843. https://doi.org/10.1071/MF9810843

Lewis, M.R., Platt, T., 1982. Scales of variability in estuarine ecosystems, in: Kennedy, V.S. (Ed.), Estuarine Comparisons. Academic Press, pp. 3–20. https://doi.org/10.1016/B978-0-12-404070-0.50007-7

Lima, F.P., Wethey, D.S., 2012. Three decades of high-resolution coastal sea surface temperatures reveal more than warming. Nat Commun 3, 1–13. https://doi.org/10.1038/ncomms1713

Liss, P.S., 1988. Tracers of air-sea gas exchange. Philos Trans Royal Soc A 325, 93–103. https://doi.org/10.1098/rsta.1988.0045

Loder, J.W., Han, G., Hannah, C.G., Greenberg, D.A., Smith, C., 1997. Hydrography and baroclinic circulation in the Scotian Shelf region: winter versus summer. Can J Fish Aquat Sci 54, 40-56.

Losordo, T.M., Piedrahita, R.H., 1991. Modelling temperature variation and thermal stratification in shallow aquaculture ponds. Ecol Modell 54, 189–226. https://doi.org/10.1016/0304-3800(91)90076-D

Mansour A., Hamoutene D., Mabrouk G., Puestow T., Barlow E., 2008 Evaluation of some environmental parameters for salmon aquaculture cage sites in Fortune Bay, Newfoundland: Emphasis on the occurrence of hypoxic conditions. Canadian Technical Report of Fisheries and Aquatic Sciences, 2814, 21pp.

Marchesiello, P., McWilliams, J.C., Shchepetkin, A., 2003. Equilibrium Structure and Dynamics of the California Current System. J Phys Oceanogr 33, 753–783. https://doi.org/10.1175/1520-0485(2003)33<753:ESADOT>2.0.CO;2

McClimans, T.A., Handå, A., Fredheim, A., Lien, E., Reitan, K.I., 2010. Controlled artificial upwelling in a fjord to stimulate non-toxic algae. Aquac Eng 42, 140–147. https://doi.org/10.1016/j.aquaeng.2010.02.002

McGinty, N., Barton, A.D., Record, N.R., Finkel, Z.V., Johns, D.G., Stock, C.A., Irwin, A.J., 2021. Anthropogenic climate change impacts on copepod trait biogeography. Glob Change Biol 27, 1431–1442. https://doi.org/10.1111/gcb.15499

McLellan, H.J., 1957. On the Distinctness and Origin of the Slope Water off the Scotian Shelf and its Easterly Flow South of the Grand Banks. J Fish Res Board Can 14, 213–239. https://doi.org/10.1139/f57-011

Mellor, G. L.,Yamada, T., 1982. Development of a turbulence closure model for geophysical fluid problems. Rev Geophys 20, 851-875.

Meyer, F.P., 1970. Seasonal fluctuations in the incidence of disease on fish farms, in: A Symposium on Diseases of Fishes and Shellfishes. Am Fish Soc, 21–29.

Mills, E.L., Fournier, R.O., 1979. Fish production and the marine ecosystems of the Scotian Shelf, eastern Canada. Mar Biol 54, 101–108. https://doi.org/10.1007/BF00386589

Molnar, L., Toal, D., 2007. A control system development for submersible sea cage system. Oceans 2007, 1-11pp. doi: 10.1109/OCEANS.2007.4449291.

Moore, J.K., Fu, W., Primeau, F., Britten, G.L., Lindsay, K., Long, M., Doney, S.C., Mahowald, N., Hoffman, F., Randerson, J.T., 2018. Sustained climate warming drives declining marine biological productivity. Science 359, 1139–1143. https://doi.org/10.1126/science.aao6379

Morales, C.E., Hormazábal, S.E., Blanco, J., 1999. Interannual variability in the mesoscale distribution of the depth of the upper boundary of the oxygen minimum layer off northern Chile (18–24S): Implications for the pelagic system and biogeochemical cycling. J Mar Res 57, 909–932. https://doi.org/10.1357/002224099321514097

Neralla, V.R., Venkatesh, S., 1989. Real-time application of an oil spill movement prediction system. Nat Hazards 2, 31–44. https://doi.org/10.1007/BF00124756

Neubauer, P., Andersen, K.H., 2019. Thermal performance of fish is explained by an interplay between physiology, behaviour and ecology. Conserv Physiol 7. https://doi.org/10.1093/conphys/coz025

Noble, C., Gismervik, K., Iversen, M. H., Kolarevic, J., Nilsson, J., Stien, L. H., Turnbull, J. F., (Eds.) 2018. Welfare Indicators for farmed Atlantic salmon: tools for assessing fish welfare 351pp.

Nunez, S., Arets, E., Alkemade, R., Verwer, C., Leemans, R., 2019. Assessing the impacts of climate change on biodiversity: is below 2 °C enough? Clim Change 154, 351–365. https://doi.org/10.1007/s10584-019-02420-x

Oberle, M., Salomon, S., Ehrmaier, B., Richter, P., Lebert, M., Strauch, S.M., 2019. Diurnal stratification of oxygen in shallow aquaculture ponds in central Europe and recommendations for optimal aeration. Aquaculture 501, 482–487. https://doi.org/10.1016/j.aquaculture.2018.12.005

O'Donncha, F., Grant, J., 2019. Precision Aquaculture. IEEE Internet of Things Magazine 2, 26–30. https://doi.org/10.1109/IOTM.0001.1900033

Oldham, T., Dempster, T., Fosse, J.O., Oppedal, F., 2017. Oxygen gradients affect behaviour of caged Atlantic salmon Salmo salar. Aquaculture Environment Interactions 9, 145–153. https://doi.org/10.3354/aei00219

Oldham, T., Oppedal, F., Dempster, T., 2018. Cage size affects dissolved oxygen distribution in salmon aquaculture. Aquac Environ Interact 10, 149–156. https://doi.org/10.3354/aei00263

Oldham, T., Nowak, B., Hvas, M., Oppedal, F., 2019. Metabolic and functional impacts of hypoxia vary with size in Atlantic salmon. Comp Biochem Physiol Part A-Mol Integr Physiol 231, 30-38. https://doi.org/10.1016/j.cbpa.2019.01.012

Oppedal, F., Juell, J.-E., Tarranger, G.L., Hansen, T., 2001. Artificial light and season affects vertical distribution and swimming behaviour of post-smolt Atlantic salmon in sea cages. J Fish Biol 58, 1570–1584. https://doi.org/10.1111/j.1095-8649.2001.tb02313.x

Oppedal, F., Dempster, T., Stien, L.H., 2011a. Environmental drivers of Atlantic salmon behaviour in sea-cages: A review. Aquaculture 311, 1–18. https://doi.org/10.1016/j.aquaculture.2010.11.020

Oppedal, F., Vagseth, T., Dempster, T., Juell., J-E., Johansson, D., 2011b. Fluctuating sea-cage environments modify the effects of stocking densities on production and welfare parameters of Atlantic salmon (*Salmo salar* L.). Aquaculture 315, 361-368. https://doi.org/10.1016/j.aquaculture.2011.02.037

Oschlies, A., Koeve, W., Landolfi, A., Kähler, P., 2019. Loss of fixed nitrogen causes net oxygen gain in a warmer future ocean. Nat Commun 10, 2805. https://doi.org/10.1038/s41467-019-10813-w

Packard, T.T., Christensen, J.P., 2004. Respiration and vertical carbon flux in the Gulf of Maine water column. J Mar Res 62, 93–115. https://doi.org/10.1357/00222400460744636

Page, F.H., Losier, R., McCurdy, P., Greenberg, D., Chaffey, J., Chang, B., 2005. Dissolved oxygen and salmon cage culture in the southwestern New Brunswick portion of the Bay of Fundy. Environmental Effects of Marine Finfish Aquaculture, 1–28. https://doi.org/10.1007/b136002

Paiva, A.M., Hargrove, J.T., Chassignet, E.P., Bleck, R., 1999. Turbulent behavior of a fine mesh (1/12°) numerical simulation of the North Atlantic. J Mar Syst 21, 307–320. https://doi.org/10.1016/S0924-7963(99)00020-2

Pawlowicz, R., 2020. "M_Map: A mapping package for MATLAB", version 1.4m, [Computer software], available online at www.eoas.ubc.ca/~rich/map.html.

Pastore, D.M., Peterson, R.N., Fribance, D.B., Viso, R., Hackett, E.E., 2019. Hydrodynamic Drivers of Dissolved Oxygen Variability within a Tidal Creek in Myrtle Beach, South Carolina. Water 11, 1723. https://doi.org/10.3390/w11081723

Paulmier, A., D. Ruiz-Pino., 2009. Oxygen minimum zones (OMZs) in the modern ocean. Prog Oceanogr 80, 113-128. doi: 10.1016/j.pocean.2008.08.001

Pei, Q., 2022. Study of circulation, hydrography and dissolved oxygen concentration over coastal waters of the Scotian Shelf. Master of Science, Department of Oceanography, Dalhousie University, Halifax, Nova Scotia, Canada.

Petrie, B., Drinkwater, K., 1978. Circulation in an Open Bay. J Fish Res Board Can 35, 1116–1123. https://doi.org/10.1139/f78-176

Petrie, B., Topliss, B.J., Wright, D.G., 1987. Coastal upwelling and eddy development off Nova Scotia. J Geophys Res- Oceans 92, 12979–12991. https://doi.org/10.1029/JC092iC12p12979

Petrie, B., Drinkwater, K., 1993. Temperature and salinity variability on the Scotian Shelf and in the Gulf of Maine 1945–1990. J Geophys Res-Oceans 98, 20079–20089. https://doi.org/10.1029/93JC02191

Petrie, B., Yeats, P., 2000. Annual and interannual variability of nutrients and their estimated fluxes in the Scotian Shelf – Gulf of Maine region. Can J Fish Aquat Sci 57. https://doi.org/10.1139/f00-235

Pingree, R.D., Maddock, L., 1979. The tidal physics of headland flows and offshore tidal bank formation. Mar Geol 32, 269–289. https://doi.org/10.1016/0025-3227(79)90068-9

Powell, M. D., Vickery, P. J., Reinhold, T. A., 2003. Reduced drag coefficient for high wind speeds in tropical cyclones. Nature 422, 279–283. https://doi.org/10.1038/nature01481

Priestly, M.B., 1981. Spectral analysis and time series. Academic Press. 890 pp.

Rabalais, N.N., Cai, W.-J., Carstensen, J., Conley, D.J., Fry, B., Hu, X., Quiñones-Rivera, Z., Rosenberg, R., Slomp, C.P., Turner, R.E., Voss, M., Wissel, B., Zhang, J., 2014. Eutrophication-Driven Deoxygenation in the Coastal Ocean. Oceanogr 27, 172–183.

Raju, K.R.S.R., Varma, G.H.K., 2017. Knowledge Based Real Time Monitoring System for Aquaculture Using IoT, in: 2017 IEEE 7th International Advance Computing Conference (IACC). Presented at the 2017 IEEE 7th International Advance Computing Conference (IACC), 318–321 pp. https://doi.org/10.1109/IACC.2017.0075

Remen, M., Oppedal, F., Imsland, A.K., Olsen, R.E., Torgersen, T., 2013. Hypoxia tolerance thresholds for post-smolt Atlantic salmon: Dependency of temperature and hypoxia acclimation. Aquaculture, 416-417, 41-47. https://doi.org/10.1016/j.aquaculture.2013.08.024

Remen, M., Aas, T. S., Vågseth, T., Torgersen, T., Olsen, R. E., Imsland, A., Oppedal, F., 2014. Production performance of Atlantic salmon (Salmo salar L.) postsmolts in cyclic hypoxia, and following compensatory growth. Aquac Res, 45, 1355–1366. Doi: 10.1111/are.12082

Remen, M., Sievers, M., Torgersen, T., Oppedal, F., 2016. The oxygen threshold for maximal feed intake of Atlantic salmon post-smolts is highly temperature-dependent. Aquaculture 464, 582–592. https://doi.org/10.1016/j.aquaculture.2016.07.037

Richards, F.A., 1957. Oxygen in the ocean. Geol Soc Am, Mem 185–238.

Ridder, N.N., England, M.H., 2014. Sensitivity of ocean oxygenation to variations in tropical zonal wind stress magnitude. Global Biogeochem Cycles 28, 909–926. https://doi.org/10.1002/2013GB004708

Rixen, T., Jiménez, C., Cortés, J., 2012. Impact of upwelling events on the sea water carbonate chemistry and dissolved oxygen concentration in the Gulf of Papagayo (Culebra Bay), Costa Rica: Implications for coral reefs. Rev Biol Trop 60, 187–195.

Rodriguez, L., Marin, V., Farias, M., Oyarce, E.,, 1991. Identification of an upwelling zone by remote sensing and in situ measurements. Mejillones del Sur Bay (Antofagasta-Chile). Sci Mar 55, 467–473.

Roegner, G.C., Needoba, J.A., Baptista, A.M., 2011. Coastal Upwelling Supplies Oxygen-Depleted Water to the Columbia River Estuary. PLOS ONE 6, e18672. https://doi.org/10.1371/journal.pone.0018672

Ross, T., Craig, S.E., Comeau, A., Davis, R., Dever, M., Beck, M., 2017. Blooms and subsurface phytoplankton layers on the Scotian Shelf: Insights from profiling gliders. J Mar Syst 172, 118–127. https://doi.org/10.1016/j.jmarsys.2017.03.007

Ruckdeschel, G.S., Davies, K.T.A., Ross, T., 2020. Biophysical Drivers of Zooplankton Variability on the Scotian Shelf Observed Using Profiling Electric Gliders. Front Mar Sci 7. https://doi.org/10.3389/fmars.2020.00627

Rumyantseva, A., Henson, S., Martin, A., Thompson, A.F., Damerell, G.M., Kaiser, J., Heywood, K.J., 2019. Phytoplankton spring bloom initiation: The impact of atmospheric forcing and light in the temperate North Atlantic Ocean. Prog Oceanogr 178, 102202. https://doi.org/10.1016/j.pocean.2019.102202

Rutherford, K., Fennel, K., 2018. Diagnosing transit times on the northwestern North Atlantic continental shelf. Ocean Sci 14, 1207–1221. https://doi.org/10.5194/os-14-1207-2018

Rutherford, K., Fennel, K., Atamanchuk, D., Wallace, D., Thomas, H., 2021. A modelling study of temporal and spatial pCO_2 variability on the biologically active and temperature-dominated Scotian Shelf. Biogeosciences 18, 6271–6286. https://doi.org/10.5194/bg-18-6271-2021

Saha, K., Zhao, X., Zhang, H., Casey, K. S., Zhang, D., Baker-Yeboah, S., Kilpatrick, K. A., Evans, R. H., Ryan, T., Relph, J. M., 2018. AVHRR Pathfinder version 5.3 level 3 collated (L3C) global 4km sea surface temperature for 1981-Present. NOAA National Centers for Environmental Information. Dataset. https://doi.org/10.7289/v52j68xx.

Saba, V.S., Griffies, S.M., Anderson, W.G., Winton, M., Alexander, M.A., Delworth, T.L., Hare, J.A., Harrison, M.J., Rosati, A., Vecchi, G.A., Zhang, R., 2016. Enhanced warming of the Northwest Atlantic Ocean under climate change. J Geophys Res- Oceans 121, 118–132. https://doi.org/10.1002/2015JC011346

Sameoto, D.D., Herman, A.W., 1990. Life cycle and distribution of Calanus finmarchicus in deep basins on the Nova Scotia shelf and seasonal changes in Calanus spp. Mar Ecol Prog Ser 66, 225–237.

Sanchez-Cabeza, J.-A., Herrera-Becerril, C.A., Carballo, J.L., Yáñez, B., Álvarez-Sánchez, L.F., Cardoso-Mohedano, J.-G., Ruiz-Fernández, A.C., 2022. Rapid surface water warming and impact of the recent (2013–2016) temperature anomaly in shallow coastal waters at the eastern entrance of the Gulf of California. Prog Oceanogr 202, 102746. https://doi.org/10.1016/j.pocean.2022.102746

Santana, R., Lessa, G.C., Haskins, J., Wasson K.. 2018. Continuous monitoring reveals drivers of dissolved oxygen variability in a small California estuary. Estuaries Coast 41, 99-113.

Sarma, V.V.S.S., Sridevi, B., Maneesha, K., Sridevi, T., Naidu, S.A., Prasad, V.R., Venkataramana, V., Acharya, T., Bharati, M.D., Subbaiah, Ch.V., Kiran, B.S., Reddy, N.P.C., Sarma, V.V., Sadhuram, Y., Murty, T.V.R., 2013. Impact of atmospheric and physical forcings on biogeochemical cycling of dissolved oxygen and nutrients in the coastal Bay of Bengal. J Oceanogr 69, 229–243. https://doi.org/10.1007/s10872-012-0168-y

Schmidtko, S., Stramma, L., Visbeck, M., 2017. Decline in global oceanic oxygen content during the past five decades. Nature 542, 335–339. https://doi.org/10.1038/nature21399

Seibel, B.A. 2011. Critical oxygen levels and metabolic suppression in oceanic oxygen minimum zones. J Exp Biol 214, 326-336. doi:10.1242/jeb.049171

Seibel, B.A., J.L. Schneider, S. Kaartvedt, K.F. Wishner, and K.L. Daly. 2016. Hypoxia tolerance and metabolic suppression in oxygen minimum zone Euphausiids: Implications for ocean deoxygenation and biogeochemical cycles. Integr Comp Biol 56, 510-523. doi:10.1093/icb/icw091

Seidov, D., Baranova, O. K., Boyer, T., Cross, S. L., Mishonov, A. V.,Parsons, A. R., 2016. Northwest Atlantic Regional Ocean Climatology, in NOAA Atlas NESDIS 80, edited by A. V. Mishonov, 56 pp., NOAA/NESDIS, Washington, D. C., doi:10.7289/V5/ATLAS-NESDIS-80

Seidov, D., Mishonov, A., Parsons, R., 2021. Recent warming and decadal variability of Gulf of Maine and Slope Water. Limnol Oceanogr 66, 3472–3488. https://doi.org/10.1002/lno.11892

Shadwick, E.H., Thomas, H., Comeau, A., Craig, S.E., Hunt, C.W., Salisbury, J.E., 2010. Air-Sea CO_2 fluxes on the Scotian Shelf: seasonal to multi-annual variability. Biogeosciences 7, 3851–3867. https://doi.org/10.5194/bg-7-3851-2010

Shadwick, E.H., Thomas, H., 2011. Carbon Dioxide in the Coastal Ocean: A Case Study in the Scotian Shelf Region. Ocean Yearbook Online 25, 171–204. https://doi.org/10.1163/22116001-92500007

Shadwick, E.H., Thomas, H., 2014. Seasonal and spatial variability in the CO2 system on the Scotian Shelf (Northwest Atlantic). Mar Chem 160, 42–55. https://doi.org/10.1016/j.marchem.2014.01.009

Shaffer, G., Olsen, S., Pedersen, J.O., 2009. Long-term ocean oxygen depletion in response to carbon dioxide emissions from fossil fuels. Nat Geosci 2. https://doi.org/10.1038/ngeo420

Shan, S., Sheng, J., 2022. Numerical study of topographic effects on wind-driven coastal upwelling on the Scotian Shelf. J Mar Sci Eng 10, 497.https://doi.org/10.3390/jmse10040497

Shore, J.A., Hannah, C.G., Loder, J.W., 2000. Drift pathways on the western Scotian Shelf and its environs. Can J Fish Aquat Sci 57, 2488-2505.

Shulenberger, E., Reid, J.L., 1981. The Pacific shallow oxygen maximum, deep chlorophyll maximum, and primary productivity, reconsidered. Deep-Sea Res I: Oceanogr Res Pap 28, 901–919. https://doi.org/10.1016/0198-0149(81)90009-1

Silvert, W., Sowles, J.W., 1996. Modelling environmental impacts of marine finfish aquaculture. J Appl Ichthyol 12, 75–81. https://doi.org/10.1111/j.1439-0426.1996.tb00066.x

Smagorinsky, J., 1963. General circulation experiments with the primitive equations: I. The basic experiment. Mon Weather Rev 91, 99-164.

Smith, P.C., 1978. Low-frequency fluxes of momentum, heat, salt, and nutrients at the edge of the Scotian Shelf. J Geophys Res- Oceans 83, 4079–4096. https://doi.org/10.1029/JC083iC08p04079

Smith, P. C., Petrie, B., Mann, C.R., 1978. Circulation, variability, and dynamics of the Scotian Shelf and Slope. J Fish Res Board Can 35, 1067-1083.

Smith, P.C., Schwing, F.B., 1991. Mean circulation and variability on the eastern Canadian continental shelf. Cont Shelf Res 11, 977–1012. https://doi.org/10.1016/0278-4343(91)90088-N

Smith, R.D., Maltrud, M.E., Bryan, F.O., Hecht, M.W., 2000. Numerical Simulation of the North Atlantic Ocean at 1/10°. J Phys Oceanogr 30, 1532–1561. https://doi.org/10.1175/1520-0485(2000)030<1532:NSOTNA>2.0.CO;2

Snieszko, S.F., 1974. The effects of environmental stress on outbreaks of infectious diseases of fishes. J Fish Biol 6, 197–208. https://doi.org/10.1111/j.1095-8649.1974.tb04537.x

Solstorm, D., Oldham, T., Solstorm, F., Klebert, P., Stien, L.H., Vagseth, T., Oppedal, F., 2018. Dissolved oxygen variability in a commercial sea-cage exposes farmed Atlantic salmon to growth limiting conditions. Aquaculture 486, 122–129. https://doi.org/10.1016/j.aquaculture.2017.12.008

Song, H., Ji, R., Stock, C., Kearney, K., Wang, Z., 2011. Interannual variability in phytoplankton blooms and plankton productivity over the Nova Scotian Shelf and in the Gulf of Maine. Mar Ecol Prog Ser 426, 105–118. https://doi.org/10.3354/meps09002

Song, H., Ji, R., Stock, C., Wang, Z., 2010. Phenology of phytoplankton blooms in the Nova Scotian Shelf–Gulf of Maine region: remote sensing and modeling analysis. J Plankton Res 32, 1485–1499. https://doi.org/10.1093/plankt/fbq086

Spietz, R.L., C.M. Williams, G. Rocap, and M.C. Horner-Devine. 2015. A dissolved oxygen threshold for shifts in bacterial community structure in a seasonally hypoxic estuary. PLoS One 10, e0135731. doi: 10.1371/journal.pone.0135731

Srithongouthai, S., Endo, A., Inoue, A., Kinoshita, K., Yoshioka, M., Sato, A., Iwasaki, T., Teshiba, I., Nashiki, H., Hama, D., Tsutsumi, H., 2006. Control of dissolved oxygen levels of water in net pens for fish farming by a microscopic bubble generating system. Fish Sci 72, 485–493. https://doi.org/10.1111/j.1444-2906.2006.01176.x

Stauffer, B.A, Gellene, A.G., Schnetzer, A., Seubert, E.L., Oberg, C., Sukhatme, G.S., Caron, D.A., 2012. An oceanographic, meterological, and biological 'perfect storm' yields a massive fish kill. Mar Ecol Prog Ser 468, 231-243. Doi: 10.3354/meps09927

Stehfast, K.M., Carter, C.G., McAllister, J.D., Ross, J.D., Semmens, J.M., 2017. Response of Atlantic salmon *Salmo salar* to temperature and dissolved oxygen extremes established using animal-borne environmental sensors. Sci Rep 4545. https://doi.org/10.1038/s41598-017-04806-2

Stortini, C.H., Shackell, N.L., Tyedmers, P., Beazley, K., 2015. Assessing marine species vulnerability to projected warming on the Scotian Shelf, Canada. ICES J Mar Sci 72, 1731–1743. https://doi.org/10.1093/icesjms/fsv022

Stramma, L., Schmidtko, S., 2019. Global evidence of ocean deoxygenation. Laffoley D, Baxter J. M (Eds). Ocean Deoxygenation – Everyone's Problem: Causes, Impacts, Consequences and Solutions. Gland, Switzerland: IUCN. 25–36.

Sutcliffe, W.H., Jr., Loucks, R.H., Drinkwater, K.F., 1976. Coastal Circulation and Physical Oceanography of the Scotian Shelf and the Gulf of Maine. J Fish Res 33, 98-115.

Sutherland, D.A., O'Neill, M.A., 2016. Hydrographic and dissolved oxygen variability in a seasonal Pacific Northwest estuary. Estuar Coast Shelf Sci 172, 47–59. https://doi.org/10.1016/j.ecss.2016.01.042

Tait, L.W., Schiel, D.R., 2013. Impacts of Temperature on Primary Productivity and Respiration in Naturally Structured Macroalgal Assemblages. PLoS ONE 8, e74413. https://doi.org/10.1371/journal.pone.0074413

Takahashi, T., Nakata, H., Hirano, K., Matsuoka, K., Iwataki, M., Yamaguchi, H., Kasuya, T., 2009. Upwelling of oxygen-depleted water (Sumishio) in Omura Bay, Japan. J Oceanogr 65, 113–120. https://doi.org/10.1007/s10872-009-0011-2

Talley, L.D., 2011. Descriptive physical oceanography: An introduction. Academic Press, 63pp.

Taranger, G.L., O. Karlsen, R.J. Bannister, K.A. Glover, V. Husa, E. Karlsbakk, B.O. Kvamme, K.K. Boxaspen, P.A. Bjorn, B. Finstad, A.S. Madhun, H.C. Morton, and T. Svasand. 2015. Risk assessment of the environmental impact of Norwegian Atlantic salmon farming. ICES J Mar Sci 72, 997-1021.

Tengberg, A., Hovdenes, J., Andersson, H.J., Brocandel, O., Diaz, R., Hebert, D., Arnerich, T., Huber, C., Körtzinger, A., Khripounoff, A., Rey, F., Rönning, C., Schimanski, J., Sommer, S., Stangelmayer, A., 2006. Evaluation of a lifetime-based optode to measure oxygen in aquatic systems. Limnol Oceanogr: Methods 4, 7–17. https://doi.org/10.4319/lom.2006.4.7

Thompson, K. R., Sheng, J., 1997. Subtidal circulation on the Scotian Shelf: Assessing the hindcast skill of a linear, barotropic model. J Geophys Res-Oceans 102, 24987-25003.

Townsend, D.W., Pettigrew, N.R., Thomas, M.A., Neary, M.G., McGillicuddy, D.J., O'Donnell, J., 2015. Water masses and nutrient sources to the Gulf of Maine. J Mar Res 73, 93–122. https://doi.org/10.1357/002224015815848811

Trenberth, K.E., 2018. Climate change caused by human activities is happening and it already has major consequences. J Energy Nat Resour Law 36, 463–481. https://doi.org/10.1080/02646811.2018.1450895

Trudel, M., Welch, D.W., 2005. Modeling the Oxygen Consumption Rates in Pacific Salmon and Steelhead: Model Development. Trans Am Fish Soc 134, 1542–1561. https://doi.org/10.1577/T04-156.1

Turner, R.E., Schroeder, W.W., Wiseman, Wm.J., 1987. The Role of Stratification in the Deoxygenation of Mobile Bay and Adjacent Shelf Bottom Waters. Estuaries 10, 13. https://doi.org/10.2307/1352020

Uchida, H., Kawano, T., Kaneko, I., Fukasawa, M., 2008. In situ calibration of optode-based oxygen sensors. J Atmos Ocean Technol 25, 2271-2281. https://doi.org/10.1175/2008JTECHO549.1

Umoh, J.U., Thompson, K.R., 1994. Surface heat flux, horizontal advection, and the seasonal evolution of water temperature on the Scotian Shelf. J Geophys Res-Oceans 99, 20403–20416. https://doi.org/10.1029/94JC01620

Vaquer-Sunyer, R., Duarte, C.M., 2008. Thresholds of hypoxia for marine biodiversity. Proc Nat Acad Sci 105, 15452–15457.

Vautard, R., Cattiaux, J., Yiou, P., Thépaut, J.-N., Ciais, P., 2010. Northern Hemisphere atmospheric stilling partly attributed to an increase in surface roughness. Nature Geosci 3, 756–761. https://doi.org/10.1038/ngeo979

Vigen, J., 2008. Oxygen variation within a seacage. European Master in Aquaculture and Fisheries, Department of Biology, University of Bergen, Bergen.

Vinci and Summerfelt 2015. 9th Annual Recirculating Aquaculture Systems Short Course. The Freshwater Institute, WV.

Wallmann, K., 2003. Feedbacks between oceanic redox states and marine productivity: A model perspective focused on benthic phosphorus cycling. Global Biogeochem Cyc 17. https://doi.org/10.1029/2002GB001968

Wang, Y., Sheng, J., Lu, Y., 2020. Examining tidal impacts on seasonal circulation and hydrography variability over the eastern Canadian shelf using a coupled circulation-ice regional model. Prog Oceanogr 189, 102448.

Wang, Z., Li, D., Xue, H., Thomas, A.C., Zhang, Y.J., Chai, F., 2022. Freshwater Transport in the Scotian Shelf and Its Impacts on the Gulf of Maine Salinity. J Geophys Res- Oceans 127, e2021JC017663. https://doi.org/10.1029/2021JC017663

Watson, A.J., Lenton, T.M., Mills, B.J.W., 2017. Ocean deoxygenation, the global phosphorus cycle and the possibility of human-caused large-scale ocean anoxia. Philos Trans Royal Soc A 375, 20160318. https://doi.org/10.1098/rsta.2016.0318

Wiebe, P.H., Hulburt, E.M., Carpenter, E.J., Jahn, A.E., Knapp III, G.P., Boyd, S.H., Ortner, P.B., Cox, J.L., 1976. Gulf stream cold core rings: large-scale interaction sites for open ocean plankton communities. Deep-Sea Res 23, 695–710. https://doi.org/10.1016/S0011-7471(76)80015-0

Wihsgott, J.U., Sharples, J., Hopkins, J.E., Woodward, E.M.S., Hull, T., Greenwood, N., Sivyer, D.B., 2019. Observations of vertical mixing in autumn and its effect on the autumn phytoplankton bloom. Prog Oceanogr 177, 102059. https://doi.org/10.1016/j.pocean.2019.01.001

Wilding, J.L., 1939. The oxygen threshold for three species of fish. Ecology 20, 253–263. https://doi.org/10.2307/1930744

Wildish, D.J., Keizer, P.D., Wilson, A.J., Martin, J.L., 1993. Seasonal changes of dissolved oxygen and plant nutrients in seawater near salmonid net pens in the macrotidal Bay of Fundy. Can J Fish Aquat Sci 50, 303–311. https://doi.org/10.1139/f93-035

Winkler, L.W. 1888. Bestimmung des im Wasser gelösten Sauerstoffes. Berichte der deutschen chemischen Gesellschaft 21, 2843-2854. doi:10.1002/cber.188802102122

Winthereig-Rasmussen, H., Simonsen, K., Patursson, O., 2016. Flow through fish farming sea cages: Comparing computational fluid dynamics simulations with scaled and full-scale experimental data. Ocean Eng 124, 21-31. https://doi.org/10.1016/j.oceaneng.2016.07.027

Winkler, L.W. 1888. Bestimmung des im Wasser gelösten Sauerstoffes. Berichte der deutschen chemischen Gesellschaft 21, 2843-2854. doi:10.1002/cber.188802102122

Wright, D., Nowak, B., Oppedal, F., Bridle, A., Dempster, T., 2017. Free-living Neoparamoeba perurans depth distribution is mostly uniform in salmon cages, but reshaped by stratification and potentially extreme fish crowding. Aquac Environ Interact 9, 269–279. https://doi.org/10.3354/aei00233

Wu, Y., Sheng, J., Senciall, D., Tang, C., 2016. A comparative study of satellite-based operational analyses and ship-based in-situ observations of sea surface temperatures over the eastern Canadian shelf. Satell. Oceanogr Meteorol 1, 29–38. http://dx.doi.org/10.18063/SOM.2016.01.003

Xia, M., Craig, P.M., Wallen, C.M., Stoddard, A., Mandrup-Poulsen, J., Peng, M., Schaeffer, B., Liu, Z., 2011. Numerical Simulation of Salinity and Dissolved Oxygen at Perdido Bay and Adjacent Coastal Ocean. J Coast Res 27, 73–86.

Xu, G., Shi, Y., Sun, X., Shen, W., 2019. Internet of Things in the marine environment monitoring: A review. Sensors 19, 1711. https://doi.org/10.3390/s19071711

Yamamoto, A., Abe-Ouchi, A., Shigemitsu, M., Oka, A., Takahashi, K., Ohgaito, R., Yamanaka, Y., 2015. Global deep ocean oxygenation by enhanced ventilation in the Southern Ocean under long-term global warming. Global Biogeochem Cycles 29, 1801–1815. https://doi.org/10.1002/2015GB005181

Yashayaev, I., Loder, J.W., 2016. Recurrent replenishment of Labrador Sea Water and associated decadal-scale variability. J Geophys Res- Oceans 121, 8095–8114. https://doi.org/10.1002/2016JC012046

Yu, L., Fennel, K., Laurent, A., 2015. A modeling study of physical controls on hypoxia generation in the northern Gulf of Mexico. J Geophys Res- Oceans 120, 5019–5039. https://doi.org/10.1002/2014JC010634

Williamson, M.A., Keen, C.E., Mudie, P.J., 1984. Foraminiferal distribution on the continental margin off Nova Scotia. Mar Micropaleontol 9, 219–239. https://doi.org/10.1016/0377-8398(84)90014-8

Winton, M., Anderson, W.G., Delworth, T.L., Griffies, S.M., Hurlin, W.J., Rosati, A., 2014. Has coarse ocean resolution biased simulations of transient climate sensitivity? Geophys Res Lett 41, 8522–8529. https://doi.org/10.1002/2014GL061523

Zehr, J.P., Ward, B.B., 2002. Nitrogen Cycling in the Ocean: New Perspectives on Processes and Paradigms. Appl Environ Microbiol 68, 1015–1024. https://doi.org/10.1128/AEM.68.3.1015-1024.2002

Zorz, J., Willis, C., Comeau, A.M., Langille, M.G.I., Johnson, C.L., Li, W.K.W., LaRoche, J., 2019. Drivers of Regional Bacterial Community Structure and Diversity in the Northwest Atlantic Ocean. Front Microbiol 10.